LYAPUNOV-BASED ROBUST AND ADAPTIVE CONTROL DESIGN FOR NONLINEAR UNCERTAIN SYSTEMS

by

KUN ZHANG
B.S. Wuhan University of Technology, 2007
M.S. Huazhong University of Science and Technology, 2011

A dissertation submitted in partial fulfilment of the requirements
for the degree of Doctor of Philosophy
in the Department of Electrical Engineering and Computer Science
in the College of Engineering and Computer Science
at the University of Central Florida
Orlando, Florida

Spring Term
2015

Major Professor: Aman Behal

ABSTRACT

The control of systems with uncertain nonlinear dynamics is an important field of control science attracting decades of focus. In this dissertation, four different control strategies are presented using sliding mode control, adaptive control, dynamic compensation, and neural network for a nonlinear aeroelastic system with bounded uncertainties and external disturbance. In Chapter 2, partial state feedback adaptive control designs are proposed for two different aeroelastic systems operating in unsteady flow. In Chapter 3, a continuous robust control design is proposed for a class of single input and single output system with uncertainties. An aeroelastic system with a trailing-edge flap as its control input will be considered as the plant for demonstration of effectiveness of the controller. The controller is proved to be robust by both mathematical proof and simulation results. In Chapter 3, a robust output feedback control strategy is discussed for the vibration suppression of an aeroelastic system operating in an unsteady incompressible flowfield. The aeroelastic system is actuated using a combination of leading-edge (LE) and trailing-edge (TE) flaps in the presence of different kinds of gust disturbances. In Chapter 5, a neural-network based model-free controller is designed for an aeroelastic system operating at supersonic speed. The controller is shown to be able to effectively asymptotically stabilize the system via both a Lyapunov-based stability proof and numerical simulation results.

ACKNOWLEDGMENTS

I am thankful to Dr. Aman Behal, my supervisor, for his insightful guidance and consistent support of my work in University of Central Florida. I would also like to express my gratitude to my committee members: Dr. Piergiovanni Marzocca, Dr. Ladislau Boloni, Dr. Michael Haralambous, Dr. Yunjun, Xu, for inspiring discussions and suggestions on my research. A special thank you to Dr. Zhao Wang whose generous and invaluable help in my research and life has enabled me to achieve all that I have this far. Finally, thanks to my family and girlfriend Fiona for all the love and support they have given to me over the years in my further education.

TABLE OF CONTENTS

LIST OF FIGURES

LIST OF TABLES

CHAPTER 1: INTRODUCTION

The control of systems with uncertain nonlinear dynamics has been an important field of control science attracting decades of focus. Engineering systems can be modeled with different kinds of mathematical tools. One of them is differential equation based modeling method which occupies a significant place in control science. However, due to the complexity of real world systems, it is extremely hard to model a system with 100% accuracy. Unpredictable uncertainties and nonlinearities in the real systems are always the obstacles that prevent engineers from modeling real systems perfectly. Control techniques like robust and adaptive control are explored to control these engineering systems. In this dissertation, several new robust- and adaptive-based control strategies are proposed to stabilize different classes of engineering systems with uncertainties and disturbances. Specially, we consider aeroelastic systems operated under various conditions as our application choice. These new control strategies are proved to be effective with both mathematical proofs and simulation results.

In Chapter 2, a particular class of trailing-edge flap-controlled 2-D aeroelastic systems with structural nonlinearities in plunging and pitching and operated in an unsteady aerodynamic incompressible flowfield is considered. By using the flap hinge torque of the trailing edge flap surface as the control input, a partial state feedback continuous adaptive controller is proposed in order to suppress the aeroelastic vibrations of the wing section model. It is shown that the control design with respect to an appropriately chosen output variable yields an asymptotic stability result for all three of the pitching, plunging, and flapping degrees-of-freedom. As an extension to the single-input and single-output (SISO) system, an extra control flap is introduced to the original model for control design. By introducing another control input, the torque of the leading-edge flap, the wing section model becomes an multiple-input-multiple-output (MIMO) system akin to the system considered in [1]. Numerical simulation results clearly demonstrate the effectiveness of the control strategy

toward suppressing aeroelastic vibration at both pre- and post-flutter flight speed regimes for SISO and MIMO aeroelastic systems.

The same SISO mathematical model of aeroelastic systems from Chapter 2 is taken into consideration in Chapter 3. By using the flap hinge torque of a trailing edge flap surface as the control input, a continuous controller is proposed to suppress the aeroelastic vibrations of the wing section model which is theoretically shown to be robust with respect to external disturbances. By exploiting an Input-to-State-Stability (ISS) property, the control design of a chosen output variable yields a semi-global asymptotic stability result. Numerical simulation results verify the efficacy of the proposed control strategy toward suppressing aeroelastic vibration in both pre- and post-flutter flight speed regimes under a multitude of external disturbances.

In Chapter 4, an output feedback controller without observer is proposed to asymptotically stabilize a 4-DOF (plunging, pitching, LE flapping, TE flapping) airfoil system under unsteady flow with unstructured nonlinear uncertainties and bounded unknown external disturbances. The goal of this control design is to design a robust controller to suppress the vibrations for the aeroelastic system only using position feedback for the aeroelastic system by taking LE and TE flap as the actuator. A specific filter error is built based on output errors to avoid using velocity sensors to measure the rates of output variables and actuator deflections. The robustness of the system to external disturbance is theoretically guaranteed by a Lyapunov function based stability proof. The proposed controller requires only minimal knowledge of the system model, namely, the signs of the leading principal minors of control gain matrix. A SDU(Symmetric Diagonal Upper triangular factorization) decomposition[2] is applied to the control gain matrix to decouple the control inputs. A Lyapunov-based analysis is applied to show that semi-global asymptotic stability can be obtained for the pitching and plunging tracking errors under application of the proposed continuous robust controller.

The model-free control of aeroelastic vibrations of a non-linear 2-D wing-flap system operating in a supersonic flight speed regime is discussed in the Chapter 5. A novel continuous robust controller design yields asymptotically stable vibration suppression in both the pitching and plunging degrees of freedom using the flap deflection as a control input. The controller also ensures that all system states remain bounded at all times during closed-loop operation. A Lyapunov method is used to obtain the global asymptotic stability result. An unsteady aerodynamic load is considered by utilization of the non-linear Piston Theory Aerodynamics (PTA) modified to account for the effect of the flap deflection. Simulation results demonstrate the performance of the robust control strategy in suppressing dynamic aeroelastic instabilities, such as non-linear flutter and limit cycle oscillations

CHAPTER 2: ADAPTIVE CONTROL FOR SISO/MIMO NONLINEAR AEROELASTIC SYSTEM

Introduction

In this chapter, two novel adaptive control strategies are proposed for aeroelastic systems with single and multiple flaps. The aeroelastic system with single control flap is considered as a single-input-single-output (SISO) system while the one with two control flaps is taken as a multiple-input-multiple-output (MIMO) system. The aeroelastic system with two control flaps is considered as an extension of the system with one control flap and an SDU decomposition is applied to decouple the control inputs. Both aeroelastic systems are operated in subsonic incompressible unsteady flow field. The unsteady aerodynamic model is based on Wagner indicial function with a description of the aerodynamic loads provided in terms of the added lag state model. For facilitation of control design without using the immeasurable aerodynamic lag states, the Duhamel integration is shown to be linearly parameterizable. Based on the linearly parameterized system, a partial state adaptive feedback controller is designed to suppress the aeroelastic vibrations on a nonlinear wing section model in pre- and post-flutter conditions. A Lyapunov-based method has been utilized to obtain the asymptotic stability result for the plunging displacement error. The system is shown to be minimum-phase when considering the plunging displacement as the system output, thereby, assuring the convergence of the internal dynamics as the plunging displacement motion is suppressed. Simulation results under different conditions show the efficacy of the control design. Although the observable states of the aeroelastic system converge to zero as time goes to infinite, it is not guaranteed that all estimations of the uncertain parameters will converge to their real values. However, the stability can be guaranteed even when the parameters are off from their nominal values.

Aeroelastic Model Configuration

A 2-D wing flap structural model is illustrated in Fig. 2.1. The equations governing the aeroelastic motion of the system can be written as follows [3], [5]

$$M\ddot{\mathbf{Y}}(t)+K\mathbf{Y}(t) = -\mathbf{L}(t) + \mathbf{L}_c(t). \tag{2.1}$$

In the above equation, the variable $\mathbf{Y}(t)$ is defined as a column vector $\mathbf{Y}(t) \triangleq [\frac{h(t)}{b}\ \alpha(t)\ \beta(t)]^T$, where $\frac{h(t)}{b}$ denotes the dimensionless plunge displacement (positive downwards), $\alpha(t)$ denotes the pitch angle (measured at the elastic axis of the airfoil, positive nose-up) and $\beta(t)$ denotes the flap deflection of the trailing edge. In (2.1), the mass and stiffness matrices M and K, respectively, are defined as follows

$$\begin{aligned} M=&\begin{bmatrix} bm & S_\alpha & S_\beta \\ bS_\alpha & I_\alpha & I_\beta + S_\beta b\,(c-a) \\ bS_\beta & I_\beta + S_\beta b\,(c-a) & I_\beta \end{bmatrix} \\ K=&\begin{bmatrix} bk_h(h) & 0 & 0 \\ 0 & k_\alpha(\alpha) & 0 \\ 0 & 0 & K_\beta \end{bmatrix}, \end{aligned} \tag{2.2}$$

while L_c is the control load which is defined as

$$\mathbf{L}_c = \begin{bmatrix} 0 & 0 & 1 \end{bmatrix}^T T_c(t),$$

where $T_c(t)$ is the control input, which is the additional flap hinge torque used to control the flap deflection β. $\mathbf{L}(t)$ represents the unsteady aerodynamic load vector which can be expressed in

terms of its components as

$$\mathbf{L}(t) = \begin{bmatrix} L & M & T \end{bmatrix}^T$$

where the lift L, the aerodynamic pitching moment $M(t)$ and the flap torque $T(t)$ are explicitly defined as follows [5]

$$\begin{aligned} L(t) = \;& \pi\rho b^2[\ddot{h}(t) - bx_{EA}\ddot{\alpha}(t) + \tfrac{b}{2\pi}\Phi_4\ddot{\beta}(t) + V\dot{\alpha}(t) + \tfrac{V}{\pi}\Phi_3\dot{\beta}(t)] + 2\pi\rho VbD(t) \\ M(t) = \;& \pi\rho b^3[-a\ddot{h}(t) + b\left(\tfrac{1}{8} + a^2\right)\ddot{\alpha}(t) + \tfrac{b}{4\pi}\Phi_7\ddot{\beta}(t) + \left(\tfrac{1}{2} - a\right)V\dot{\alpha}(t) + \tfrac{V}{2\pi}\Phi_6\dot{\beta}(t) \\ & + \tfrac{V^2}{\pi b}\Phi_5\beta(t)] - 2\pi\rho b^2\left(\tfrac{1}{2} + a\right)VD(t) \\ T(t) = \;& \pi\rho b^2[\tfrac{b}{2\pi}\Phi_4\ddot{h}(t) + \tfrac{b^2}{4\pi}\Phi_7\ddot{\alpha}(t) + \tfrac{b^2}{2\pi^2}\Phi_{12}\ddot{\beta}(t) + \left(\tfrac{bV_f}{2\pi}\Phi_9\right)\dot{\alpha}(t) + \tfrac{bV}{2\pi^2}\Phi_{11}\dot{\beta}(t) \\ & + \tfrac{V^2}{\pi^2}\Phi_{10}\beta(t)] + \rho Vb_8^2\Phi_8 D(t), \end{aligned} \tag{2.3}$$

In (2.3) above, $\Phi_i = \Phi_i(\phi)$ are Theodorsen's constants [6][7] which have been listed in Appendix A, $\phi = \arccos(-c)$, while $D(t)$ denotes the Duhamel integration which yields

$$D(t) = Q(t) - A_1B_1(t) - A_2B_2(t) \tag{2.4}$$

based on the following standard two-term Jones' approximation of Wagner's function [8]

$$\Phi(\tau) = 1 - A_1e^{-\beta_1\tau} - A_2e^{-\beta_2\tau} \tag{2.5}$$

where $\tau = Vt/b$ is dimensionless time and $A_1, A_2, \beta_1, \beta_2$ are constants whose values will be explicitly chosen in the sequel. In (2.4), $Q(t)$ is a measure of circulation that is expressed as follows

$$Q(t) = \dot{h} + b\left(\frac{1}{2} - a\right)\dot{\alpha} + \frac{b}{2\pi}\Phi_2\dot{\beta} + \frac{V}{\pi}\Phi_1\beta + V\alpha \tag{2.6}$$

and $B_1(t)$,$B_2(t)$ are the state variables associated with the unsteady aerodynamics that are represented as follows

$$\begin{aligned} \dot{B}_1(t) + w_1 B_1(t) &= \dot{Q}(t) \\ \dot{B}_2(t) + w_2 B_2(t) &= \dot{Q}(t) \end{aligned} . \tag{2.7}$$

where $w_i = \beta_i(\frac{V}{b}), i = 1, 2.$

Given the expressions of (2.6) and (2.4), the aerodynamic loads given in (2.3) can be rewritten as follows

$$\begin{aligned} L(t) = \; & \pi\rho b^2[b\frac{\ddot{h}(t)}{b} - ba\ddot{\alpha}(t) + \frac{b}{2\pi}\Phi_4\ddot{\beta}(t) + 2V\frac{\dot{h}(t)}{b} + 2V\left(1-a\right)\dot{\alpha} + \frac{V}{\pi}(\Phi_3+\Phi_2)\dot{\beta} \\ & + \frac{2V^2}{b}\alpha(t) + \frac{2V^2}{\pi b}\Phi_1\beta(t) - \frac{2VA_1}{b}B_1(t) - \frac{2VA_2}{b}B_2(t)]. \\ M(t) = \; & \pi\rho b^2[-ab^2\frac{\ddot{h}(t)}{b} + b^2\left(\frac{1}{8}+a^2\right)\ddot{\alpha}(t) + \frac{b^2}{4\pi}\Phi_7\ddot{\beta}(t) - 2bV_f\left(\frac{1}{2}+a\right)\frac{\dot{h}(t)}{b} \\ & -2bVa\left(\frac{1}{2}-a\right)\dot{\alpha}(t) + \tfrac{Vb}{\pi}\left\{\frac{1}{2}\Phi_6 - \left(\frac{1}{2}+a\right)\Phi_2\right\}\dot{\beta}(t) - 2V^2\left(\frac{1}{2}+a\right)\alpha(t) \\ & + \frac{V^2}{\pi}\left\{\Phi_5 - 2\left(\frac{1}{2}+a\right)\Phi_1\right\}\beta(t) + 2V\left(\frac{1}{2}+a\right)A_1B_1(t) + 2V\left(\frac{1}{2}+a\right)A_2B_2(t)]. \\ T(t) = \; & \pi\rho b^2[\frac{b^2}{2\pi}\Phi_4\frac{\ddot{h}(t)}{b} + \frac{b^2}{4\pi}\Phi_7\ddot{\alpha}(t) + \frac{b^2}{4\pi}\Phi_{12}\ddot{\beta}(t) + \frac{Vb}{\pi}\Phi_8\frac{\dot{h}(t)}{b} + \frac{Vb}{\pi}\left(\frac{\Phi_9}{2} + \left(\tfrac{1}{2}-a\right)\Phi_8\right)\dot{\alpha}(t) \\ & + \frac{Vb}{2\pi^2}(\Phi_{11}+\Phi_2\Phi_8)\dot{\beta}(t) + \frac{V^2}{\pi}\Phi_8\alpha(t) + \frac{V^2}{\pi^2}(\Phi_{10}+\Phi_1\Phi_8)\beta(t) \\ & - \frac{V}{\pi}\Phi_8A_1B_1(t) - \frac{V}{\pi}\Phi_8A_2B_2(t)]. \end{aligned} \tag{2.8}$$

Based on the expressions in (2.8) above, the dynamics represented by (2.1) and (2.7) can be manipulated into the following state-space form

$$\begin{aligned} \dot{\mathbf{x}} = \; & A\mathbf{x} + \mathbf{f}(\frac{h}{b}, \alpha) + \mathbf{B}u \\ y = \; & \mathbf{C}^T\mathbf{x} \end{aligned} \tag{2.9}$$

where the state variable vector $\mathbf{x}$ is defined as follows

$$\mathbf{x} = \begin{bmatrix} \frac{\dot{h}(t)}{b} & \dot{\alpha}(t) & \dot{\beta}(t) & \frac{h(t)}{b} & \alpha(t) & \beta(t) & B_1(t) & B_2(t) \end{bmatrix}^T, \tag{2.10}$$

while u is used to denote the flap hinge torque $T_c(t)$. Explicit definitions for the system matrices $A, \mathbf{B}, \mathbf{C}$ and the nonlinear vector $\mathbf{f}(\frac{h}{b}, \alpha)$ are provided in Appendix A.

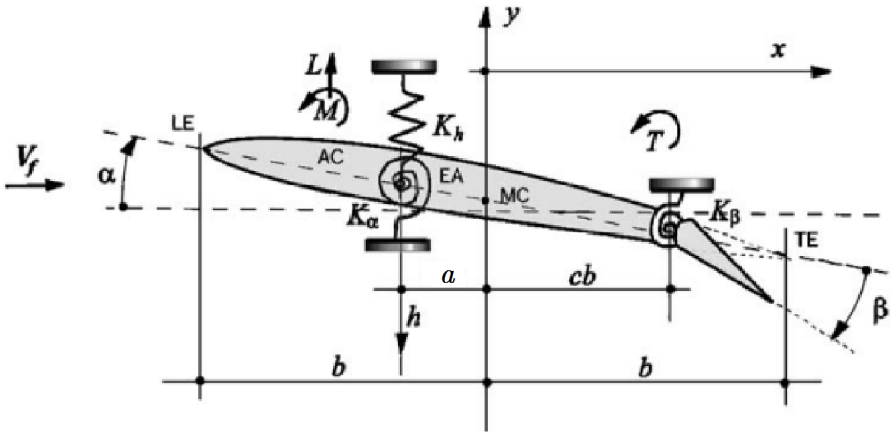

Figure 2.1: A 2-D wing flap structural model

Problem Definition and Open-Loop Error System Development

Based on the knowledge of the structure of the aeroelastic model, the control objective is to design a control strategy to drive the dimensionless plunge displacement $\frac{h}{b}$ to zero while adaptively compensating for parametric uncertainties in the system model. In next section, the system is shown to be minimum-phase with respect to the chosen input and output, thereby, assuring the stability of the zero dynamics to prove that the pitching and trailing edge flap deflections will converge to the origin along with the convergence of the plunging displacement. The state variables $\frac{h}{b}, \alpha, \beta, \frac{\dot{h}}{b}, \dot{\alpha},$

and $\dot{\beta}$ are considered to be measurable, since these six variables are deflections (and rates of deflection) associated with the physical structure of the airfoil. However, the state variables B_1 and B_2 are immeasurable for they are modeling approximations for the unsteady aerodynamics. All model parameters are considered to be unknown except for the sign of the coefficient of the control input.

To facilitate the subsequent stability analysis, an error signal $e(t) \in \Re$ for the plunging degree of freedom can be defined as

$$e \triangleq \frac{h_d}{b} - \frac{h}{b}, \tag{2.11}$$

where $\frac{h_d}{b} \in \Re$ is the desired output variable. Since the control objective is to suppress the plunging aeroelastic vibrations, $\frac{h_d}{b}$ will be simply chosen to be zero for all time. Next, to simplify the subsequent control design, a filtered error signal $r(t) \in \Re$ is introduced as follows

$$r = \dot{e} + \kappa e \tag{2.12}$$

where κ is a control gain.

Motivated by [9], by utilizing (2.2), (2.3) and the governing equation (2.1), one can obtain the following input-output representation of the plunging variable which is amenable to the ensuing adaptive feedback control design

$$\frac{\ddot{h}}{b} = c_1\frac{h}{b} + c_2\frac{\dot{h}}{b} + c_3\alpha + c_4\dot{\alpha} + c_5\beta + c_6\dot{\beta} + g_1 D(t) + f_{n1}(\frac{h}{b}, \alpha) + b_1 u \tag{2.13}$$

The definitions of the parameters and expressions in (2.13) are given in Appendix A. Then the above open-loop dynamics of (2.13) can be compactly rewritten as follows

$$\frac{\ddot{h}}{b} = F\left(x_1, x_2, x_3, x_4, x_5, x_6, D(t)\right) + b_1 u, \tag{2.14}$$

where $x_i, \forall\, i = 1-6$ denote the measurable system state variables and $F(\cdot)$ is expressed as

$$F(\cdot) \triangleq c_1\frac{h}{b} + c_2\frac{\dot{h}}{b} + c_3\alpha + c_4\dot{\alpha} + c_5\beta + c_6\dot{\beta} + g_1 D(t) + f_{n1}(\frac{h}{b}, \alpha)$$

However, the Duhamel integral term $D(t)$ in (2.14) appears to be immeasurable. In order to circumvent this issue, the solution for (2.7) is written as follows

$$\begin{aligned} B_1(t) &= e^{-w_1 t}B_1(0) + \dot{Q}(t) * e^{-w_1 t} \\ B_2(t) &= e^{-w_1 t}B_2(0) + \dot{Q}(t) * e^{-w_2 t} \end{aligned} \tag{2.15}$$

where '*' denotes the convolution operator. By substituting (2.15) into (2.4), one can obtain an expression for $D(t)$ as follows

$$D(t) = Q(t) - A_1 e^{-w_1 t}B_1(0) - A_2 e^{-w_1 t}B_2(0) - \dot{Q}(t) * \left[A_1 e^{-w_1 t} + A_2 e^{-w_2 t}\right]. \tag{2.16}$$

By taking advantage of the fact that the convolution terms in (2.16) can be written as follows

$$\dot{Q}(t) * A_i e^{-w_i t} \;\; = A_i \int_0^t \dot{Q}(\tau) e^{-w_i(t-\tau)} d\tau, \forall i = 1, 2, \tag{2.17}$$

one can utilize integration by parts to rewrite (2.17) into

$$\dot{Q}(t) * A_i e^{-w_i t} = A_i \left[Q(t) - Q(0) e^{-w_i t} - w_i Q(t) * e^{-w_i t}\right], \forall i = 1, 2. \tag{2.18}$$

By Substituting (2.18) into (2.16), one can write $D(t)$ as follows

$$\begin{aligned} D(t) = \;& (1 - A_1 - A_2) Q(t) + (A_1 e^{-w_1 t} + A_2 e^{-w_2 t}) Q(0) + Q(t) * (A_1 w_1 e^{-w_1 t} + A_2 w_2 e^{-w_2 t}) \\ & - A_1 e^{-w_1 t}B_1(0) - A_2 e^{-w_1 t}B_2(0) \end{aligned} \tag{2.19}$$

.

The third terms in the left side of can be written in the Laplace domain as follows

$$\mathcal{L}\left[Q(t) * \left(A_1 w_1 e^{-w_1 t} + A_2 w_2 e^{-w_2 t}\right)\right] = G_1(s)Q(s) \tag{2.20}$$

where $G_1(s) \triangleq \left[\dfrac{A_1 w_1}{s+w_1} + \dfrac{A_2 w_2}{s+w_1}\right]$. After utilizing (2.20), with a slight abuse of notation, $D(t)$ of (2.19) can be rewritten as follows

$$D(t) = \quad G(s)Q(t) + A_1 e^{-w_1 t}\left[Q\left(0\right) - B_1(0)\right] + A_2 e^{-w_2 t}\left[Q\left(0\right) - B_2(0)\right] \ . \tag{2.21}$$

where

$$G(s) \triangleq 1 - A_1 - A_2 + G_1(s). \tag{2.22}$$

By using (2.6), $D(t)$ can be linearly parameterizable as follows

$$D(t) = \mathbf{W}_\Delta \boldsymbol{\theta}_\Delta \tag{2.23}$$

where the measurable regression vector $\mathbf{W}_\Delta$ and the unknown parameter vector $\boldsymbol{\theta}_\Delta$ are explicitly defined as follows

$$\begin{aligned}
\mathbf{W}_\Delta &= \left[\begin{array}{cccccc} G(s)\dfrac{\dot{h}}{b} & G(s)\dot{\alpha} & G(s)\dot{\beta} & G(s)\beta & G(s)\alpha & e^{-w_1 t} \quad e^{-w_2 t} \end{array}\right], \\
\boldsymbol{\theta}_\Delta &= \left[\begin{array}{cccccc} b & b\left(\dfrac{1}{2} - a\right) & \dfrac{b}{2\pi}\Phi_2 & V & \dfrac{V}{\pi}\Phi_1 & A_1\left[Q\left(0\right) - B_1(0)\right] \quad A_2\left[Q\left(0\right) - B_2(0)\right] \end{array}\right]^T
\end{aligned} \tag{2.24}$$

Since the structural nonlinearity $f_{n1}(\frac{h}{b}, \alpha)$ is also linear parameterizable, the function $F\left(\cdot\right)$ in open-loop dynamic (2.14) can be linearly parameterized as follows

$$F\left(x_1, x_2, x_3, x_4, x_5, x_6, D(t)\right) = \mathbf{W}_F \boldsymbol{\theta}_F, \tag{2.25}$$

where $\mathbf{W}_F$ is a measurable nonlinear regression vector and $\boldsymbol{\theta}_F$ is a vector of unknown parameters.

After taking the time derivative of (2.12), premultiplying both sides of the result by $\frac{1}{|b_1|}$ and taking advantage of (2.14), one can obtain

$$\frac{1}{|b_1|}\dot{r} = \mathbf{W}\boldsymbol{\theta} - sgn(b_1)u, \tag{2.26}$$

where the linear parameterization $\mathbf{W}\boldsymbol{\theta} \in \Re$ is defined as follows

$$\mathbf{W}\boldsymbol{\theta} = \frac{1}{|b_1|}\left[-\mathbf{W}_F\boldsymbol{\theta}_F + \kappa\dot{e}\right]. \tag{2.27}$$

Analysis of Zero Dynamics

Since the subsequent control design is predicated on the system being minimum-phase, the stability of the system zero dynamics need to be assured, i.e., the system dynamics when the output has been regulated to the origin. Given our choice of $\frac{h}{b}$ as the output variable, it is straightforward to see from (2.13) that the system has strong relative degree 2. The analysis begins by defining a linear state transformation

$$\digamma : \mathbf{x} \rightarrow \left(\boldsymbol{\mu}, \boldsymbol{\zeta}^T\right)^T \in \mathbf{R}^8.$$

where $\boldsymbol{\mu} = \begin{bmatrix} \mu_1 & \mu_2 \end{bmatrix}^T \in \mathbf{R}^2$ and $\boldsymbol{\zeta} \in \mathbf{R}^6$ are partitions of the state vector with the system represented in the normal form. Specifically, $\boldsymbol{\mu}$ and $\boldsymbol{\zeta}$ are defined as follows

$$\digamma \mathbf{x} = \left(\boldsymbol{\mu}, \boldsymbol{\zeta}^T\right) \triangleq \begin{bmatrix} \frac{h}{b} \\ \frac{\dot{h}}{b} \\ b_2 \frac{h}{b} - b_1 \dot{\alpha} \\ b_3 \dot{\alpha} - b_2 \dot{\beta} \\ b_2 \frac{h}{b} - b_1 \alpha \\ b_3 \alpha - b_2 \beta \\ b_7 \frac{h}{b} - b_2 B_1 \\ B_1 - B_2 \end{bmatrix}. \tag{2.28}$$

It can be verified that the transformation matrix $\digamma$ is non-singular by computing its determinant. By taking the time derivative of (2.28), one can find that the control variable u does not appear in $\dot{\boldsymbol{\zeta}}$. Hence, the state space equations (2.9) can be transformed into following normal form

$$\begin{aligned} \dot{\mu}_1 &= \mu_2 \\ \dot{\mu}_2 &= a\left(\boldsymbol{\mu}, \boldsymbol{\zeta}\right) + b_1 u \ \cdot \\ \dot{\zeta} &= \mathbf{w}\left(\boldsymbol{\mu}, \boldsymbol{\zeta}\right) \end{aligned} \tag{2.29}$$

Explicit expressions for $a\left(\boldsymbol{\mu}, \boldsymbol{\zeta}\right) \in \mathbf{R}$ and $\mathbf{w}\left(\boldsymbol{\mu}, \boldsymbol{\zeta}\right) \in \mathbf{R}^6$ are nonlinear functions that can be computed from the matrix A, vectors $\mathbf{B}, \mathbf{C}$ and the nonlinear vector $\mathbf{f}(\frac{h}{b}, \alpha)$ defined in (2.9). By substituting $\mu_1 = \mu_2 \equiv 0$ into (2.29), the zero dynamics can be obtain as follows

$$\dot{\boldsymbol{\zeta}} = \boldsymbol{\Pi}(\boldsymbol{\zeta}) \tag{2.30}$$

where $\mathbf{\Pi}(\boldsymbol{\zeta}) = \mathbf{w}(\mathbf{0}, \boldsymbol{\zeta})$ denotes a nonlinear vector function of $\boldsymbol{\zeta}$ with $\mathbf{\Pi}(0) = 0$ which implies that $\boldsymbol{\zeta} = 0$ is an equilibrium point (EP) for the system (2.30). The local stability of the origin of this system can be verified by checking the eigenvalues of the linearized system

$$\dot{\boldsymbol{\zeta}} = K^* \boldsymbol{\zeta} \tag{2.31}$$

where $K^* \triangleq \dfrac{\partial \mathbf{\Pi}(\boldsymbol{\zeta})}{\partial \boldsymbol{\zeta}}(0)$. Thus, the origin of the zero dynamics is locally exponentially stable if K^* is a Hurwitz matrix. By utilizing nominal values of the system parameters, the eigenvalues of K^* were seen to lie in the open left half of the complex plane. The aforementioned facts imply that the zero dynamics of the nominal system are locally stable. Thus, as the plunging displacement is asymptotically regulated to the origin, the internal dynamics of the system will simultaneously converge to the origin.

Control Design and Stability Analysis

Based on the open-loop dynamics of Eq. (2.26) and the subsequent stability analysis, the following state feedback adaptive control law is proposed

$$u(t) = sgn(b_1)\left(\mathbf{W}\hat{\boldsymbol{\theta}} + K_r r\right) \tag{2.32}$$

where $K_r \in \Re$ is a control gain and $\hat{\boldsymbol{\theta}}(t) \in \Re^p$ denotes a gradient-based online estimation of $\boldsymbol{\theta}$ which is dynamically generated as follows

$$\dot{\hat{\boldsymbol{\theta}}} = Proj\left\{\Gamma \mathbf{W}^T r, \hat{\boldsymbol{\theta}}\right\} \tag{2.33}$$

where $\Gamma \in \Re^{p\times p}$ is a constant diagonal, positive definite matrix and p is determined by the dimension of the regression vector $\mathbf{W}$. Motivated by [10], the parameter projection operator $Proj\left\{\cdot\right\}$ is designed to bound $\hat{\boldsymbol{\theta}}\left(t\right)$ in a known compact set Ω_{ε} in the sense that

$$\hat{\boldsymbol{\theta}}\left(t\right) \in \Omega_{\varepsilon}\ \forall t > 0 \text{ if } \hat{\boldsymbol{\theta}}\left(0\right) \in \Omega_{\varepsilon}. \tag{2.34}$$

where the numerical definition of Ω_{ε} is given in next Section. After substituting the control law (2.32) into Eq. (2.26), one can obtain the following closed-loop system dynamics

$$\frac{1}{|b_1|}\dot{r} = \mathbf{W}\tilde{\boldsymbol{\theta}} - K_r r \tag{2.35}$$

where $\tilde{\boldsymbol{\theta}}\left(t\right) \in \Re^{p}$ is a parameter estimation error defined as follows

$$\tilde{\boldsymbol{\theta}}\left(t\right) \triangleq \boldsymbol{\theta} - \hat{\boldsymbol{\theta}}.$$

A non-negative Lyapunov candidate function $V_1\left(t,r\right) \in \Re$ as follows

$$V_1\left(t,r\right) = \frac{1}{2\left|b_1\right|}r^2 + \frac{1}{2}\tilde{\boldsymbol{\theta}}^T\Gamma^{-1}\tilde{\boldsymbol{\theta}}. \tag{2.36}$$

By taking the time derivative of (2.36) along the dynamics of (2.35) and the adaptive update law of (2.33), one can obtain the following result for $\dot{V}_1\left(t,r\right)$

$$\dot{V}_1\left(t,r\right) \leq -K_r r^2 \tag{2.37}$$

where the fact that $\dot{\tilde{\theta}}(t) = -\dot{\hat{\theta}}$ is used. In (2.37), the equality is in effect when $\hat{\boldsymbol{\theta}}\left(t\right)$ lies inside the compact set Ω_{ε} defined in (2.34) while the inequality is in force on the boundary of Ω_{ε}. From (2.36) and (2.37), one can conclude that $r\left(t\right) \in \mathcal{L}_2 \cap \mathcal{L}_{\infty}$ and $\tilde{\boldsymbol{\theta}} \in \mathcal{L}_{\infty}$, which also directly implies

that $e(t)$, $\dot{e}(t) \in \mathcal{L}_2 \cap \mathcal{L}_\infty$ and $\hat{\boldsymbol{\theta}}(t) \in \mathcal{L}_\infty$. Since $h_d = \dot{h}_d \equiv 0$, it is straightforward to see that $\frac{h}{b}, \frac{\dot{h}}{b} \in \mathcal{L}_\infty$.$\frac{h}{b}$ and $\frac{\dot{h}}{b}$ are bounded to a compact set as follows. From (2.36) and (2.37), one can have

$$V_1(t, r) \leq V_1(0, r_0) \tag{2.38}$$

where $r_0 = r(t_0)$ denotes the initial condition for $r(t)$. Substituting (2.36) into (2.38), one can obtain the following inequality

$$\frac{1}{2|b_1|} r^2 \leq V_1(0, r_0) - \frac{1}{2} \tilde{\boldsymbol{\theta}}^T \Gamma^{-1} \tilde{\boldsymbol{\theta}}.$$

Since $\frac{1}{2} \tilde{\boldsymbol{\theta}}^T \Gamma^{-1} \tilde{\boldsymbol{\theta}} \geq \mathbf{0}$, r can be bounded as

$$|r| \leq \sqrt{2|b_1| V_1(0, r_0)}. \tag{2.39}$$

Given $h_d = \dot{h}_d \equiv 0$, from the definitions of (2.11), (2.12), and (2.36), the bound given in (2.39), as well as the fact that $\tilde{\boldsymbol{\theta}}(0)$ remains inside a compact set, one can state that $\frac{h}{b}, \frac{\dot{h}}{b}$ remain inside a compact set $\mathcal{D}_1 \triangleq \left\{ \boldsymbol{\mu} \in \mathbf{R}^2 \;\middle|\; \|\boldsymbol{\mu}\| \leq K(|r_0|, \Gamma) \right\} \forall t$ where $K(\cdot)$ is a monotonically increasing function of r_0 and Γ^{-1}. Furthermore, by an appropriate choice of r_0 and Γ, the bound $K(\cdot)$ can be made as small as possible.Before the remainder of the stability analysis, motivated by [11], a critical Lemma is given to establish the conditions for boundedness of the system states.

Lemma 1 *: Given that the zero dynamics (2.30) of the nonlinear system (2.29) are locally exponentially stable and that* $\mathbf{w}(\boldsymbol{\mu}, \boldsymbol{\zeta})$ *defined in (2.29) is locally Lipschitz in* $\boldsymbol{\mu}, \boldsymbol{\zeta}$*, then, the internal dynamics* $\boldsymbol{\zeta}$ *of system (2.29) are bounded provided that the state vector initial condition lies inside an appropriately defined compact set.*

Based on Lemma 1, it is clear to see that the state vector $\mathbf{x}(t) \in \mathcal{L}_\infty$. Since $+(\cdot)$ is a bounded

function of the system states, this also implies that the control input $u(t)$ remains bounded for all time by virtue of (2.32). Furthermore, from (2.35), it is clear to see that $\dot{r}(t) \in \mathcal{L}_\infty$ which implies the uniform continuity of $r(t)$. Thus, Barbalat's Lemma [4] is utilized to show that $r(t) \to 0$ as $t \to \infty$. From (2.12), it is clear to see that $e_1(t), \dot{e}_1(t) \to 0$ as $t \to \infty$ which implies that $\frac{h}{b}, \frac{\dot{h}}{b} \to 0$ as $t \to \infty$. Furthermore, from the asymptotic stability of the zero dynamics, all system states are guaranteed to asymptotically converge to the origin.

Simulations and Results

Model and Control Parameters

In (2.2), the nonlinear stiffness functions $bk_h(h)$ and $k_\alpha(\alpha)$ are considered to be polynomial nonlinearities and are explicitly defined in the sequel. Section of fourth- and second- degree, respectively. They are defined as [12]

$$\begin{aligned} bk_h(h) &= bK_h\left(1 + 0.09h^2\right) \text{ N/m} \\ &= bK_h + k_{n_h}(h) \\ k_\alpha(\alpha) &= K_\alpha(1 - 22.1\alpha + 1315.5\alpha^2 + 8580\alpha^3 - 17289.7\alpha^4) \text{ Nm/rad} \\ &= k_{h_0} + k_{n_\alpha}(\alpha). \end{aligned} \tag{2.40}$$

Numerical simulation results are presented for a nonlinear aeroelastic system controlled by the flap torque of trailing-edge. The nonlinear unsteady aerodynamic model was simulated using (2.1) and (2.3). Within this aeroelastic formulation the aerodynamic-lag states B_1, B_2 were introduced to substitute the Duhamel Integration $D(t)$ as show in (2.4). The plunging and pitching spring stuffiness were modeled as polynomial nonlinearities as shown in (2.40). Model parameters ar given in Table 2.1. Note that all the parameters used in the aeroelastic and aerodynamic model

were considered to be unknown for the purpose of control design, except the sign of b_1.

In this simulation example, the desired trajectory variable $\frac{\dot{h}_d}{b}$ and $\frac{h_d}{b}$ were simply selected as zero. The initial conditions for pitch angle $\alpha(t)$ and plunge displacement $h(t)$ were set to be $\alpha(0) = 5.729$ [deg] and $h(0) = 0$ [m] while all other state variables were also selected as zero. The model parameters used in the simulation were the same as those used in [5], listed in Table 1 and lead to a flutter speed of $V_f = 128.87$ [m.s^{-1}]. The controller parameter is selected as $K_r = 10$, while the estimator gain are set as Γ=$500\mathbf{I}^{19\times 19}$ and the initial parameter estimates are set to zero. The compact set Ω_ε is given as

$$\Omega_\varepsilon = \left\{ \boldsymbol{\theta} \epsilon R^{19\times 1} \;\middle|\; \begin{array}{c} |\theta_i| < 20, i = 1,2,3,4,10,11,19 \\ |\theta_j| < 6000, j = 5,6,7,12,13 \\ |\theta_k| < 1000, k = 8,9,14, \\ |\theta_l| < 1e+6, l = 15,16,17,18 \end{array} \right\}$$

where $\theta_i, \theta_j, \theta_k, \theta_l$ are the components of vector $\boldsymbol{\theta}$.

Table 2.1: Model Parameters

Parameter	Value	Parameter	Value
b	0.305 [m]	K_h	$500m$
a	$-\frac{1}{2}$	K_α	$2000I_\alpha$
c	1.0	K_β	$18000I_\beta$
m	90.04 [kg]	ρ	1.225 [kg/m^3]
I_β	0.552 [kg·m^2]	I_α	1.512 [kg·m^2]
S_β	0.441 [kg]	S_α	7.062 [kg]
V_f	128.87 [m/s]	A_1	0.165
A_2	0.335	β_1	0.041
β_2	0.300		

For validating the effectiveness of the control strategy with respect to external disturbance, a triangular external disturbances is considered according to [5]. The external gust disturbance $\mathbf{L}_g(t)$ is

given as

$$\mathbf{L}_g(t) = [\ L_g \quad M_g \quad 0\ ],$$

where

$$\begin{aligned} L_g &= 4\pi\dot{\psi} w_G(\tau) \\ M_g &= L_g\left(\tfrac{1}{2} + \tfrac{a}{b}\right) \end{aligned} . \tag{2.41}$$

In (2.41), $\psi\,(t)$ denotes Kussner's function which is approximated by

$$\psi(t) = 1 - 0.5e^{-0.13t} - 0.5e^{-t}$$

while $w_G(\tau)$ denotes the disturbance velocity; here, τ is a dimensionless time variable. The velocity distribution function for $w_G(\tau)$ is given as

$$w_G(\tau) = 2w_0\frac{\tau}{\tau_G}\left(H\left(\tau\right) - H\left(\tau - \frac{\tau_G}{2}\right)\right) - 2w_0\left(\frac{\tau}{\tau_G} - 1\right)\left(H\left(\tau - \tau_G\right) - H\left(\tau - \frac{\tau_G}{2}\right)\right)$$

where $H(\cdot)$ denotes a unit step function and given $t_G = 0.25$ [s]. This triangular gust lasts 0.5 [s] from $t = 5$ to 5.5 [s].

Results

In this section, two set of simulations are investigated: in the pre-flutter condition, $V = 103.09$ [m.s^{-1}] and in the post-flutter condition $V = 141.7556$ [m.s^{-1}]. Fig. (2.2) shows the open-loop response of the wing-section model at pre-flutter speed $V = 103.09$ [m.s^{-1}]$< V_f = 128.87$ [m.s^{-1}].Both the plunging and pitching responses to initial conditions along with the flap deflection are displayed. Consistent with their dynamic parameters, the response of the individual states occurs at different frequencies. In particular, the higher frequency content in the torsional modes is evident when compared with the corresponding bending frequency. These frequencies are flight

speed dependent, and in this case with the simulations conducted well below the flutter speed, no coalescence of frequencies is evident. Instead, the three main frequencies, i.e., bending, pitch and flap torsion are well distinct. In this uncontrolled open-loop case, the control torque applied at the flap is zero. Fig. (2.3) is the response of the aerodynamic lag states B_1 and B_2.

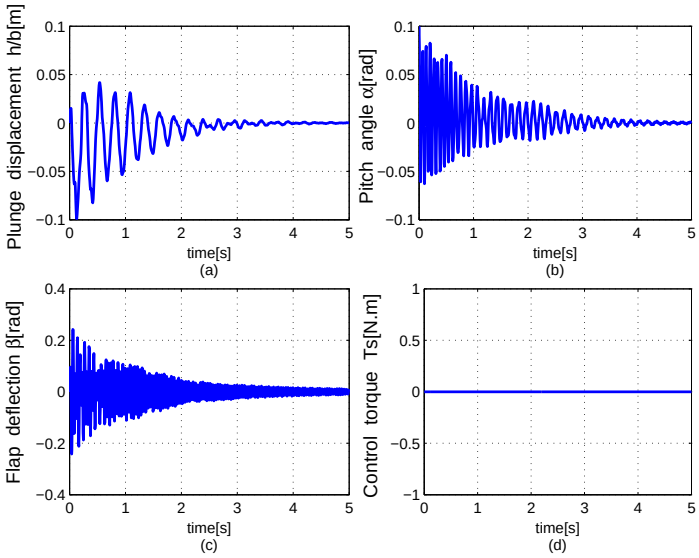

Figure 2.2: Open-loop system response at pre-flutter speed $V = 0.8V_f$

In Fig. (2.4), one can see that the proposed control law suppresses the plunging displacement in 3[s] while the pitching displacement is driven to zero in 6[s]. In Fig. (2.5), the aerodynamic lag states B_1, B_2 are affected by the control that in turn changes the dynamics of the system. It is expected that the dynamic response of the states B_1 and B_2 is quickly controlled when compared to the uncontrolled open-loop case. Note that in these simulations the controller was turned on at $t = 0$ [s].

Figs. (2.6) and (2.7) show the system response at a post-flutter speed $V = 141.76$ [m.s^{-1}]>128.87 [m.s^{-1}]. Without any control input, limit cycle oscillations appear in the system response due to

the nonlinearities in the system model. The plunging and pitching post-flutter responses are now in synchronization and the bending and torsional frequencies of the system reach close proximity. A linear flutter analysis will show that a coalescence of frequency has been reached, since this system does not include structural damping.

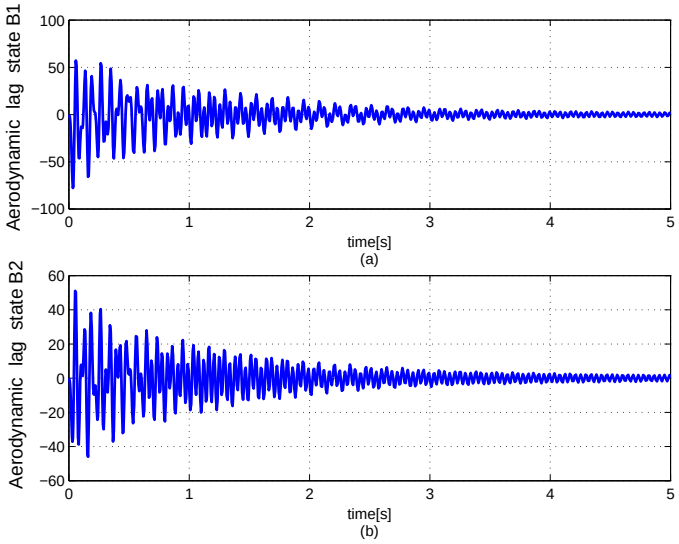

Figure 2.3: Open-loop aerodynamic lag states B_1,B_2 pre-flutter speed $V = 0.8V_f$

In Figs. (2.8) and (2.9), the control is turned on at $t = 5$ [s]. The vibration of plunging displacement is suppressed in less than 2[s] without oscillation, while it takes a little longer for pitch degree and aerodynamic lag states to converge to zero.

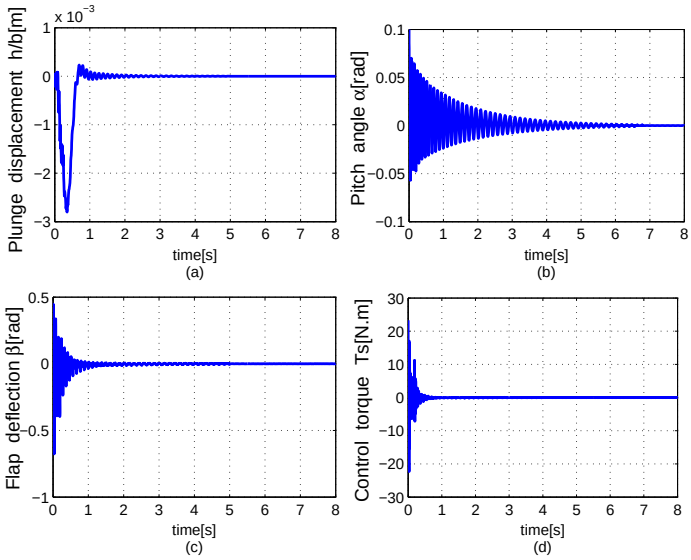

Figure 2.4: Closed-loop system response at pre-flutter speed $V = 0.8V_f$

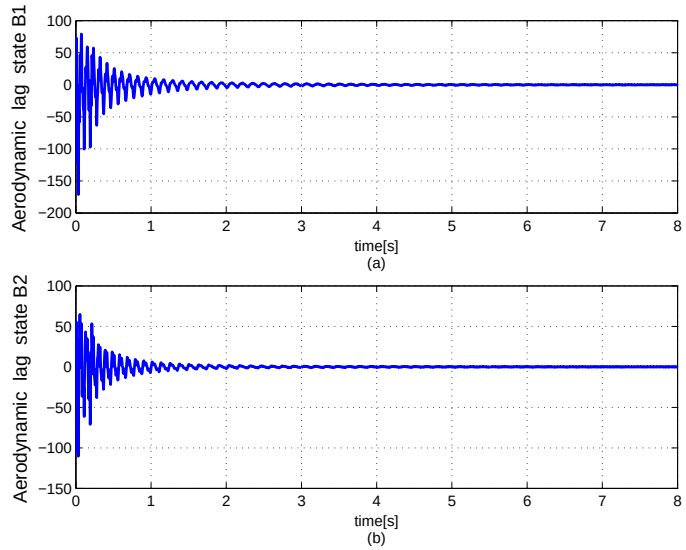

Figure 2.5: Closed-loop aerodynamic lag states B_1,B_2 at pre-flutter speed $V = 0.8V_f$

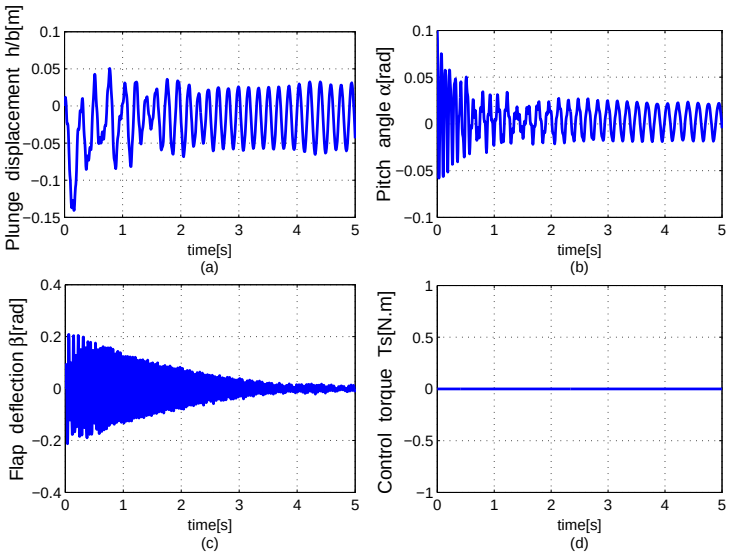

Figure 2.6: Open-loop system response at post-flutter speed $V = 1.2V_f$

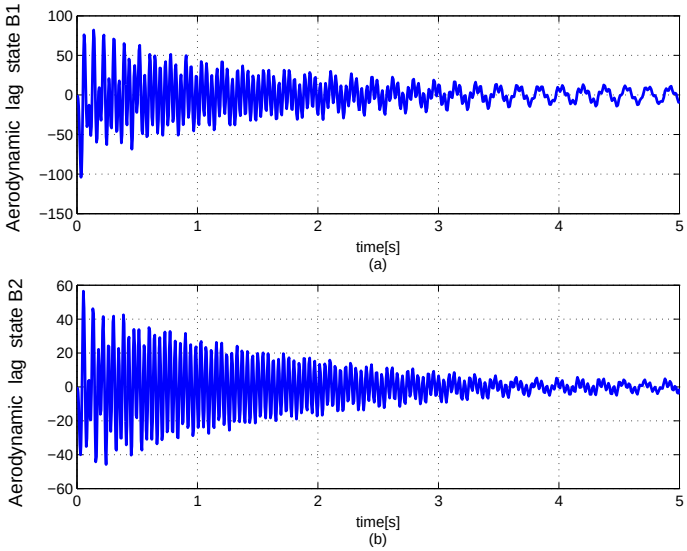

Figure 2.7: Open-loop aerodynamic lag states B_1,B_2 at post-flutter speed $V = 1.2V_f$

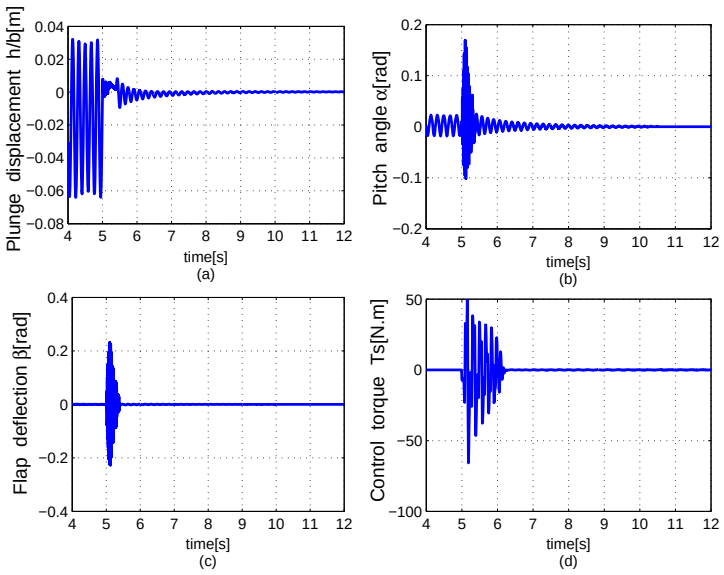

Figure 2.8: Closed-loop system response at post-flutter speed $V = 1.2V_f$

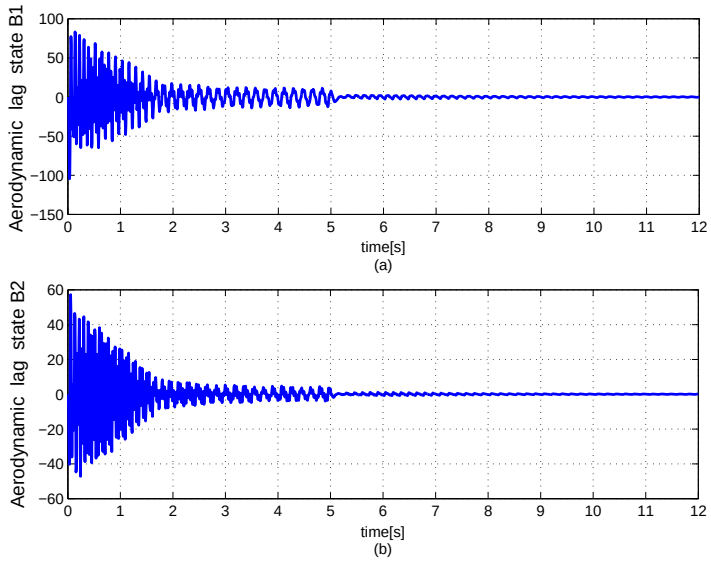

Figure 2.9: Closed-loop aerodynamic lag states B_1,B_2 at post-flutter speed $V = 1.2V_f$

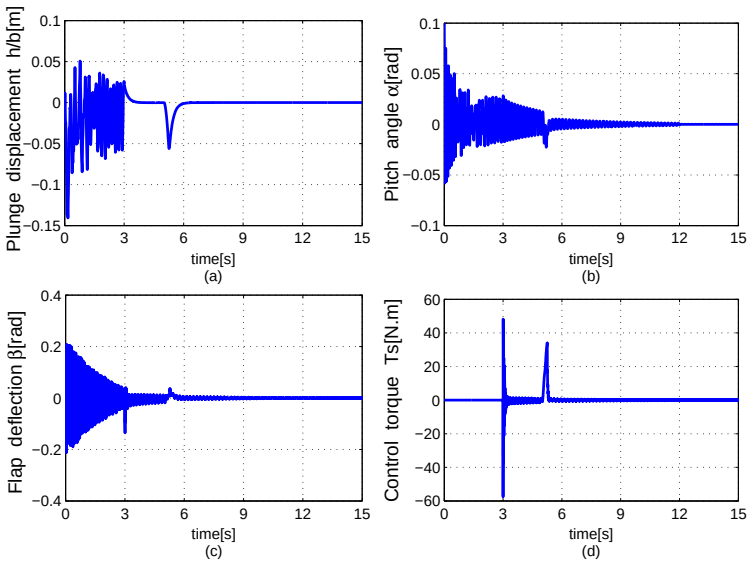

Figure 2.10: Closed-loop system response at post-flutter speed $V = 1.2V_f$ under triangular gust

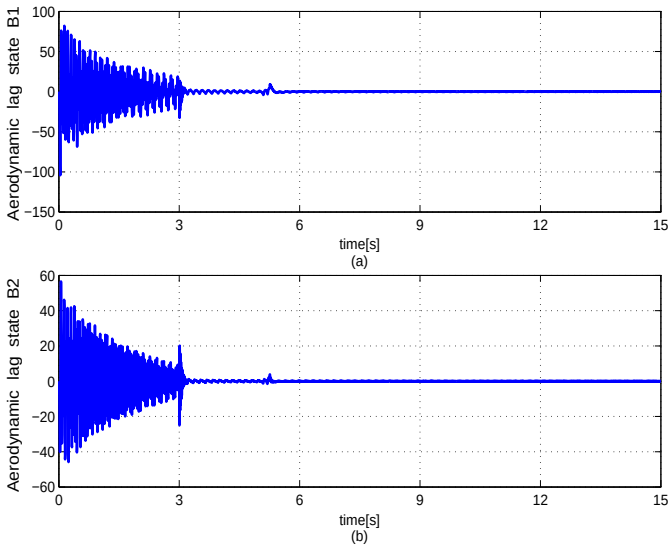

Figure 2.11: Closed-loop aerodynamic lag states B_1,B_2 at post-flutter speed $V = 1.2V_f$ under triangular gust

The closed-loop responses of the system at post-flutter speed under a triangular gust disturbance are shown in Fig. (2.10) and (2.11). The disturbance is applied at $t = 5$ [s] and lasts for 0.5 [s]. One can see from Fig. (2.10) and (2.11) that the pitching and plunging displacements are suppressed in 5 [s] and the internal dynamics B_1 and B_2 also converge in less than 5 [s]. Note that in this case the control is turned on at $t = 3$ [s]. These simulation results reveal that the control strategy proposed effectively suppresses the oscillation of the plunging displacement and consequently the system internal dynamics at both pre- and post-flutter speeds.

MIMO system Extension

Model Derivation and Control Design

In this section, we will briefly discuss extension an adaptive control strategy for the wing section model as a 4-DOF system (plunging, pitching, LE flapping, TE flapping) with two control inputs and accounting for unsteady aerodynamics loads. A wing section model with 4-DOFs in plunging displacement $h(t)$, pitching angle $\alpha(t)$, TE flap deflection $\beta(t)$, and LE flap deflection $\gamma(t)$ is presented in Figure 2.12. The hinge torques u_β and u_γ of the TE- and LE-flaps, respectively, are taken as control inputs. The aeroelastic governing equations are developed based on the model proposed in [6][5]

$$M_s\ddot{\mathbf{x}} = -K_s\mathbf{x} - K(h,\alpha)\,\mathbf{x} + \frac{1}{m_s b^2}\mathbf{L} + T\mathbf{u} \tag{2.42}$$

where $\mathbf{L}(t)$ represents the unsteady aerodynamic load, m_s is the total mass of wing and flaps per unit length, b is the semi-chord, the state vector $\mathbf{x} \triangleq \begin{bmatrix} \frac{h}{b} & \alpha & \beta & \gamma \end{bmatrix}^T$, while M_s and K_s denote the structural mass and stiffness matrices which are explicitly given in the Appendix. The control gain matrix T is defined as $T \triangleq \begin{bmatrix} 0_2 & \frac{1}{m_s b^2} I_2 \end{bmatrix}^T$[1], $\mathbf{u} \triangleq \begin{bmatrix} u_\beta & u_\gamma \end{bmatrix}^T$, while $K(h,\alpha) \triangleq$

[1]Throughout the note, the notation 0_n and I_n denote, respectively, the $n \times n$ zero and identity matrices.

diag$\{k_h(h), k_\alpha(\alpha), 0, 0\}$ denotes the structural nonlinearity in the pitching and plunging stiffnesses explicit choices are presented in next part. The aerodynamical load $\mathbf{L}(t)$ in (2.42) is expressed as sum of circulatory and non-circulatory components as

$$\mathbf{L} = \mathbf{L}_c + \mathbf{L}_{nc}. \tag{2.43}$$

In the above equation, the non-circulatory aerodynamic load component is defined as

$$\mathbf{L}_{nc} = \rho_\infty b^4 M_{nc}\ddot{\mathbf{x}} + \rho_\infty b^3 U_\infty B_{nc}\dot{\mathbf{x}} + \rho_\infty b^2 U_\infty^2 K_{nc}\mathbf{x} \tag{2.44}$$

where U_∞ is the freestream velocity, ρ_∞ is the air density, M_{nc}, B_{nc}, K_{nc} denote the non-circulatory loads aerodynamic matrices reported in the Appendix, while $\mathbf{L}_c(t)$ is the circulatory load defined as follows

$$\mathbf{L}_c = \rho_\infty b^2 U_\infty P^T R D(t). \tag{2.45}$$

In the above equation, $R \in \mathfrak{R}^{4\times 1}$ is a constant vector and $P \in \mathfrak{R}^{4\times 4}$ denotes a coordination transformation matrix (see the Appendix for explicit definitions), while $D(t)$, commonly referred to as the Duhamel integral, is expressed as follows

$$D(t) = Q(t) - a_1 B_1(t) - a_2 B_2(t). \tag{2.46}$$

The expression above is based on Jones' approximation of Wagner's function as shown in (2.5). In (2.46), $Q(t) \in \mathfrak{R}$ is a measure of circulation expressed as follows

$$Q(t) \triangleq U_\infty \mathbf{S}_1 P\mathbf{x} + b\mathbf{S}_2 P\dot{\mathbf{x}}, \tag{2.47}$$

while B_1 and B_2 are aerodynamic lag state variables satisfying the following dynamics

$$\dot{B}_i(t) + w_i B_i(t) = \dot{Q}(t), i = 1, 2 \tag{2.48}$$

where $w_i \triangleq \beta_i U_\infty / b$, $i = 1, 2$. We note that $\mathbf{S}_1, \mathbf{S}_2 \in \Re^{1\times 4}$ used in (2.47) are constant vectors whose expressions are also given in the Appendix. For more details about the unsteady aerodynamic development above, the readers are referred to [13]. After defining a state vector $\mathbf{X} \triangleq \begin{bmatrix} \dot{\mathbf{x}}^T & \mathbf{x}^T & \mathbf{x}_B^T \end{bmatrix}^T \in \Re^{10\times 1}$ where $\mathbf{x}_B = \begin{bmatrix} B_1 & B_2 \end{bmatrix}^T$, one can utilize (2.42), (2.43), (2.45), (2.46), (2.47), and (2.48) to obtain the system state-space dynamics as

$$\begin{aligned} \dot{\mathbf{X}} &= A\mathbf{X} + \mathbf{f}(\mathbf{y}) + H\mathbf{u} \\ \mathbf{y} &\triangleq \begin{bmatrix} \frac{h}{b} & \alpha \end{bmatrix}^T \end{aligned} \tag{2.49}$$

where $\mathbf{y} \in \Re^2$ is the system output, while the system matrix $\mathbf{A}$, the nonlinearity $\mathbf{f}(\mathbf{y})$, and the control gain matrix $H \in \Re^{10\times 2}$ are explicitly defined in the Appendix. Given the above choice of the output variable, it is straightforward to demonstrate that the internal dynamics of (2.49) is globally exponentially stable from the eigenvalues of the nominal system matrix of the zero dynamics.

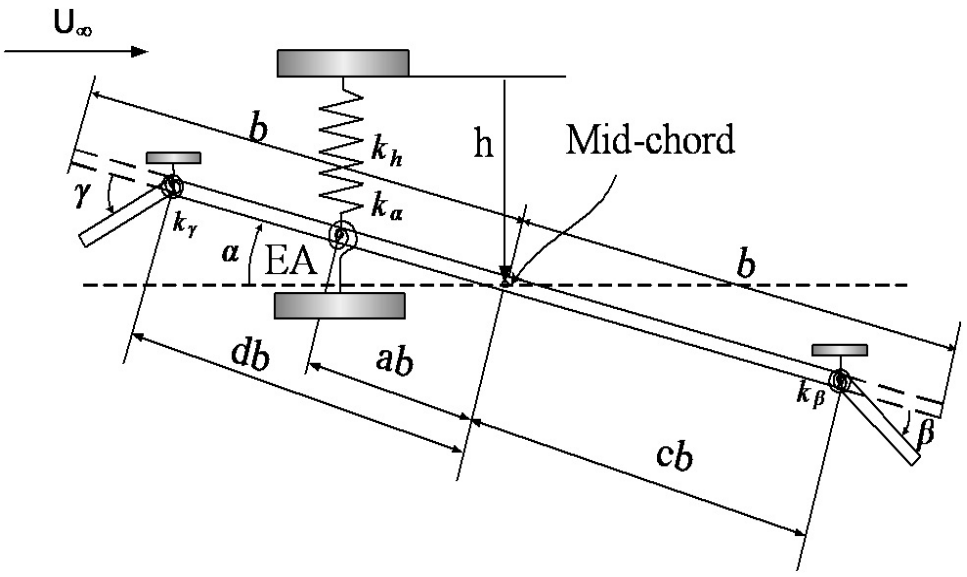

Figure 2.12: Wing Section with Leading- and Trailing-Edge Flaps

Then the output dynamics can be cast as follows

$$\ddot{\mathbf{y}} = \Psi\left(\mathbf{x}, \dot{\mathbf{x}}\right) + \mathbf{F} D\left(t\right) + G\mathbf{u} \tag{2.50}$$

where$\Psi\left(\mathbf{x}, \dot{\mathbf{x}}\right) \in \Re^2$ is an auxiliary function defined in Appendix, $F \in \Re^{2\times 1}$ is a constant parameter matrix while G is an input gain matrix with nonzero leading principal minors defined as the first two rows of the control gain matrix H. Since the aerodynamic lag states B_1, B_2 are immeasurable, (2.46) suggests that $D\left(t\right)$ cannot be directly obtained as a linear regression. However, using a convolution based method described in previous section in (2.23)[13] that utilizes (2.46), (2.47), and (2.48), $D\left(t\right)$ can be linearly parameterized as follows

$$D\left(t\right) = \mathbf{W}_{\Delta}^{T} \boldsymbol{\theta}_{\Delta} \tag{2.51}$$

where the measurable regression vector $\mathbf{W}_{\Delta}\left(x, \dot{x}, t\right) \in \Re^{10}$ and the unknown parameter vector

$\boldsymbol{\theta}_\Delta \in \Re^{10}$ are explicitly defined as follows

$$\mathbf{W}_\Delta = \begin{bmatrix} G(s)\dot{x}^T & G(s)x^T & e^{-w_1 t} & e^{-w_2 t} \end{bmatrix}^T,$$
$$\boldsymbol{\theta}_\Delta = \begin{bmatrix} (S_2 P)^T & (S_1 P)^T & a_1 \left[Q\left(0\right) - B_1(0)\right] & a_2 \left[Q\left(0\right) - B_2(0)\right] \end{bmatrix}^T$$

where $G(s)$ is given in 2.22. Similar to the error definition given in (2.11)(2.12), we define a group of error signals as follows

$$\begin{aligned} \mathbf{e} &= \mathbf{y}_d - \mathbf{y}, \\ \mathbf{r} &= \dot{\mathbf{e}} + \kappa \mathbf{e} \end{aligned} \tag{2.52}$$

where $\mathbf{y}_d \triangleq \begin{bmatrix} \frac{h_d}{b} & \alpha_d \end{bmatrix}^T \in \Re^{2\times 1}$, $\mathbf{y}_d$ can either be simply chosen to be zero for all time or it can be allowed to smoothly converge to the origin, κ is a positive, diagonal gain matrix. The open-loop error dynamics is obtained by taking the derivative of $\mathbf{r}$ in (2.52) as follows

$$\dot{\mathbf{r}} = \ddot{\mathbf{y}}_d + \kappa \dot{\mathbf{e}} - \Phi\left(\mathbf{x}, \dot{\mathbf{x}}\right) - F\mathbf{W}_\Delta^T \boldsymbol{\theta}_\Delta - G\mathbf{u}. \tag{2.53}$$

Since the leading principal minors of G are nonzero, it can be decomposed as $G = S\bar{D}U$, where S is a symmetric positive-definite matrix, $\bar{D}$ is a diagonal matrix with diagonal entries $+1$ or -1, and U is an unknown unity upper-triangular matrix . The reader is referred to [14] for explicit definitions of $S, \bar{D}$, and U. Based on this SDU decomposition, one can perform some algebraic manipulations on (2.53) in order to obtain the following convenient form of the open-loop error dynamics.

$$M\dot{\mathbf{r}} = \mathbf{N} - \bar{D}\mathbf{u}. \tag{2.54}$$

where $M \triangleq S^{-1}$, while the vector $\mathbf{N}\left(\mathbf{x}, \dot{\mathbf{x}}, \mathbf{u}, t\right) \in \Re^{2\times 1}$ is defined as

$$N = M\left[\ddot{\mathbf{y}}_d + \kappa \dot{e} - \Phi\left(\mathbf{x}, \dot{\mathbf{x}}\right) - F\mathbf{W}_\Delta^T \boldsymbol{\theta}_\Delta\right] + \left(\bar{D} - \bar{D}U\right)\mathbf{u}. \tag{2.55}$$

The matrix $\left(\bar{D}-\bar{D}U\right)$ is strictly upper triangular so that

$$\mathbf{N}\left(\cdot\right)=\left[\begin{array}{cc} N_1\left(\mathbf{x},\dot{\mathbf{x}},u_2,t\right) & N_2\left(\mathbf{x},\dot{\mathbf{x}},t\right)\end{array}\right]^T.$$

It is clear to see from (2.55) that $\mathbf{N}\left(\cdot\right)$ can be linearly parameterized as follows

$$\mathbf{N}=W\left(\mathbf{x},\dot{\mathbf{x}},\mathbf{u},t\right)\boldsymbol{\theta}=\left[\begin{array}{cc} \mathbf{W_3}^T\left(\mathbf{x},\dot{\mathbf{x}},u_2,t\right) & 0 \\ 0 & \mathbf{W_4}^T\left(\mathbf{x},\dot{\mathbf{x}},t\right)\end{array}\right]\left[\begin{array}{c}\boldsymbol{\theta_1}\\ \boldsymbol{\theta_2}\end{array}\right]$$

where the measurable regression vectors $\mathbf{W_3}\left(\cdot\right)\in\Re^{24}$ and $\mathbf{W_4}\left(\cdot\right)\in\Re^{23}$ are defined as follows

$$\begin{aligned}\mathbf{W}_3 &\triangleq \left[\begin{array}{ccc}\mathbf{W}_\Delta^T & \mathbf{W}_\mathbf{1}^T & u_2\end{array}\right]^T\\ \mathbf{W}_4 &\triangleq \left[\begin{array}{cc}\mathbf{W}_\Delta^T & \mathbf{W}_\mathbf{1}^T\end{array}\right]^T\\ \mathbf{W}_\mathbf{1} &\triangleq \left[\begin{array}{ccccccccccccc}\dot{h} & \dot{\alpha} & h & \alpha & \dot{\beta} & \dot{\gamma} & \beta & \gamma & h^3 & \alpha^2 & \alpha^3 & \alpha^4 & \dot{e}\end{array}\right]\end{aligned} \tag{2.56}$$

while $\boldsymbol{\theta}_1\in\Re^{24}$ and $\boldsymbol{\theta}_2\in\Re^{23}$ denote unknown parameter vectors defined as follows

$$\begin{aligned}\boldsymbol{\theta_1} &= \left[\begin{array}{cccc}\theta_{1,1} & \ldots & \theta_{1,23} & \theta_u\end{array}\right]^T\\ \boldsymbol{\theta_2} &= \left[\begin{array}{ccc}\theta_{2,1} & \ldots & \theta_{2,23}\end{array}\right]^T\end{aligned}. \tag{2.57}$$

Under knowledge of the signs of the leading principal minors (*i.e.,* knowledge of control direction), an adaptive control law is postulated as follows

$$\mathbf{u}=\bar{D}^{-1}\left[W\hat{\boldsymbol{\theta}}+K\mathbf{r}\right] \tag{2.58}$$

where $\mathbf{K}=diag\{k_1,k_2\}\in\Re^{2\times2}$ is a constant, positive definite control gain matrix, while the

parameter estimate $\hat{\boldsymbol{\theta}}(t)$ is dynamically generated by the following update law

$$\dot{\hat{\boldsymbol{\theta}}} = \Gamma \mathbf{W}^T \mathbf{r} \tag{2.59}$$

where $\Gamma \in \Re^{41\times 41}$ is a constant, positive definite adaptive gain matrix. By substituting (2.58) into (2.54), one can obtain the closed-loop error dynamics as follows

$$M\dot{\mathbf{r}} = \mathbf{W}\tilde{\boldsymbol{\theta}} - K\mathbf{r} \tag{2.60}$$

where $\tilde{\boldsymbol{\theta}} \triangleq \boldsymbol{\theta} - \hat{\boldsymbol{\theta}} \in \Re^{41}$ denotes the parameter estimation errors. To analyze the stability of the proposed control law, a non-negative Lyapunov function $V_0(t)$ is given as follows

$$V_0(t) = \frac{1}{2}\mathbf{r}^T M \mathbf{r} + \frac{1}{2}\tilde{\boldsymbol{\theta}}^T \Gamma^{-1} \tilde{\boldsymbol{\theta}} \tag{2.61}$$

After taking the time derivative of (2.61) along the dynamics of (2.60) and (2.59), one obtains

$$\dot{V}_0 = -\mathbf{r}^T K \mathbf{r} \leq 0 \tag{2.62}$$

From (2.61) and (2.62), one can conclude that $r(t) \in \mathcal{L}_2 \cap \mathcal{L}_\infty$, $\tilde{\boldsymbol{\theta}} \in \mathcal{L}_\infty$, which also implies that $\mathbf{e}(t), \dot{\mathbf{e}}(t) \in \mathcal{L}_2 \cap \mathcal{L}_\infty$ and $\hat{\boldsymbol{\theta}} \in \mathcal{L}_\infty$. By virtue of the boundedness and smoothness properties of the reference trajectory, one can conclude that $\frac{h}{b}, \frac{\dot{h}}{b}, \alpha$, and $\dot{\alpha} \in \mathcal{L}_\infty$. Since the system of (2.49) is minimum-phase, one can straightforwardly prove that the internal states $\beta, \gamma, \dot{\beta}, \gamma, B_1$, and $B_2 \in \mathcal{L}_\infty$. From the aforementioned boundedness assertions, one can conclude that $u_2(t) \in \mathcal{L}_\infty$ and consequently $u_1(t) \in \mathcal{L}_\infty$. Based on all previous boundedness assertions, from (2.54) $\dot{\mathbf{r}}(t) \in \mathcal{L}_\infty$ which implies uniform continuity of $\mathbf{r}(t)$. Now, using Barbalat's Lemma [4], one can show that $\lim_{t\to\infty} \mathbf{r}(t) = \mathbf{0}$, and from (2.52), one can state that $\lim_{t\to\infty} h(t), \alpha(t) = 0$. Finally, from the asymptotic stability of the zero dynamics, one can also guarantee the asymptotic convergence of all system

states to the origin.

Simulation Results and Discussion

The wing section model is based on the structural and aerodynamic equations of (2.42) and (2.43). The model parameter settings are quite similar to those utilized in [6] and are given in Table 2.2 as follows.

Table 2.2: Model parameters

Parameter	Value	Parameter	Value
ω_α	40 [rad/s]	b	1 [m]
ω_h	35 [rad/s]	d	-0.8
ω_β	300 [rad/s]	c	0.8
ω_γ	300 [rad/s]	x_α	0.2
μ	40	r_α^2	0.25
a	-0.4	x_β, x_γ	0.0125
$\zeta_\beta, \zeta_\gamma$	0.1	r_β^2, r_γ^2	0.00625
ρ_∞	1.292 [kg/m^3]		

The nonlinear stiffness functions are selected as $k_\alpha(\alpha) = K_\alpha(1 - 22.1\alpha + 1315.5\alpha^2)$ and $k_h(h) = K_h\,(1 + 0.09h^2)$ while $K_h \triangleq \omega_h^2 m_s$, $K_\alpha \triangleq \omega_\alpha^2 I_\alpha$, where $m_s = \pi\rho b^2\mu$ denotes the mass of wing per unit length and $I_\alpha = r_\alpha^2 m_s b^2$ denotes the inertia per unit length of wing section about elastic EA. The dimensionless flight speed $V \triangleq \frac{U_\infty}{b\omega_\alpha}$. Given the parameters settings in Table 1, one can compute the flutter speed to be $U_f = 100.40$ [m/s] while the dimensionless flutter speed $V_f \triangleq \frac{U_f}{b\omega_\alpha} = 2.51$. The desired trajectory variables $\dot{h}_d, h_d, \dot{\alpha}_d, \alpha_d$ are simply set to zero. The initial conditions for pitching angle $\alpha(t)$ and plunge displacement $h(t)$ are set to be $\alpha(0) = 5$ [deg] and $h(0) = 0.1$ [m], respectively, while all other plant state variables are initially selected to be zero. The adaptive controller law is implemented via (2.58) and (2.59). From (2.57) and (2.56) one can see that the regression variables corresponding to $\theta_{i,15}$ and $\theta_{i,16}$, $i = 1, 2$ are $\dot{\beta}$ and $\dot{\gamma}$, respectively; therefore,

damping in the β and γ dynamics is introduced by specifying the initial value of $\theta_{i,15}$ and $\theta_{i,16}$ in the controller to limit the maximum amplitude of the flap deflections. In this case, there is no need to consider structural damping structure in the wing section model. Thus, parameter estimates are initialized to zero except for $\theta_{i,15}$ and $\theta_{i,16}$, $i = 1, 2$ that are initialized to 1. Table 2.3 shows the controller gain settings that were utilized to ensure satisfactory system closed-loop performance.

Table 2.3: Controller Parameters

Parameter	Pre-flutter	Post-flutter
k_1	2	5
k_2	2	5
κ	2	5
Γ	$5I_{41}$	$2I_{41}$

Figure (2.15) represents the closed-loop response of the pitching, plunging, and flap deflections at pre-flutter speed. In this simulation, the controller is turned on at $t = 0.2$ [s].

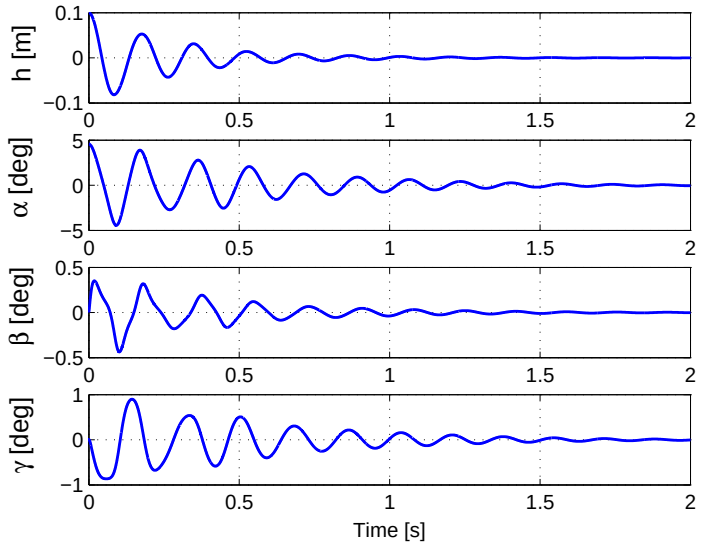

Figure 2.13: Open-loop response at pre-flutter speed $V_\infty = 2.26 < V_f$

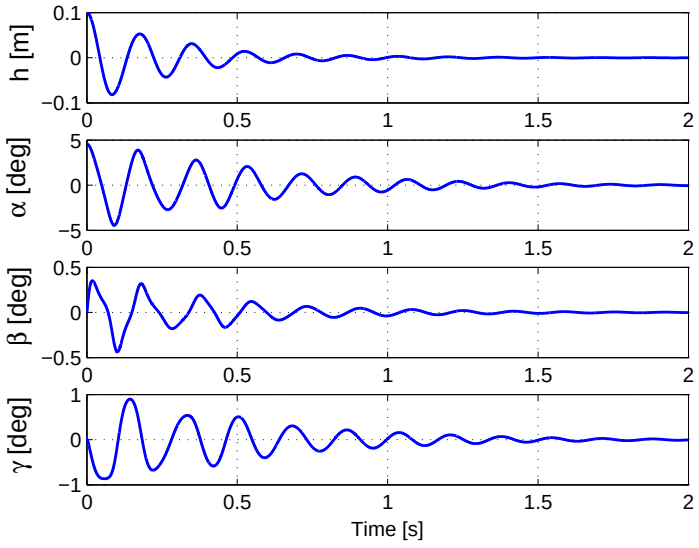

Figure 2.14: Open-loop response at pre-flutter speed $V_\infty = 2.26 < V_f$

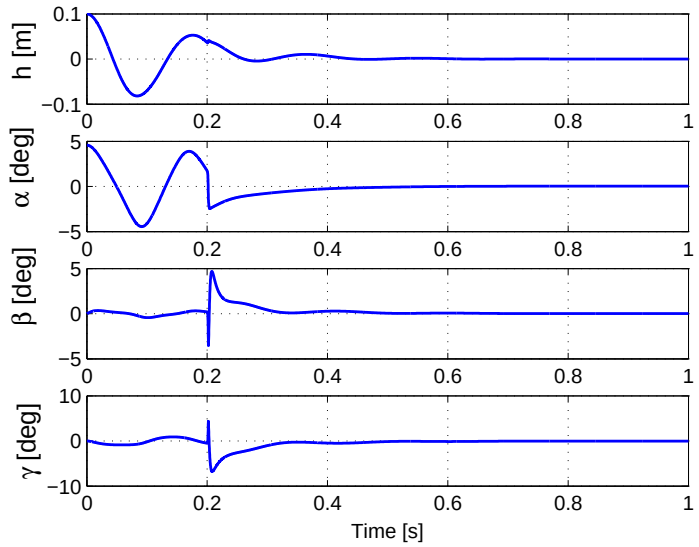

Figure 2.15: Closed-loop response at pre-flutter speed $V_\infty = 2.26 < V_f$

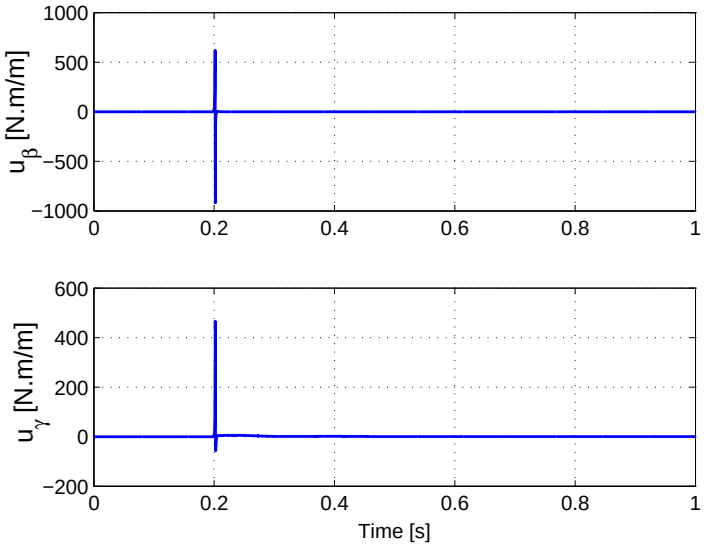

Figure 2.16: LE- and TE-flap hinge torque inputs at pre-flutter speed $V_\infty = 2.26 < V_f$

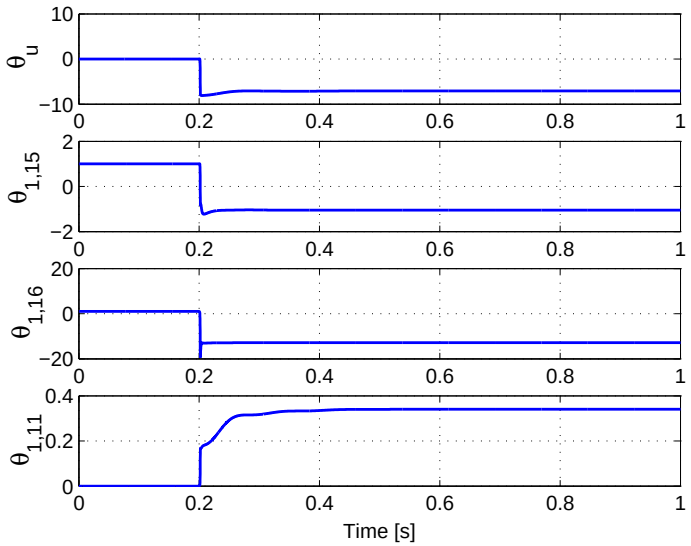

Figure 2.17: Time evolution of sample parameter estimates at pre-flutter speed $V_\infty = 2.26 < V_f$

By comparing Figures (2.14) and (2.15), one can find that the adaptive control law can significantly decrease the system settling time. The control input is presented in Figure (2.16) and sample parameter estimates are shown in Figure (2.17).

The second simulation is carried out at post-flutter speed $V_\infty = 2.76 > V_f$. The controller is also turned on at $t = 0.2$ [s]. As one can see from Figure (2.18), both the pitching and plunging DOFs are stabilized in 0.2 [s] and the LCOs are effectively suppressed by the proposed adaptive controller. The control torque input is shown in Figure (2.19), while the estimates of selected parameters are shown in Figure (2.20).

Figures (2.21) and (2.22) show the advantages of the proposed control strategy implemented with two control flaps as compared with only the TE flap. The controller was turned on at $t = 0.2$ [s] for both cases and the same parameters settings were used. The solid line is system response with LE and TE flaps. The dotted line is system response with only TE flap as control input.

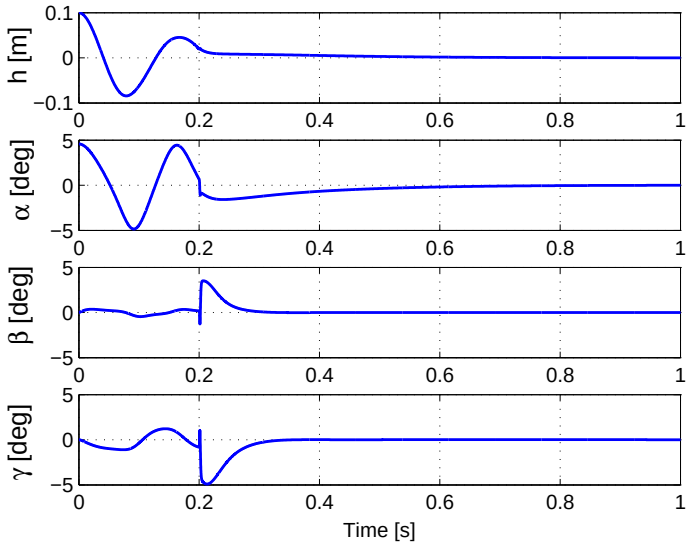

Figure 2.18: Closed-loop response at post-flutter speed $V = 2.76 > V_f$

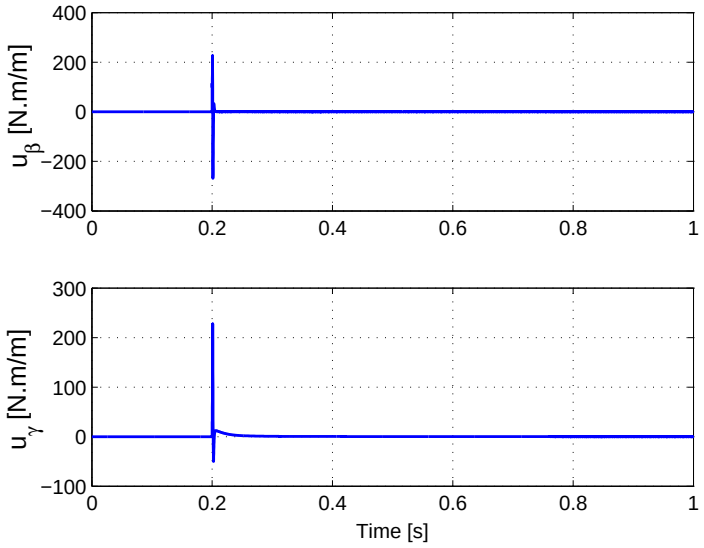

Figure 2.19: LE- and TE-flap hinge torque inputs at post-flutter speed $V = 2.76 > V_f$

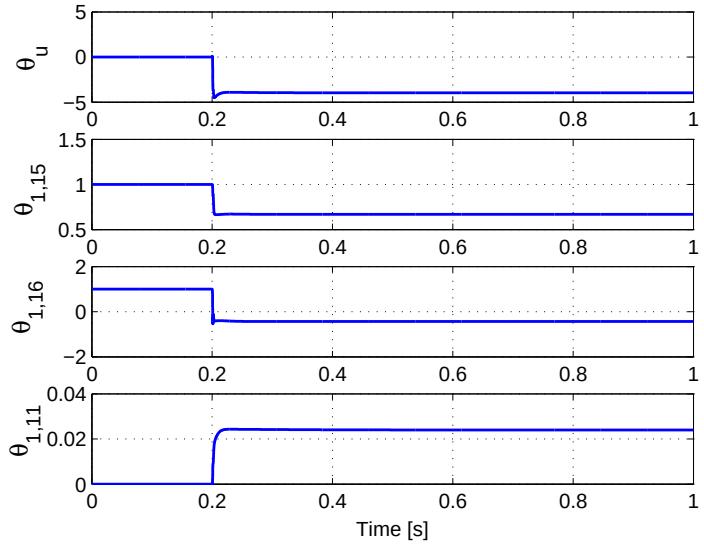

Figure 2.20: Time evolution of sample parameter estimates at post-flutter speed $V = 2.76 > V_f$

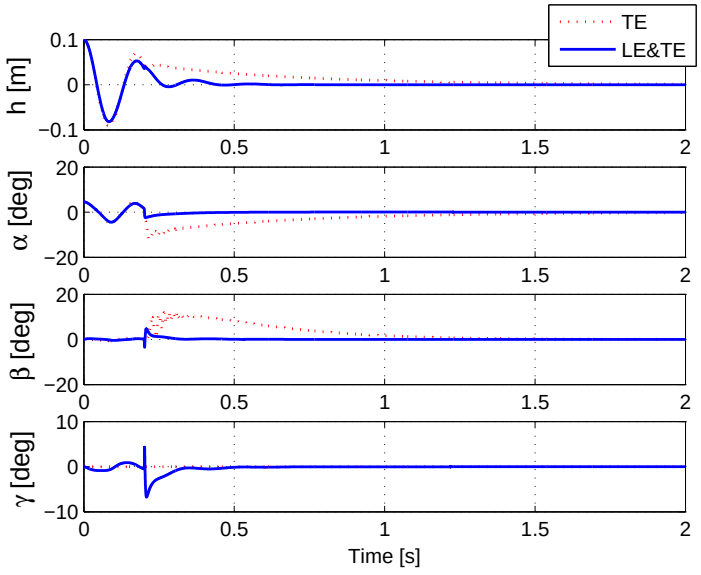

Figure 2.21: Closed-loop system response at pre-flutter speed $V_\infty = 2.26 < V_f$.

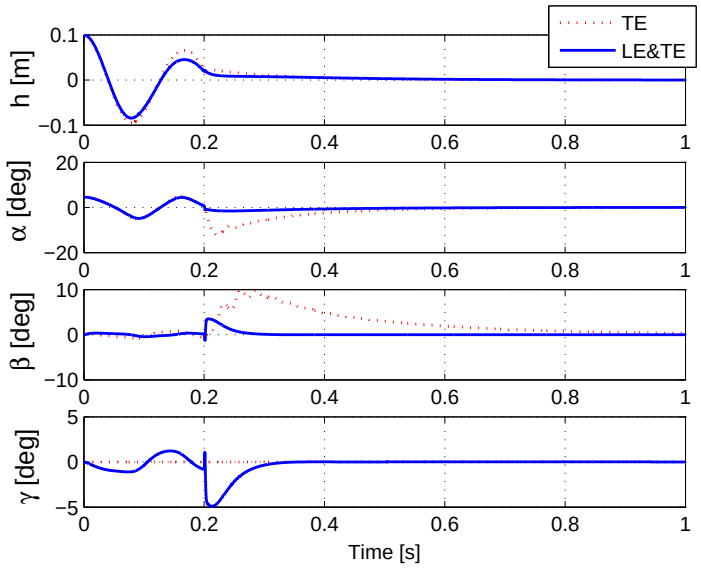

Figure 2.22: Closed-loop system response at post-flutter speed $V_\infty = 2.76 > V_f$.

Results illustrate that at both pre- and post- flutter speeds the pitching and plunging displacements of the system converge much faster when using the two flaps collectively. With only the TE flap, the plunging displacement converges fast (being the directly controlled variable) while the pitching displacement converges naturally according to the internal dynamics of the system. Another advantage of the proposed control strategy with two flaps is that the maximum amplitude of the both the TE and LE control flap deflections is much smaller than that of control strategy with only the TE flap. Furthermore, the very low amplitude of the leading edge deflection minimizes potential flow separation induced by the control surface operation.

Conclusion

Partial state feedback adaptive control designs are developed for SISO/MIMO aeroelastic systems exposed to incompressible unsteady flow. The immeasurable unsteady aerodynamic states resulted from the formulation based on Wagner's indicial function were estimated implicitly during the control design using a convolution based method. Both system is shown to be minimum-phase with the chosen variables as the system output, thereby, assuring the convergence of the internal dynamics as the plunging displacement motion is suppressed. Lyapunov-based method has been utilized to obtain the asymptotic stability result for both situations.

In the control design for MIMO system, an SDU (Symmetric p.d. + Diagonal + Upper Triangular) decomposition was utilized to decouple the control inputs resulting in a singularity free controller that produced a global asymptotic stability result. Numerical simulations showed that the controller could suppress Limit Cycle Oscillations (LCOs) at post-flutter speed while also having the ability to dramatically decrease the settling time of the system at pre-flutter speed.

CHAPTER 3: CONTINUOUS ROBUST CONTROL FOR AEROELASTIC SYSTEM

Introduction

In this chapter, a continuous robust controller is proposed to asymptotically stabilize the 2-D airfoil system that presented in Chapter 2. However, several kinds of bounded unknown external disturbances are applied to the system. A single-input/single-output (SISO) continuous robust controller is designed to suppress the vibrations for the aeroelastic system using a TE flap as the actuator. The novelty of this work is that we theoretically guarantee robustness to external disturbances which (to the best of our knowledge) has not been achieved before using an unsteady formulation. The proposed controller requires only minimal knowledge of the system model, namely, the sign of the control gain. The design of this control law is motivated by a continuous robust SISO result presented in [15] which was applicable to flat systems. The challenge in extending the controller of [15] to the 2-D system model utilized in this paper lies in proving the stability of the internal dynamics induced by the combination of the unsteady aerodynamics and the dynamics of the plunging degree of freedom which is not directly controlled. These internal dynamics appear as a disturbance term in the dynamics of the pitching displacement. We address these internal dynamics in a two-step fashion by utilizing Input-to-State Stability (ISS) concepts [4]. First, we prove that the system internal dynamics can be bounded as the summation of a nondecreasing function of the tracking error of the chosen output variable (specifically, the pitching DOF) and the bounds of the external disturbance. Then, given this boundedness of the internal states of the system as a function of the output error, a Lyapunov-based analysis is applied to show that semi-global asymptotic stability can be obtained for the pitching angle tracking error under application of the proposed continuous robust controller. The advantages of the proposed robust controller compared with the

adaptive control designed in our previous work in [13] are *three-fold*: firstly, the proposed control design is low-order since there are no parameters that need to be estimated; secondly, this is a partial state feedback controller in which only the output variable and its derivative are utilized, and finally, the control design theoretically guarantees robustness to a class of bounded disturbances..

Dynamic System and Open-Loop Error System Development

The 2-D wing flap structural model presented in Chapter 2 and illustrated in Fig. 2.1 is taken into consideration. While different from the situation in Chapter 2, pitching displacement is taken as the system output and nonlinearity are restricted in pitching displacement. We can get a similar state space representation of the overall system dynamics as shown in (2.1) such that

$$M\ddot{\mathbf{Y}}(t)+K\mathbf{Y}(t) = -\mathbf{L}(t) + \mathbf{L}_c(t) - \mathbf{L}_g(t)\,. \tag{3.1}$$

where $\mathbf{L}_g(t)$ represent the unsteady aerodynamic load and gust loads. All the matrices definition in (3.1) is the same as those in (2.1) except the stiffness matrix is defined as

$$K = \begin{bmatrix} K_h & 0 & 0 \\ 0 & k_\alpha(\alpha) & 0 \\ 0 & 0 & K_\beta \end{bmatrix}$$

In (3.1), the gust loading $\mathbf{L}_g(\tau)$ is defined as follows [16][5].

$$\begin{aligned} \mathbf{L}_g(\tau) &= \begin{bmatrix} L_G(\tau) & M_{yG}(\tau) & T_T(\tau) \end{bmatrix}^T \\ &= \rho V b \int_0^\tau \begin{bmatrix} I_{LG}(\tau-\tau_0) & I_{MG}(\tau-\tau_0) & I_{fG}(\tau-\tau_0) \end{bmatrix}^T w_G(\tau_0) d\tau \end{aligned} \tag{3.2}$$

where $\tau = Vt/b$ is the dimensionless time and $w_G(\tau)$ is the gust variable velocity which is assumed to be $\mathcal{C}^0$, while I_{LG}, I_{MG} and I_{fG} are the related aerodynamic indicial functions. For incompressible flow, they are expressed as

$$\begin{bmatrix} I_{LG}(\tau-\tau_0) & I_{MG}(\tau-\tau_0) & I_{fG}(\tau-\tau_0) \end{bmatrix}^T = \begin{bmatrix} 4\pi\dot{\psi} & bI_{LG}\left(\frac{1}{2}-a\right) & 0 \end{bmatrix}^T \tag{3.3}$$

where ψ denotes the Kussner function which is approximated by

$$\psi = 1 - 0.5e^{-0.13\tau} - 0.5e^{-\tau}. \tag{3.4}$$

From Eqs.(3.1)-(3.3), the state space representation of the overall system dynamics can be obtained as follows

$$\begin{aligned} \dot{\mathbf{x}} &= A\mathbf{x} + \mathbf{f}(\alpha) + \mathbf{B}\mathbf{u} + G\mathbf{w}_g \\ y &= \mathbf{C}^T\mathbf{x} \end{aligned} \tag{3.5}$$

where $\mathbf{w}_g \triangleq \begin{bmatrix} w_L(t) & w_M(t) & w_T(t) \end{bmatrix}^T$ denotes the external gust disturbance which is $\mathcal{C}^1$ since $w_G(\tau) \in \mathcal{C}^0$, $A, \mathbf{B}, \mathbf{C}, G$, and $\mathbf{f}(\alpha)$ are, respectively, parameter matrices and a nonlinear vector, whose explicit definitions have been given in Appendix A.

From (3.5), the pitching displacement dynamics are expressed as follows

$$\ddot{\alpha} = \lambda(\mathbf{x}) + b_2 u + \mathbf{G}_2\mathbf{w}_g, \tag{3.6}$$

where the expression for $\lambda(\mathbf{x})$ is given in Appendix B, while b_2 and $\mathbf{G}_2$, respectively, denote the second component of the control input vector $\mathbf{B}$ and the second row of the disturbance matrix G. For the sake of design of a continuous controller using an integral of the standard signum function, we begin by taking the derivative of (3.6) and utilizing (3.5) to obtain the dynamics in the following

form amenable to further analysis

$$\alpha^{(3)} = \dot{\lambda}\left(\mathbf{x}\right) + b_2 \dot{u} + d(t) \tag{3.7}$$

where $d(t)$ is a time-varying bounded disturbance term for which an explicit expression has been provided in Appendix B. To facilitate the following controller design, the tracking error e_1 is defined as

$$e_1 = \alpha_d - \alpha, \tag{3.8}$$

where α_d is the desired bounded output variable that is designed to be $\mathcal{C}^3$ smooth in deference to the requirements of the subsequent control design. Next, the auxiliary error signals e_2 and r are defined as follows

$$e_2 = \dot{e}_1 + e_1, \tag{3.9}$$

$$r = \dot{e}_2 + e_2. \tag{3.10}$$

Based on above definitions, a composite error signal $\mathbf{e}(t)$ can be defined as follows

$$\mathbf{e} = \begin{bmatrix} e_1 & e_2 & r \end{bmatrix}^T. \tag{3.11}$$

By taking the derivative of r, substituting from the derivative of (3.9) and applying the definitions given in (3.7), (3.9), and (3.10), we obtain

$$\frac{1}{|b_2|}\dot{r} = \frac{1}{|b_2|}\left[(\ddot{\alpha}_d + 2\dot{e}_2 - \dot{e}_1) - \dot{\lambda}\left(\mathbf{x}\right)\right] - sgn(b_2)\dot{u} - \frac{1}{|b_2|}d(t) \tag{3.12}$$

We now arrange (3.12) into following open-loop dynamics form

$$\frac{1}{|b_2|}\dot{r} = N(\mathbf{x}, \dot{\mathbf{x}}, t) - sgn(b_2)\dot{u} - e_2 \tag{3.13}$$

where the auxiliary function $N(\mathbf{x}, \dot{\mathbf{x}}, t)$ is defined as follows

$$N = \frac{1}{|b_2|}\left[(\ddot{\alpha}_d + 2\dot{e}_2 - \dot{e}_1) - \dot{\lambda}(\mathbf{x})\right] - \frac{1}{|b_2|}d(t) + e_2. \tag{3.14}$$

Note here that the function $N(\mathbf{x}, \dot{\mathbf{x}}, t)$ will be split into different parts based on their boundedness to facilitate the subsequent control design.

Boundedness of Internal Dynamics

Before we delve into the control design, we introduce a Lemma which can provide the boundedness of system states in terms of the input, output, and initial state values. We start by transforming (3.5) into a normal form by applying a linear diffeomorphism [13] $F : R^8 \to R^8$ to the original system states $\mathbf{x}(t)$ as follows

$$F\mathbf{x} = \begin{bmatrix} \alpha & \dot{\alpha} & \boldsymbol{\zeta}^T \end{bmatrix}^T \tag{3.15}$$

such that

$$\frac{d}{dt}\begin{bmatrix} \alpha \\ \dot{\alpha} \\ \boldsymbol{\zeta} \end{bmatrix} = FAx + F\mathbf{f}(\alpha) + F\mathbf{B}u + F\mathbf{G}\mathbf{w}_g(t) \tag{3.16}$$

where (3.5) has been utilized; here, $\digamma$ has been designed s.t. $\digamma \mathbf{B} = \begin{bmatrix} 0 & b_2 & 0^{6\times 1} \end{bmatrix}^T$, which implies that the $\boldsymbol{\zeta} \triangleq \digamma_{sub}\mathbf{x} \in R^{6\times 1}$ dynamics are independent of the control variable u as follows

$$\dot{\boldsymbol{\zeta}} = \digamma_{sub} A\mathbf{x} + \digamma_{sub}\mathbf{f}(\alpha) + \digamma_{sub}\mathbf{G}\mathbf{w}_g(t) \tag{3.17}$$

where $\digamma_{sub}$ is the appropriate submatrix of $\digamma$ derived from (3.15). Then a higher-order state vector $\mathbf{Z} = \begin{bmatrix} \boldsymbol{\mu}^T & \boldsymbol{\eta}^T \end{bmatrix}^T$ is defined as follows where $\boldsymbol{\mu} \triangleq \begin{bmatrix} \alpha & \dot{\alpha} & \ddot{\alpha} \end{bmatrix}^T$ and $\boldsymbol{\eta} \triangleq \begin{bmatrix} \boldsymbol{\zeta}^T & \dot{\boldsymbol{\zeta}}^T \end{bmatrix}^T$. By utilizing (3.7) and the time derivative of (3.17), the dynamics of $\mathbf{Z}(t)$ can be succinctly written as follows

$$\dot{\mathbf{Z}} = \mathbf{F}(\mathbf{Z}) + \mathbf{T}\dot{u} + \mathbf{D}(\mathbf{t}) \tag{3.18}$$

while $\mathbf{F}$, $\mathbf{T}$, and $\mathbf{D}$ are defined as follows

$$\mathbf{F}(\mathbf{Z}) \triangleq \begin{bmatrix} \dot{\alpha} \\ \ddot{\alpha} \\ \dot{\mathbf{x}}^T \dfrac{\partial \lambda(\mathbf{x})}{\partial \mathbf{x}} \\ \mathbf{f}_{\boldsymbol{\eta}}(\boldsymbol{\mu}, \boldsymbol{\eta}) \end{bmatrix}, \quad \mathbf{T} \triangleq \begin{bmatrix} 0 \\ 0 \\ b_2 \\ 0^{12\times 1} \end{bmatrix}, \quad \mathbf{D}(\mathbf{t}) \triangleq \begin{bmatrix} 0 \\ 0 \\ d(t) \\ \mathbf{d}_{\boldsymbol{\zeta}}(t) \end{bmatrix} \tag{3.19}$$

where the auxiliary vector $\mathbf{f}_{\boldsymbol{\eta}}(\boldsymbol{\mu}, \boldsymbol{\eta}) \in R^{12\times 1}$ and the disturbance vector function $\mathbf{d}_{\boldsymbol{\zeta}}(t) \in R^{12\times 1}$ are defined as follows

$$\mathbf{f}_{\boldsymbol{\eta}}(\boldsymbol{\mu}, \boldsymbol{\eta}) \triangleq \begin{bmatrix} \dot{\boldsymbol{\zeta}}^T & \digamma_{sub} A\dot{\mathbf{x}} + \digamma_{sub}\dot{\mathbf{f}}(\alpha) \end{bmatrix}^T \qquad \mathbf{d}_{\boldsymbol{\zeta}}(t) \triangleq \begin{bmatrix} 0^{1\times 6} & \left(\digamma_{sub}\mathbf{G}\dot{\mathbf{w}}_g(t)\right)^T \end{bmatrix}^T. \tag{3.20}$$

It is clear to see from the definitions above that $\mathbf{f}_{\boldsymbol{\eta}}(\boldsymbol{\mu}, \boldsymbol{\eta})$ can be written out as follows

$$\mathbf{f}_{\boldsymbol{\eta}}(\boldsymbol{\mu}, \boldsymbol{\eta}) = \mathbf{f}_{\boldsymbol{\eta}}(\mathbf{0}, \boldsymbol{\eta}) + \mathbf{f}_{\boldsymbol{\eta}}(\boldsymbol{\mu}, \mathbf{0}). \tag{3.21}$$

Since $\mathbf{f}_{\boldsymbol{\eta}}(\mathbf{0}, \boldsymbol{\eta})$ denotes the nominal zero dynamics and the system is assumed to be minimum phase, a converse theorem [4] can be employed to obtain the following upperbound

$$\boldsymbol{\eta}^T \mathbf{f}_{\boldsymbol{\eta}}(\mathbf{0}, \boldsymbol{\eta}) \leq -K_\eta \|\boldsymbol{\eta}\|^2 \tag{3.22}$$

where K_η is a system constant. With all of the above definitions, a Input-to-State Stability like Lemma is introduced as follows

Lemma 2 *Consider the system (3.19) with a bounded initial state $\mathbf{Z}_0$; given a positive constant C_0 such that $\left\|\boldsymbol{\eta}_0 \triangleq \boldsymbol{\eta}(t_0)\right\| < C_0$, there exists a corresponding positive constant C_1 such that $\forall t > t_0$, the internal dynamics $\boldsymbol{\eta}$ satisfy*

$$\|\boldsymbol{\eta}\| \leq \rho_1(\|\mathbf{e}\|)\|\mathbf{e}\| + C_1, \tag{3.23}$$

where $\rho_1(\cdot)$ is a positive invertible nondecreasing function.

Proof. *We define a positive definite function $V_1(t)$ as follows*

$$V_1 = \frac{1}{2}\boldsymbol{\eta}^T\boldsymbol{\eta} \tag{3.24}$$

Taking the time derivative of V_1 along the trajectory of (3.18) yields

$$\dot{V}_1 = \boldsymbol{\eta}^T \mathbf{f}_{\boldsymbol{\eta}}(\mathbf{0}, \boldsymbol{\eta}) + \boldsymbol{\eta}^T\left(\mathbf{f}_{\boldsymbol{\eta}}(\boldsymbol{\mu}, \mathbf{0}) + \mathbf{d}_{\boldsymbol{\zeta}}(t)\right) \tag{3.25}$$

where we have utilized (3.21). By adding and subtracting $\boldsymbol{\eta}^T \mathbf{f}_{\boldsymbol{\eta}}(\boldsymbol{\mu}_d, \mathbf{0})$ to the right hand side of the above expression and using (3.22), $\dot{V}_1$ can be bounded as

$$\dot{V}_1 \leq -K_{\boldsymbol{\eta}}\|\boldsymbol{\eta}\|^2 + \|\boldsymbol{\eta}\|\left(\|\mathbf{f}_{\boldsymbol{\eta}}(\boldsymbol{\mu}, \mathbf{0}) - \mathbf{f}_{\boldsymbol{\eta}}(\boldsymbol{\mu}_d, \mathbf{0})\| + \|\mathbf{f}_{\boldsymbol{\eta}}(\boldsymbol{\mu}_d, \mathbf{0}) + \mathbf{d}_{\boldsymbol{\zeta}}(t)\|\right).$$

An application of the Mean Value Theorem [15] allows us to obtain the inequality

$$\|\mathbf{f}_{\boldsymbol{\eta}}(\boldsymbol{\mu}, \mathbf{0}) - \mathbf{f}_{\boldsymbol{\eta}}(\boldsymbol{\mu}_d, \mathbf{0})\| \leq \rho_0(\|\mathbf{e}\|)\|\mathbf{e}\|$$

where $\rho_0(\cdot)$ *is a positive nondecreasing function and* $\mathbf{e}(t)$ *is a composite error signal previously defined in (3.11). The desired higher-order output trajectory* $\boldsymbol{\mu}_d \triangleq \begin{bmatrix} \alpha_d & \dot{\alpha}_d & \ddot{\alpha}_d \end{bmatrix} \in \mathcal{L}_\infty$ *is bounded by design while the disturbance* $\mathbf{d}_{\boldsymbol{\zeta}}(t)$ *is bounded by assumption. Thus, one can obtain a further upperbound on* $\dot{V}_1$ *as follows*

$$\dot{V}_1 \leq -K_{\boldsymbol{\eta}}\|\boldsymbol{\eta}\|(\|\boldsymbol{\eta}\| - \rho_1(\|\mathbf{e}\|)\|\mathbf{e}\| - C) \tag{3.26}$$

where $C \triangleq \frac{1}{K_{\boldsymbol{\eta}}}\|\mathbf{f}_{\boldsymbol{\eta}}(\boldsymbol{\mu}_d, \mathbf{0}) + \mathbf{d}_{\boldsymbol{\zeta}}(t)\|_\infty$ *and* $\rho_1(\cdot) \triangleq \frac{1}{K_{\boldsymbol{\eta}}}\rho_1(\|\mathbf{e}\|)\|\mathbf{e}\|$ *is an invertible nondecreasing function. We define a set* D_1 *as follows*

$$D_1 = \{\boldsymbol{\eta} | \|\boldsymbol{\eta}\| \leq \rho_1(\|\mathbf{e}\|)\|\mathbf{e}\| + C\}$$

which is invariant because $\dot{V}_1$ *is negative on its boundary. Based on this definition, we define another set* $D_{\boldsymbol{\eta}}$ *s.t.* $D_1 \subset D_{\boldsymbol{\eta}}$ *as follows*

$$D_{\boldsymbol{\eta}} = \{\boldsymbol{\eta} | \|\boldsymbol{\eta}\| \leq \rho_1(\|\mathbf{e}\|)\|\mathbf{e}\| + C_1\}$$

where C_1 *is a positive constant defined as*

$$C_1 \triangleq C_0 + C \tag{3.27}$$

where C_0 *is the least upper bound of* $\|\boldsymbol{\eta}_0\|$*. It is clear to see that* $D_{\boldsymbol{\eta}}$ *is invariant for* $\forall t > t_0$ *which implies that* $\boldsymbol{\eta}(t) \in D_{\boldsymbol{\eta}}\ \forall t \geq t_0$ *since* $\|\boldsymbol{\eta}_0\| \in D_{\boldsymbol{\eta}}$*. This completes the proof.* ■

Control Development and Stability Analysis

Given that both the pitch degree and its derivative are measurable and the sign of control gain is known, we are motivated by the structure of open-loop error dynamics in (3.13) to propose a continuous controller as follows

$$u = sgn(b_2)\left[(k_s+1)e_2 - (k_s+1)\,e_2(t_0) + \int_{t_0}^{t}\left[(k_s+1)\,e_2(\tau) + k_d sgn(e_2(\tau))\right]d\tau\right] \tag{3.28}$$

where k_s and k_d are positive gain constants. The derivation of (3.28) is given as

$$\dot{u} = sgn(b_2)\left[(k_s+1)r + k_d sgn\left(e_2(t)\right)\right] \tag{3.29}$$

After substituting (3.29) into (3.13), the closed-loop dynamics can be expressed in the following manner

$$\frac{1}{|b_2|}\dot{r} = N - (k_s+1)r - k_d sgn(e_2(t)) - e_2. \tag{3.30}$$

It is clear to see from the definitions of $\boldsymbol{\mu}$ and $\boldsymbol{\eta}$ as well as (3.15) and (3.16) that $N\left(\mathbf{x}, \dot{\mathbf{x}}, t\right)$ defined in (3.14) can be split into two parts as follows

$$N\left(\mathbf{x}, \dot{\mathbf{x}}, t\right) = N_\mu\left(\boldsymbol{\mu}, t\right) + N_\eta\left(\boldsymbol{\eta}\right) \tag{3.31}$$

where $N_\eta\left(\boldsymbol{\eta}\right) \triangleq \mathbf{K}_{N_\eta}\boldsymbol{\eta}$ and $\mathbf{K}_{N_\eta} \in R^{1\times 12}$ is a constant vector comprised of system constants. After defining $N_{\mu d}\left(t\right) \triangleq N_\mu\left(\boldsymbol{\mu}_d, t\right)$ and $\tilde{N}_\mu \triangleq N_\mu\left(\boldsymbol{\mu}, t\right) - N_{\mu d}\left(t\right)$, one can rewrite the closed-loop dynamics of (3.30) as follows

$$\frac{1}{|b_2|}\dot{r} = N_{\mu d} + \tilde{N}_\mu + N_\eta - (k_s+1)r - k_d sgn(e_2(t)) - e_2. \tag{3.32}$$

One can utilize (3.23) to upperbound N_η as follows

$$\|N_\eta\| \leq \rho_2 (\|\mathbf{e}\|) \|\mathbf{e}\| + C_2 \tag{3.33}$$

while the Mean Value Theorem [15] can be utilized to upperbound $\tilde{N}_\mu$ in the following manner

$$\left\|\tilde{N}_\mu\right\| \leq \rho_3 (\|\mathbf{e}\|) \|\mathbf{e}\| \tag{3.34}$$

where $\rho_2(\cdot)$ and $\rho_3(\cdot)$ are positive nondecreasing functions while C_2 is a system constant. To facilitate the subsequent stability analysis, the following Lemmas are needed.

Lemma 3 *For any differentiable function $e(t) : R^+ \rightarrow R$ with $e(t), \dot{e}(t) \in \mathcal{L}_\infty$, there exist positive constants ε_1 and ε_2 such that*

$$\int_{t_0}^{t} |\dot{e}(t)| \, d\tau \leq \varepsilon_1 + \varepsilon_2 \int_{t_0}^{t} |e(t)| \, d\tau + |e(t)| \quad \forall t > t_0.$$

Proof. *The proof of Lemma 3 can be found in [35].* ■

Lemma 4 *An auxiliary function $L(t) \in R$ is defined as follows*

$$L(t) = r(\bar{N}_{\mu d} - k_d sgn(e_2)). \tag{3.35}$$

where

$$\bar{N}_{\mu d} = N_{\mu d} + C_2 sgn(r)$$

If the control gain k_d is chosen to be sufficient large as follows

$$k_d > (1 + \varepsilon_2) ||\bar{N}_{\mu d}||_\infty, \tag{3.36}$$

then the integral of $L(t)$ can be upperbounded in the following manner

$$\int_{t_0}^{t} L(\tau)d\tau \leq \epsilon \triangleq \varepsilon_1 ||\bar{N}_{\mu d}||_\infty + k_d \left| e_2 \left(t_0 \right) \right|. \tag{3.37}$$

Proof. *The proof of Lemma 4 is given in Appendix A.* ■

The stability analysis is carried out in two steps. First, the error signals e_1, e_2, and r are proven to be ultimately bounded. Then, Lemmas 3 and 4 are utilized to prove the semi-global asymptotic stability of the error signals. We begin by defining a nonnegative Lyapunov candidate function V_2 as follows

$$V_2 = \frac{1}{2}e_1^2 + \frac{1}{2}e_2^2 + \frac{1}{2}\frac{1}{|b_2|}r^2 \tag{3.38}$$

Since the Lyapunov function is continuously differentiable, V_2 can be bounded as

$$\min\left\{\frac{1}{2}, \frac{1}{2|b_2|}\right\}\|\mathbf{e}\|^2 \leq V_2\left(\mathbf{e}\right) \leq \max\left\{\frac{1}{2}, \frac{1}{2|b_2|}\right\}\|\mathbf{e}\|^2 \tag{3.39}$$

The time derivative of (3.38) along (3.32) can be obtained as follows

$$\dot{V}_2 = e_1 e_2 - e_1^2 - e_2^2 - (k_s+1)r^2 + r\left[N_{\mu d} + \tilde{N}_\mu + N_\eta - k_d sgn(e_2\left(t\right))\right].$$

By utilizing the bounds of (3.33) and (3.34) in the above expression, one can obtain the following upperbound for $\dot{V}_2$

$$\begin{aligned}\dot{V}_2 &\leq -\frac{1}{2}\left(e_1^2+e_2^2\right)-(k_s+1)r^2+|r|\left(\rho_3\left(\|\mathbf{e}\|\right)\|\mathbf{e}\|+\rho_2\left(\|\mathbf{e}\|\right)\|\mathbf{e}\|+C_2\right)\\ &\quad +r\left[N_{\mu d}-k_d sgn(e_2\left(t\right))\right]\\ &\leq -\frac{1}{2}\left(e_1^2+e_2^2\right)-(k_s+1)r^2+|r|\,\rho\left(\|\mathbf{e}\|\right)\|\mathbf{e}\|+C_4\,|r|\end{aligned}$$

where $\rho\left(\|\mathbf{e}\|\right) \triangleq \rho_3\left(\|\mathbf{e}\|\right)+\rho_2\left(\|\mathbf{e}\|\right)$ while $C_4 \triangleq \left\|N_{\mu d}+C_2 sgn\left(r\right)-k_d sgn(e_2\left(t\right))\right\|_\infty$. After completing squares to obtain the inequality $-k_s r^2+|r|\,\rho\left(\|\mathbf{e}\|\right)\|\mathbf{e}\| \leq \frac{1}{4k_s}\rho^2\left(\|\mathbf{e}\|\right)\|\mathbf{e}\|^2$, one can further upperbound $\dot{V}_2$ as follows

$$\dot{V}_2 \leq -\frac{1}{2}\left(e_1^2+e_2^2\right)-r^2+\frac{1}{4k_s}\rho^2\left(\|\mathbf{e}\|\right)\|\mathbf{e}\|^2+C_4\,|r|\,.$$

where $\dot{V}_2$ can be further bounded as

$$\dot{V}_2 \leq -\frac{1}{2}\|\mathbf{e}\|^2-\left(\frac{1}{2}-\frac{1}{4\sigma_1}\right)r^2+\frac{1}{4k_s}\rho^2\left(\|\mathbf{e}\|\right)\|\mathbf{e}\|^2+\sigma_1 C_4^2$$

by utilizing the identity $C_4\,|r| \leq \frac{1}{4\sigma_1}|r|^2+\sigma_1 C_4^2$ where σ_1 is an arbitrary positive constant. By choosing σ_1 such that $\frac{1}{2}-\frac{1}{4\sigma_1} \geq 0$, $\dot{V}_2$ can be bounded as

$$\dot{V}_2 \leq -\left(\frac{1}{2}-\frac{1}{4k_s}\rho^2\left(\|\mathbf{e}\|\right)\right)\|\mathbf{e}\|^2+\sigma_1 C_4^2.$$

Finally, one can utilize (3.39) to obtain the following upperbound renders the following inequality

$$\dot{V}_2 \leq -C_5 V_2+\sigma_1 C_4^2 \tag{3.40}$$

$\forall \|\mathbf{e}\| \leq \rho^{-1}\left(\sqrt{2k_s}\right)$, where C_5 is a positive constant. It is now easy to conclude that V_2 is semi-global uniformly ultimately bounded which implies that $e_1, e_2, r \in \mathcal{L}_\infty$. Therefore, we can apply Lemma 3 and subsequently Lemma 4 to define a nonnegative function $P(t)$ as follows

$$P \triangleq \epsilon - \int_{t_0}^{t} L(\tau)d\tau \geq 0. \tag{3.41}$$

To show asymptotic stability, we begin by considering the following Lyapunov function candidate

$$V_3 = V_2 + P. \tag{3.42}$$

By utilizing the definition of (3.41), the time derivative of $V_3(t)$ along (3.32) can be obtained as follows

$$\dot{V}_3 = e_1 e_2 - e_1^2 - e_2^2 - (k_s+1)r^2 + r\left[N_{\mu d} + N_\eta + \tilde{N}_\mu - k_d sgn(e_2(t))\right] - L(t)$$

Following similar procedures as utilized to bound $\dot{V}_2$, we can find an upperbound for $\dot{V}_3$ as follows

$$\dot{V}_3 \leq -\frac{1}{2}\|\mathbf{e}\|^2 - k_s r^2 + r\rho(\|\mathbf{e}\|)\|\mathbf{e}\| + \{r[N_{\mu d} + C_2 sgn(r) - k_d sgn(e_2(t))] - L(t)\}.$$

The term in braces nets out to zero by virtue of (3.35) so that the upperbound above can be simplified as follows

$$\dot{V}_3 \leq -\left(\frac{1}{2} - \frac{1}{4k_s}\rho^2(\|\mathbf{e}\|)\right)\|\mathbf{e}\|^2 \tag{3.43}$$

Then one can state from (3.43) that $\dot{V}_3(t)$ is negative semi-definite on the region

$$\mathcal{S} = \left\{\mathbf{e} \in \mathcal{R}^3 \middle| \, ||\mathbf{e}|| < \rho^{-1}\left(\sqrt{2k_s}\right)\right\}. \tag{3.44}$$

We note here that the region of attraction $\mathcal{S}$ can be made arbitrarily large to include any initial value of $e_1(t), e_2(t), r(t)$ by increasing the control gain k_s. From (3.42) and (3.43), one can infer that $e_1(t), e_2(t), r(t) \in \mathcal{L}_\infty \cap \mathcal{L}_2$ which implies that $\dot{e}_1(t), \dot{e}_2(t) \in \mathcal{L}_\infty$ from (3.9) and (3.10). From the boundedness and smoothness of $\alpha_d(t)$ and the the previous boundedness assertions, once can infer that $\alpha(t), \dot{\alpha}(t), \ddot{\alpha}(t) \in \mathcal{L}_\infty$ from the definitions of (3.8), (3.9), and (3.10). From (3.15)and (3.23), it is easy to see that $\mathbf{x}(\mathbf{t}), \dot{\mathbf{x}}(\mathbf{t}) \in \mathcal{L}_\infty$ which implies from (3.30) that $\dot{r}(t) \in \mathcal{L}_\infty$. Thus the right hand side of the inequality of (3.43) is uniformly continuous which allows us to utilize Barbalat's Lemma to show the asymptotic stability of $e_1(t), e_2(t), r(t)$ to the origin. This result is valid under any bounded $\mathcal{C}^0$ external disturbance $\omega_G(\tau)$. It is also clear to see by virtue of (3.6) that the control input $u(t)$ remains bounded for all time as well. Thus, all system states and the control input remain bounded for all time during closed loop operation. While the nominal internal dynamics are asymptotically stable, the internal states can not be expected to converge to the origin under application of finite external disturbances; however, it can be guaranteed boundedness of all system states under bounded disturbance.

Numerical Simulation Results

In this section, various simulations were run to test the nominal system response as well as that under the external disturbances given in Eqs.(3.45-3.47). The nonlinear polynomial representing pitching spring stiffness is chosen as $k_\alpha(\alpha) = K_\alpha(1 - 22.1\alpha + 1315.5\alpha^2 + 8580\alpha^3 - 17289.7\alpha^4)$ [N·m/rad]. The parameters settings are chosen as shown in Table 3.1 leading to a flutter speed of $V_f = 83.56$ [m.s^{-1}].The desired trajectory variable α_d and its derivatives are simply selected to be zero.

The initial conditions for pitch angle $\alpha(t)$ and plunge displacement $h(t)$ are set to be $\alpha(0) = 5.729$ [deg] and $h(0) = 0.1$ [m] while all other state variables are initially selected to be zero.

Table 3.1: Model parameters

Parameter	Value	Parameter	Value
b	0.305 [m]	K_h	$500m$
a	-0.5	K_α	$1200I_\alpha$
c	0.5	K_β	$15000I_\beta$
m	90 [kg/m]	ρ	1.225 [kg/m^3]
I_β	0.552 [kg·m^2/m]	I_α	22.08 [kg·m^2/m]
S_β	0.441 [kg]	S_α	7.062 [kg]

In this paper, the following three external disturbances are considered according to [16]. The first type of external disturbance is modeled as a triangular gust, whose velocity distribution function is given as

$$w_G(\tau) = 2w_0\frac{\tau}{\tau_G}\left(H\left(\tau\right) - H\left(\tau - \frac{\tau_G}{2}\right)\right) - 2w_0\left(\frac{\tau}{\tau_G} - 1\right)\left(H\left(\tau - \tau_G\right) - H\left(\tau - \frac{\tau_G}{2}\right)\right), \tag{3.45}$$

where $H(\cdot)$ denotes a unit step function and $\tau_G = V_f t_G/b$ given $t_G = 0.25$ [s]. This triangular gust lasts for 0.5 [s] from $t = 0$ to 0.5 [s]. The second disturbance is modeled as a sustained disturbance beyond the transient response time of the closed-loop aeroelastic system. It is given in the from of a graded gust with its velocity distribution shown as

$$w_G(\tau) = H(\tau)w_0\left(1 - e^{-0.75\tau}\right). \tag{3.46}$$

The third type of external disturbance is modeled as a sinusoidal gust with the following velocity distribution function $w_G(\tau)$

$$w_G(\tau) = H\left(\tau\right)w_0 \sin\omega\tau \tag{3.47}$$

where $\omega = 0.5$ [rad/s]. For all 3 disturbances, we set w_0 to be 0.5 [m/s] for both pre- and post-flutter

speed simulations. These external disturbances cover three main kinds of disturbance: ephemeral disturbance, steady sustained disturbance, and time-varying sustained disturbance. The contribution of these disturbances to the system response will be presented in the form of gust loading as shown in (3.2). Both the disturbance velocity distribution and the corresponding gust load will be presented along with the system response. For all simulations, we implement the controller of (3.28) with gains selected as $k_s = 50$ and $k_d = 40$.

Fig. 3.1 shows the open-loop and closed-loop response of wing section model at pre-flutter speed $V = 0.9V_f$ without disturbance. The controller in the closed-loop simulation was turned on at $t = 1.5$ [s]. It can be seen from Fig. 3.1 that the pitching displacement converged in 2 [s]. The plunging displacement converged according to the internal dynamics of the system - it is driven to zero in 2 [s] as shown in (3.1).

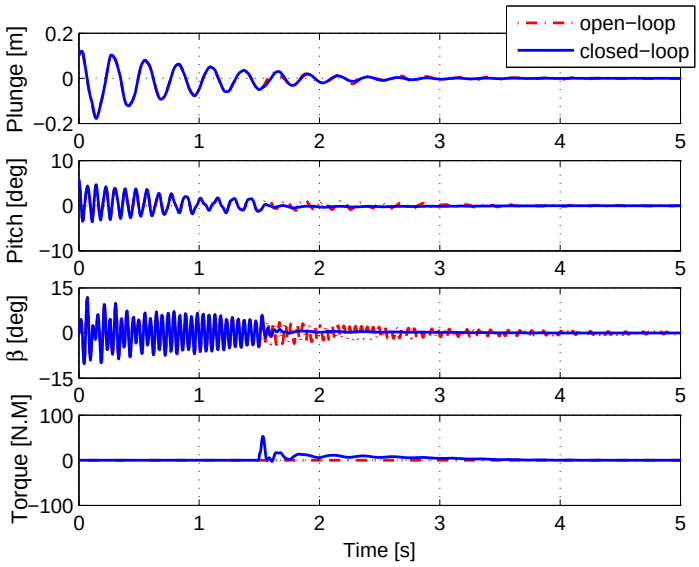

Figure 3.1: Open-loop and closed-loop response without gust disturbance at pre-flutter speed $V = 0.9V_f$

Fig. 3.2 shows the open-loop and closed-loop responses of the model section at post-flutter speed $V = 1.1V_f$ without disturbance. As shown in Fig. 3.2, the controller is turned on at $t = 1.5$ $[s]$. The limit cycle oscillations (LCO) of the pitching and plunging displacements are suppressed within 2 [s].

The triangular gust disturbance is the first type of the external disturbance considered in the simulation. Since an external gust disturbance impacts the aerodynamic in terms of gust loading $\mathbf{L}_g(t)$, it would be intuitive to analyze the response of the wing section model with the corresponding plot of gust load. Since from (3.2) and (3.3), we can see that I_{MG} and I_{fG} is the linear function of I_{LG}, we only show the plot of I_{LG}. As shown in Fig. 3.3, the gust starts at 1 [s] and lasts for 0.5 [s].However, after filtering by Kussner's function (3.4), the loading produced by the gust is seen to be smoother and longer lasting than the gust itself.

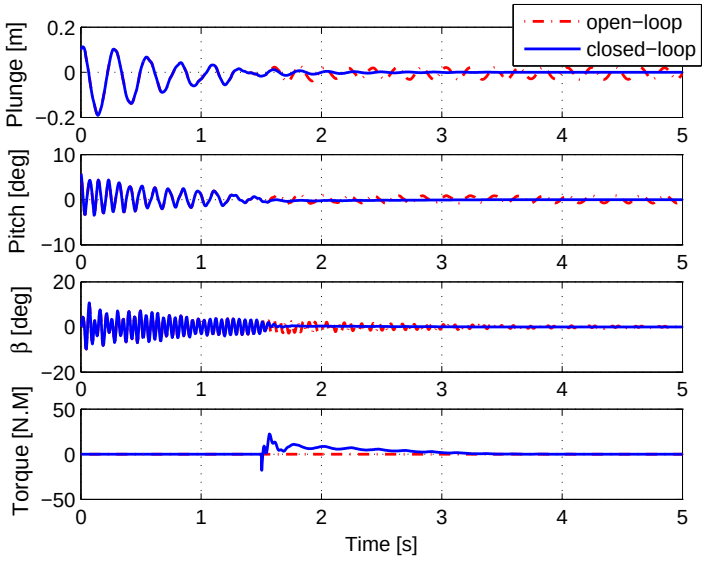

Figure 3.2: Open-loop and closed-loop response without gust disturbance at post-flutter speed $V = 1.1V_f$

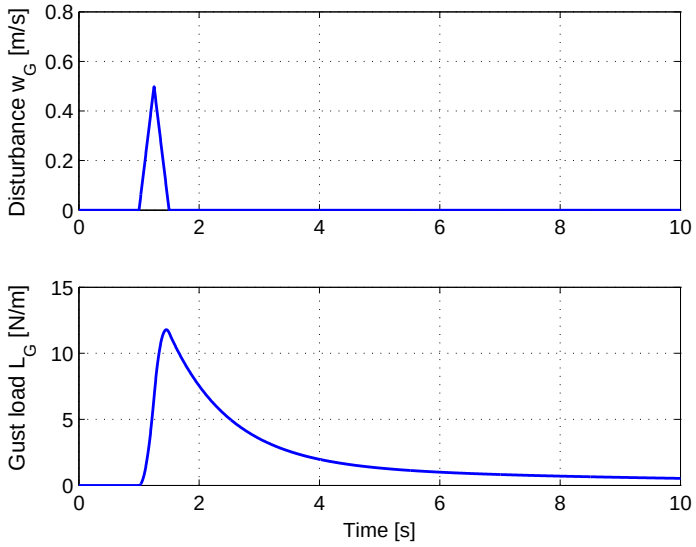

Figure 3.3: Triangular gust disturbance and corresponding gust loading

Fig. 3.4 presents the open- and closed-loop response of the wing section model under triangular gust at pre-flutter speed with $V = 0.9V_f$. As shown in Fig. 3.4, the triangular gust has an obvious impact on the plunge and pitch displacement between $t = 1$ [s] and $t = 4$ [s]. Fig. 3.5 shows the open- and closed-loop response of the wing section model under triangular gust at post-flutter speed with $V = 1.1V_f$.

In Figs. 3.4 and 3.5, the controller is turned on at $t = 2$ [s] and in both of these two simulations, plunge and pitch displacement are driven to zero in 2 [s]. While the pitching and plunging disturbances converge to the origin relatively quickly, the flap torque converges to zero only at the rate of convergence of the external disturbance.

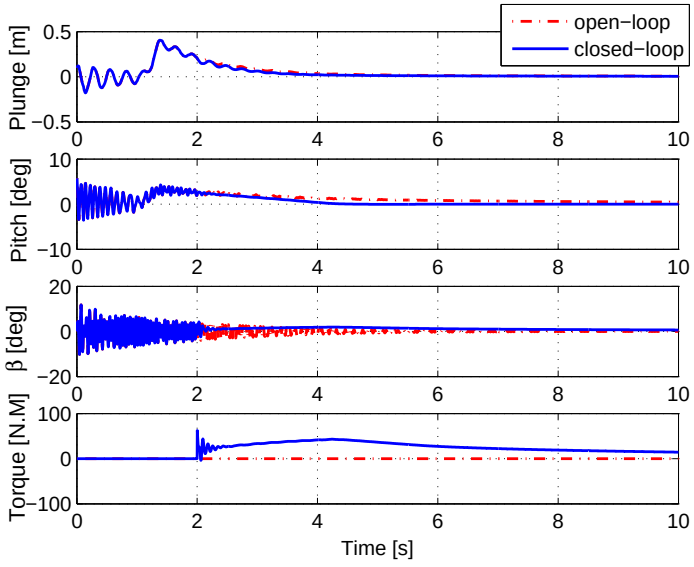

Figure 3.4: Open-loop and closed-loop under triangular gust at pre-flutter speed $V = 0.9V_f$

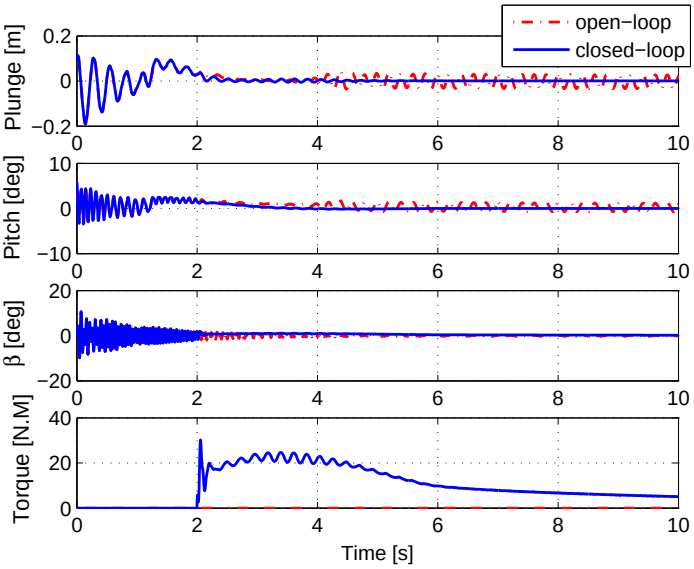

Figure 3.5: Open-loop and closed-loop under triangular gust at post-flutter speed $V = 1.1V_f$

The third set of simulations was run under the graded external gust disturbance; as shown in Fig. 3.6, the graded gust load starts at $t = 1[s]$ and exponentially goes to a constant loading value as time goes on. At both pre- and post-flutter speeds as shown in Figs. 3.7 and 3.8, the proposed controller is turned on at $t = 2$ [s] and is seen to successfully drive the output to zero. As expected, the persistent disturbance causes the control signal to not converge to zero along with the output. However, it is clear to see that the control signal is able to compensate for the unknown graded disturbance injected into the wing section model.

Sinusoid gust disturbance was considered in the fourth set of simulations. The disturbance and its gust load is presented in Fig. 3.9. The open- and closed-loop responses of the wing section model under sinusoid gust disturbance at pre- and post-flutter speed are displayed in Figs. 3.10 and 3.11, respectively. The disturbance starts at $t = 0$ and the controller is turned on at $t = 2$ [s] at both pre- and post- flutter speed.

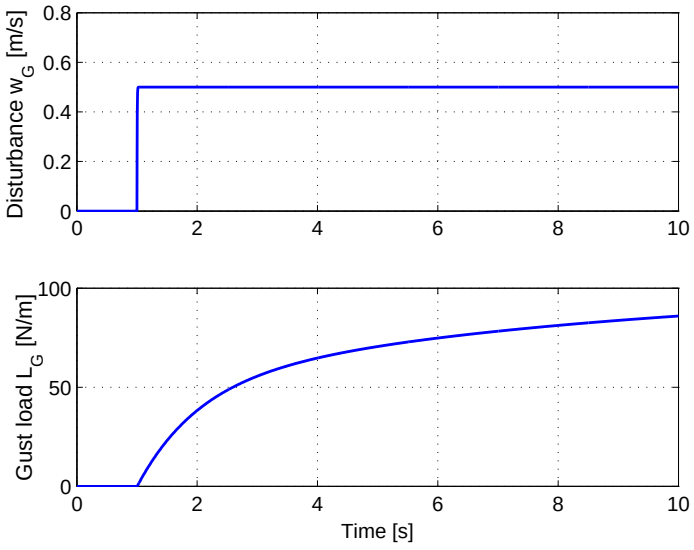

Figure 3.6: Graded gust disturbance and corresponding gust loading

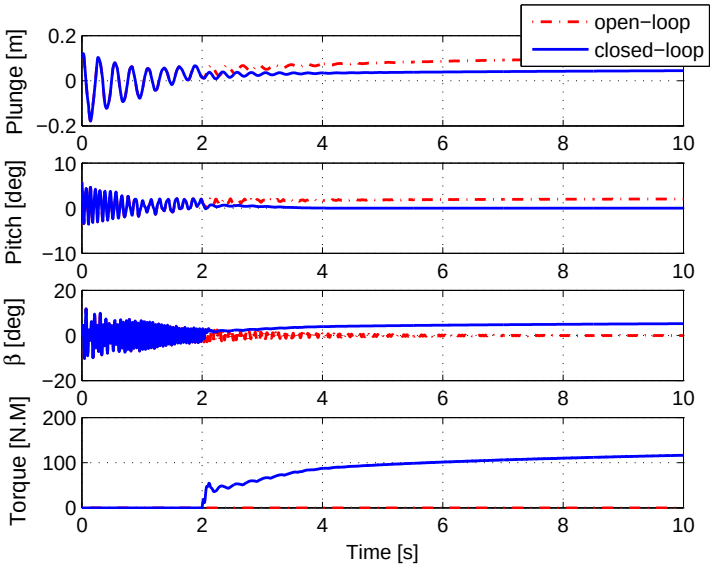

Figure 3.7: Open-loop and closed-loop response under graded gust at pre-flutter speed $V = 0.9V_f$

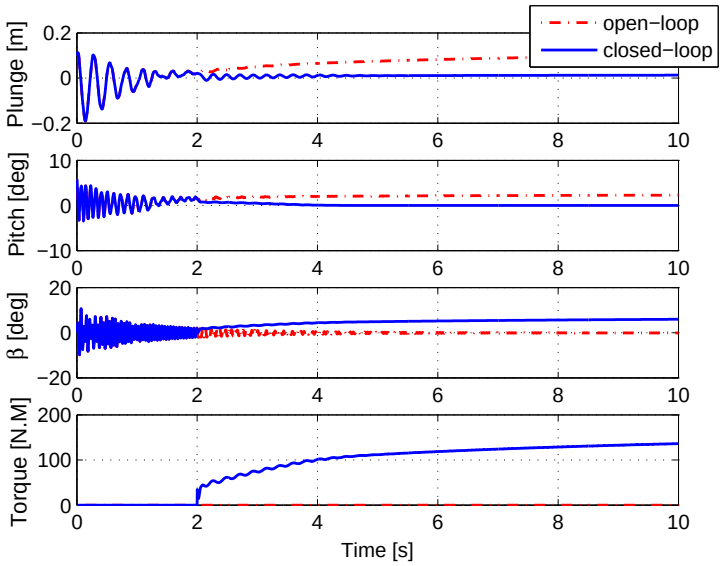

Figure 3.8: Open-loop and closed-loop response under graded gust at post-flutter speed $V = 1.1V_f$

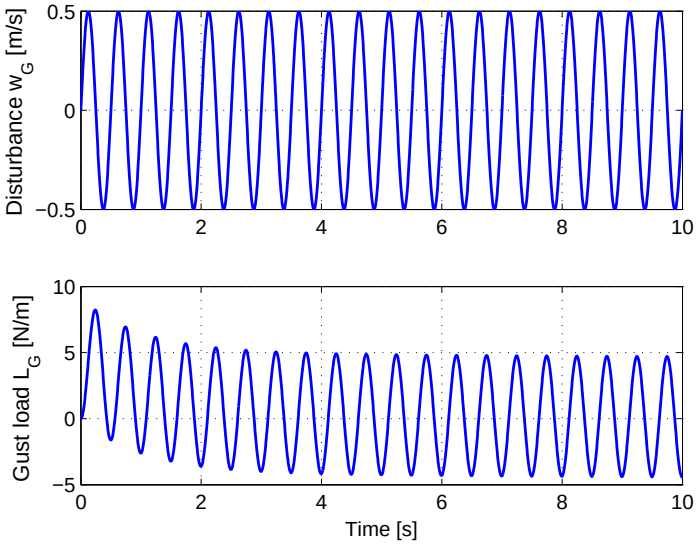

Figure 3.9: Sinusoid gust disturbance and corresponding gust loading

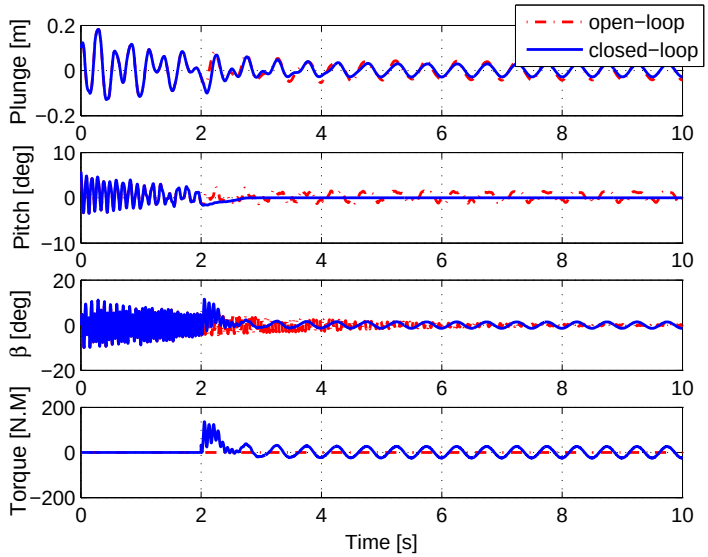

Figure 3.10: Open- and closed-loop response under sinusoidal gust at pre-flutter speed $V = 0.9V_f$

As shown in Figs. 3.10 and 3.11, after the pitching degree (which is the directly controlled DOF) converges, there are still small residual oscillations in the responses of h and β. Although the system (3.5) is minimum-phase and the output α converges under the proposed control, due to the sustained bounded external disturbance, the zero dynamics just stay bounded but are not able to converge as predicted by the bound shown in (3.23).

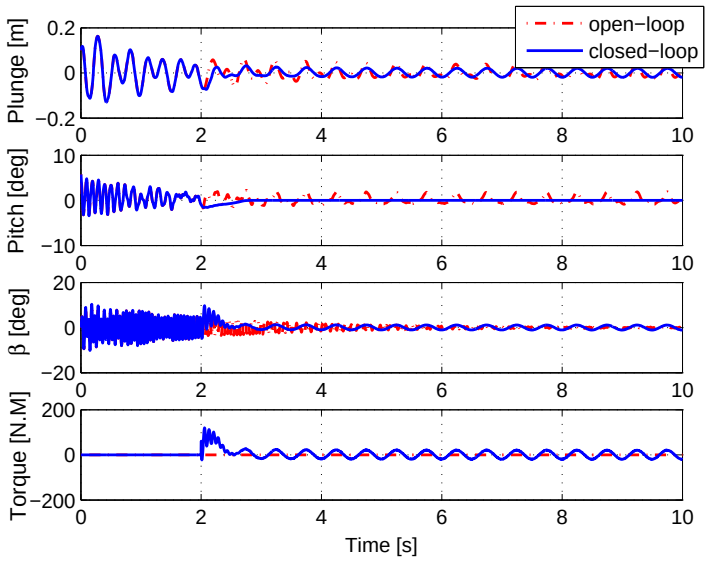

Figure 3.11: Open- and closed-loop response under sinusoidal gust at post-flutter speed $V = 1.1V_f$

Conclusion

The active aeroelastic control of 2-D wing-flap systems is modeled which is operating in an incompressible flowfield and exposed to three different kinds of external gust loads. By utilizing the property of Input-to-State Stability (ISS), the system internal states are proved to be bounded as a function of the output tracking error and its derivatives. Then, a continuous robust controller is proposed to suppress the aeroelastic vibration subject to external disturbance on a nonlinear plung-

ing and pitching wing section subject to unsteady aerodynamics. The control strategy requires minimal system and disturbance knowledge and is implemented by a trailing-edge flap torque. Lyapunov-based stability analysis is provided to obtain a semi-global asymptotic stability result on the pitching DOF tracking error. The robustness and efficacy of the controller is validated by simulation results under different operating conditions and disturbances. The investigated gust disturbances in this chapter are the most typical ones encountered. While it is impossible to present the system response under all possible kinds of disturbances, one can expect satisfactory simulation results under other disturbances based on the rigorous stability analysis presented in this chapter.

CHAPTER 4: ROBUST OUTPUT FEEDBACK CONTROL FOR 2-DOF MIMO NONLINEAR SYSTEM

Introduction

The goal of this chapter is to design a robust controller to suppress the vibrations for the aeroelastic system only using position feedback for the aeroelastic system by taking LE and TE flap as the actuator. The wing section model used in this chapter is the same as MIMO aeroelastic system shown in Chapter 2 except we have introduced external disturbance into the system. Inspired by [17], we design a filter error signal based on output errors to avoid using velocity sensor to measure the rates of the output variables and the actuator deflection. The robustness of the system to external disturbance is theoretically guaranteed by Lyapunov function based stability proof. The proposed controller requires only minimal knowledge of the system model, namely, the signs of the leading principal minors of control gain matrix. A SDU [2] decomposition is applied to the control gain matrix to decouple the control inputs. The internal dynamics induced by the unsteady aerodynamics appear as a disturbance term in the dynamics of the pitching and plunging displacement. Similar to the continuous robust control design in Chapter 3 for a SISO system (albeit the controller relied on partial state feedback), we address these internal dynamics in a two-step fashion by utilizing Input-to-State Stability (ISS) concepts. First, we prove that the system internal dynamics can be bounded as the summation of a nondecreasing function of the tracking error of the chosen output variable (specifically, the pitching and plunging DOF) and the bounds of the external disturbance. Then, given this boundedness of the internal states of the system as a function of the output error, a Lyapunov-based analysis is applied to show that semi-global asymptotic stability can be obtained for the pitching and plunging tracking errors under application of the proposed sliding mode controller. While the control torque input is discontinuous for this

design, the flap deflections are smooth and low amplitude such that the modeling construct remains valid and the potential for flow separation is mitigated.

System Modeling and Open Loop Error System Development

The wing section model with 4-DOFs in plunging displacement $h\left(t\right)$, pitching angle $\alpha\left(t\right)$, TE flap deflection $\beta\left(t\right)$, and LE flap deflection $\gamma\left(t\right)$ shown in section MIMO system Extension of Chapter 2 and illustrated in Fig. 2.12 will be taken as the prototypical system for control design. With considering the gust disturbance term L_g, the aeroelastic governing equations shown in (2.42) can be developed as

$$M_s\ddot{\mathbf{x}} = -K_s\mathbf{x} - K\left(h,\alpha\right)\mathbf{x} + \frac{1}{m_s b^2}\left(\mathbf{L} - \mathbf{L}_g\right) + T\mathbf{u} \tag{4.1}$$

where $\mathbf{L}_g(t)$ represent the unsteady aerodynamic load and gust loads. The gust load given in (4.1) is defined as follows

$$\mathbf{L}_g(\tau) \;\; = \left[\begin{array}{ccc} L_G(\tau) & M_{yG}(\tau) & 0^{2\times 1} \end{array} \right]^T \tag{4.2}$$

where the definitions of $L_G(\tau)$ and $M_{yG}(\tau)$ is given in (3.2) and (3.3). Then one can compactly write the system state space dynamics as

$$\begin{array}{l} \dot{\mathbf{X}}{=}A\mathbf{X} + \mathbf{f}(\mathbf{y}){+}H\mathbf{u}{+}\overline{\mathbf{\Delta}}\left(t\right) \\ \mathbf{y} = \left[\begin{array}{cc} \alpha & h \end{array} \right]^T \end{array} \tag{4.3}$$

which is similar to state space equation (2.49) we derived in chapter 2. The bounded unknown external disturbance $\overline{\mathbf{\Delta}}\left(t\right) \in \mathbb{R}^{10}$ are explicitly defined in Appendix B. As we have already shown, with specified choice of the output, the nominal system of (4.3) are globally exponentially stable. Since the system is of relative degree 2, a linear diffeomorphism $\digamma : \mathbb{R}^{10} \to \mathbb{R}^{10}$ (as similarly done in chapter 3 for the SISO aeroelastic system) is applied to the original system states $\mathbf{X}\left(t\right)$ such that

$$\begin{bmatrix} \boldsymbol{\mu} \\ \boldsymbol{\zeta} \end{bmatrix} \triangleq \digamma \mathbf{X}$$

where $\digamma \in \mathbb{R}^{10\times 10}$ is an invertible matrix which has been designed s.t.

$$\digamma H = \begin{bmatrix} 0^{2\times 2} & G^T & 0^{2\times 6} \end{bmatrix}^T \tag{4.4}$$

and $\boldsymbol{\mu}(t) \triangleq \begin{bmatrix} \alpha(t) & h(t) & \dot{\alpha}(t) & \dot{h}(t) \end{bmatrix}^T = \begin{bmatrix} \mathbf{y}^T(t) & \dot{\mathbf{y}}^T(t) \end{bmatrix}^T$ which implies that the dynamics of $\boldsymbol{\zeta}(t) \triangleq \digamma_{sub}\mathbf{X}(t) \in \mathbb{R}^{6\times 1}$ are independent of the control variable $u(t)$ as follows

$$\dot{\boldsymbol{\zeta}} = \digamma_{sub} A\mathbf{X} + \digamma_{sub}\mathbf{f}(\mathbf{y}) \tag{4.5}$$

where $\digamma_{sub} \in \mathbb{R}^{6\times 10}$ is a submatrix of $\digamma$.Then, one can obtain the normal form of (4.3) as follows

$$\begin{aligned} \dot{\boldsymbol{\mu}} &= \begin{bmatrix} \dot{\mathbf{y}} \\ \Phi(\boldsymbol{\mu}, \boldsymbol{\zeta}) + \boldsymbol{\Delta}_1(t) + Gu \end{bmatrix}. \\ \dot{\boldsymbol{\zeta}} &= \Psi(\boldsymbol{\mu}, \boldsymbol{\zeta}) + \boldsymbol{\Delta}_2(t) \end{aligned} \tag{4.6}$$

Explicit definitions for $\Phi(\cdot), \Psi(\cdot), \boldsymbol{\Delta}_1(t)$, $\boldsymbol{\Delta}_2(t)$, and G have been provided in Appendix B.

The objective of this chapter is to design a sliding mode controller to suppress the vibrations in the pitching (*i.e.*, $\alpha(t)$) and plunging (*i.e.*, $h(t)$) degrees of freedom using only measurements of these output variables. The output tracking error $e(t) \in \mathbb{R}^{2\times 1}$ is defined as

$$\mathbf{e}(t) = \mathbf{y}_d - \mathbf{y} \tag{4.7}$$

where $\mathbf{y}_d(t) \triangleq \begin{bmatrix} \alpha_d(t) & h_d(t) \end{bmatrix}^T$ is the desired bounded output variable that is designed to be

C^2 smooth. In order to compensate for lack of measurements of $\dot{\mathbf{y}}(t)$, a measurable filter tracking error $\mathbf{e}_f(t) \in \mathbb{R}^2$ is defined as

$$\mathbf{e}_f = -K\mathbf{e} + \mathbf{p} \tag{4.8}$$

where $\bar{K} \triangleq -K \in \mathbb{R}^{2\times 2}$ is a Hurwitz lower triangular gain matrix, while $\mathbf{p}(t) \in \mathbb{R}^2$ is generated via the following differential expression

$$\dot{\mathbf{p}} = -(K + 2I_2)\mathbf{p} + (K + K^2)\mathbf{e} \qquad \mathbf{p}(0) = Ke \tag{4.9}$$

where I_n denotes an $n \times n$ identity matrix. An unimplementable but analytically convenient expression for the dynamics of $\mathbf{e}_f(t)$ can be written as follows

$$\dot{\mathbf{e}}_f = -2\mathbf{e}_f - K\mathbf{r}. \tag{4.10}$$

where $\mathbf{r}(t) \in \mathbb{R}^2$ is an immeasurable filtered tracking error defined as

$$\mathbf{r} = \mathbf{e} + \mathbf{e}_f + \dot{\mathbf{e}} \tag{4.11}$$

based on the definitions of (4.7), (4.8), and (4.9). We define a composite error vector $\mathbf{z}(t) \in \mathbb{R}^6$ as follows

$$\mathbf{z} = \begin{bmatrix} \mathbf{e}^T & \mathbf{e}_f^T & \mathbf{r}^T \end{bmatrix}^T. \tag{4.12}$$

Finally, based on the definitions of error signals in (4.8)-(4.11), we define a measurable auxiliary error signal $\mathbf{E}(t) \in \mathbb{R}^2$ as follows

$$\mathbf{E}(t) = (K + I)^{-1}(\mathbf{e} - \mathbf{e}_f) \tag{4.13}$$

such that

$$\mathbf{r}(t) = \dot{\mathbf{E}}(t) + \mathbf{E}(t). \tag{4.14}$$

After taking the time derivative of $\mathbf{r}(t)$ along the trajectory of (4.6) and performing some algebraic manipulation, the open-loop filtered tracking error dynamics can be compactly written as follows

$$M\dot{\mathbf{r}} = \mathbf{N}(\boldsymbol{\mu}, \boldsymbol{\zeta}, t) + \boldsymbol{\Pi} - D\mathbf{u} - MK\mathbf{r} - \mathbf{e} - \mathbf{r} \tag{4.15}$$

where the auxiliary function $\mathbf{N}(\boldsymbol{\mu}, \boldsymbol{\zeta}, t) \in \mathbb{R}^2$ is defined as

$$\mathbf{N}(\boldsymbol{\mu}, \boldsymbol{\zeta}, t) = M\ddot{\mathbf{y}}_d - M\Phi_{\mathbf{1}}(\boldsymbol{\mu}) - M\Phi_{\mathbf{2}}(\boldsymbol{\zeta}) - M\boldsymbol{\Delta}_1(t) + M(r - e - e_f) - 2Me_f + \mathbf{e} + \mathbf{r} \tag{4.16}$$

where we have utilized the fact that $\Phi(\boldsymbol{\mu}, \boldsymbol{\zeta}) = \Phi_{\mathbf{1}}(\boldsymbol{\mu}) + \Phi_{\mathbf{2}}(\boldsymbol{\zeta})$ and we have applied an SDU decomposition [18, 19] to the control gain matrix G as follows

$$G = SDU$$

where $S \in \mathbb{R}^{2\times 2}$ is a symmetric positive-definite matrix, $M \triangleq S^{-1}$, $D \in \mathbb{R}^{2\times 2}$ is a diagonal matrix with $+1$ or -1 as its diagonal entries, and U is a unity upper-triangular matrix. Π is defined as

$$\begin{aligned} \Pi &= (D - DU)\, u \\ &= \begin{bmatrix} -U_{12}u_2 & 0 \end{bmatrix}^T \end{aligned} \tag{4.17}$$

where U_{ij} denotes the $(i, j)^{th}$ entry of the U matrix. From the structure of (4.16), one can rewrite $\mathbf{N}(\boldsymbol{\mu}, \boldsymbol{\zeta}, t)$ as

$$\mathbf{N}(\boldsymbol{\mu}, \boldsymbol{\zeta}, t) = \mathbf{N}_{\mu}(t) + \mathbf{N}_{\zeta}(t) \tag{4.18}$$

where $\mathbf{N}_{\mu}(t)$ and $\mathbf{N}_{\zeta}(t)$ are defined as

$$\begin{aligned} \mathbf{N}_{\mu}(t) &= \mathbf{N}(\boldsymbol{\mu}, 0, t) &= M\ddot{\mathbf{y}}_d - M\Phi_{\mathbf{1}}(\boldsymbol{\mu}) - M\boldsymbol{\Delta}_1(t) \\ & & + M(r - e - e_f) - 2Me_f + \mathbf{e} + \mathbf{r} \end{aligned} \tag{4.19}$$

$$\mathbf{N}_{\boldsymbol{\zeta}}(t) = \mathbf{N}(0, \boldsymbol{\zeta}, 0) = -M\Phi_{\mathbf{2}}(\boldsymbol{\zeta}) \tag{4.20}$$

$\mathbf{N}_{\mu}(t)$ can be further split into two parts with different boundednesses Definitions of $\mathbf{N}(\mathbf{t})$ functions are shown as

$$\mathbf{N}_{\mu}(t) = \mathbf{N}_d(t) + \tilde{\mathbf{N}}(t) \tag{4.21}$$

where $\mathbf{N}_d(t)$ and $\tilde{\mathbf{N}}(t)$ are defined as

$$\begin{aligned} \mathbf{N}_d &= \mathbf{N}(\boldsymbol{\mu}_d, 0, t) = M\ddot{\mathbf{y}}_d - M\Phi_{\mathbf{1}}(\boldsymbol{\mu}_d) - M\boldsymbol{\Delta}_1(t) \\ \tilde{\mathbf{N}} &= \mathbf{N}_{\mu} - \mathbf{N}_d \end{aligned} \tag{4.22}$$

By applying Mean Value theorem to $\tilde{\mathbf{N}}$ in (4.22), one can bound $\tilde{\mathbf{N}}$ as

$$\left|\tilde{N}_i\right| \leq \rho_{1,i}(\|\mathbf{z}\|)\|\mathbf{z}\|, i = 1, 2 \tag{4.23}$$

where $\rho_1(\cdot)$ is nondecreasing positive invertible function. Provided the fact that $\boldsymbol{\mu}_d, \boldsymbol{\Delta}_1(t) \in \mathcal{L}_{\infty}$, one can know that

$$\mathbf{N}_d \in \mathcal{L}_{\infty}.$$

Since the nonlinearities of the system only depends on the output states $\boldsymbol{\mu}$, from (4.20) one can know $\mathbf{N}_{\boldsymbol{\zeta}}(t)$ is a linear function of $\boldsymbol{\zeta}$ and it can be bounded as

$$|\mathbf{N}_{\boldsymbol{\zeta},\mathbf{i}}(t)| \leq K_{\zeta,i}\|\boldsymbol{\zeta}\|, i = 1, 2 \tag{4.24}$$

where $K_{\zeta,i}$ is a positive constant. Substituting (4.18)(4.21)(4.22) into (4.15), one can rewritten the open loop dynamic as

$$M\dot{\mathbf{r}} = \mathbf{N}_d(t) + \tilde{\mathbf{N}}(t) + \mathbf{N}_{\boldsymbol{\zeta}}(t) + \boldsymbol{\Pi} - D\mathbf{u} - MK\mathbf{r} - \mathbf{e} - \mathbf{r} \tag{4.25}$$

The following Lemma is presented to get the bounds of $N_{\boldsymbol{\zeta}}(t)$.

Lemma 5 *Consider the system (4.6) with bounded initial states $\boldsymbol{\mu}_0, \boldsymbol{\zeta}_0$, for all $t > t_0$ there exists two positive constant C_0 and C_1 such that for $\|\boldsymbol{\zeta}_0\| < C_1$ the internal dynamics ζ satisfy*

$$\|\boldsymbol{\zeta}\| \leq \rho_0(\|\mathbf{z}\|)\|\mathbf{z}\| + C_0, \tag{4.26}$$

where $\rho_0(\cdot)$ is a positive invertible nondecreasing function.

The proof of Lemma 5 is similar to Lemma 2. Reader can refer to [20]. By using (4.24) and (4.26), $N_{\boldsymbol{\zeta}}(t)$ can be further bounded as

$$|N_{\boldsymbol{\zeta},i}(t)| \leq \rho_{2,i}(\|\mathbf{z}\|)\|\mathbf{z}\| + C_{\boldsymbol{\zeta},i}, i = 1, 2 \tag{4.27}$$

where $\rho_{2,i}(\|\mathbf{z}\|)\|\mathbf{z}\| \triangleq K_{\boldsymbol{\zeta},i}\rho_0(\|\mathbf{z}\|)\|\mathbf{z}\|$ and $C_{\boldsymbol{\zeta},i} \triangleq K_{\boldsymbol{\zeta},i}C_0$.

Control Design and Stability Analysis

In this section, it is assumed that both pitching displacement and plunging displacement are measurable. Furthermore, M and U are assumed to be unknown, while the diagonal matrix D comprising the signs of the leading principal minors of G is assumed to be known. Given the previous

assumption, the following output feedback control law is proposed as

$$\mathbf{u} = D\left[-K^T\mathbf{e}_f + K_d sgn\left(\mathbf{E}\left(t\right)\right)\right] \tag{4.28}$$

where $E\left(t\right)$ is defined as

$$\mathbf{E}\left(t\right) = \left(K + I\right)^{-1}\left(\mathbf{e} - \mathbf{e}_f\right) \tag{4.29}$$

and gain matrices $K, K_d \in \mathbb{R}^{2\times 2}$ are defined as

$$K = \begin{bmatrix} k_1 & \\ k_2 & k_3 \end{bmatrix}, K_d = \begin{bmatrix} k_{d,1} & \\ & k_{d,2} \end{bmatrix}. \tag{4.30}$$

where the method for selecting K is given in Appendix. By substituting (4.28) into (4.25), one can obtain the following closed-loop dynamics as

$$M\dot{\mathbf{r}} = N_d + \tilde{N} + N_{\boldsymbol{\zeta}} + \boldsymbol{\Pi} + K^T e_f - K_d sgn\left(\mathbf{E}\left(t\right)\right) - MK\mathbf{r} - \mathbf{e} - \mathbf{r} \tag{4.31}$$

Substituting (4.28) into (4.17), Π can be rewritten as

$$\Pi = \begin{bmatrix} D_2U_2k_3e_{f,2} - D_2U_2k_{d,2}sgn\left(E_2\left(t\right)\right) & 0 \end{bmatrix}^T,$$

while it can be splited into two parts as

$$\Pi = \Phi + \Psi \tag{4.32}$$

where

$$\begin{aligned} \Phi &= \begin{bmatrix} D_2U_2k_3e_{f,2} & 0 \end{bmatrix}^T \\ \Psi &= \begin{bmatrix} -D_2U_2k_{d,2}sgn\left(E_2\left(t\right)\right) & 0 \end{bmatrix} \end{aligned} \tag{4.33}$$

To facilitate the stability analysis of (4.31) with respect to the control design (4.28), the following Lemmas is proposed.

Lemma 6 *For any differentiable function $f : \mathbb{R}^+ \to \mathbb{R}$ with $f(t), \dot{f}(t) \in \mathcal{L}_\infty$, there exist positive constants ε_1 and ε_2 such that*

$$\int_0^t \left| \dot{f}(t) \right| d\tau \leq \varepsilon_1 + \varepsilon_2 \int_0^t |f(t)| \, d\tau + |f(t)| \tag{4.34}$$

for any t>0. [35]

Lemma 7 *A auxiliary function $L(t) \in \mathbb{R}$ is defined as follows:*

$$L(t) = r^T \left(\bar{\mathbf{N}}_d - K_d sgn\left(\mathbf{E}(t) \right) \right). \tag{4.35}$$

where

$$\bar{N}_d \triangleq \begin{bmatrix} N_{d,1} + C_{\zeta,1} sgn(r_1) - D_2 U_2 k_{d,2} sgn\left(E_2(t) \right) \\ N_{d,2} + C_{\zeta,2} sgn\left(r_2 \right) \end{bmatrix} \in L_\infty \tag{4.36}$$

If the control gain k_d is chosen as

$$k_{d,i} \geq c_{\bar{N}_{d,i}} + \frac{1}{2} c_{\bar{N}_{d,i}} \varepsilon_{1,i}, i = 1, 2$$

where $k_{d,i}$ is the diagonal elements of k_d and $c_{\bar{N}_{d,i}} \triangleq \left| \bar{N}_{d,i} \right|_{\mathcal{L}_\infty}$ then one have

$$\int_0^t L(t) d\tau \leq C_d \tag{4.37}$$

where the positive constant C_d is defined as

$$C_d = \frac{1}{2}\sum_{i=1}^{2}\left(c_{\bar{N}_{d,i}}\varepsilon_1 + k_{d,i}\left|E_i\left(t_0\right)\right|\right).$$

While the proof of Lemma (7) is given in the appendix A. Then the stability analysis is composed of two steps. First, we prove the boundedness of the error signals of the closed loop dynamics (4.31). Then by using this result and Lemma 6, one can prove Lemma 7 and construct a non-negative terms for another Lyapunov function that can be utilized to prove the asymptotic stability of the closed-loop system.

Now, we consider the following Lyapunov function

$$V_2 = \frac{1}{2}r^T M r + \frac{1}{2}e^T e + \frac{1}{2}e_f^T e_f. \tag{4.38}$$

By taking derivative of V_2 along (4.31) and ultilizing (4.10)(4.11), we have

$$\begin{aligned}\dot{V}_2 &= r^T\left(\mathbf{N}\left(\boldsymbol{\mu},\boldsymbol{\zeta},t\right)+\mathbf{\Pi}+K^T e_f - K_d sgn\left(\mathbf{E}\left(t\right)\right) - MK\mathbf{r}\right) - r^T r - r^T e \\ &\quad + e^T\left(r - e_f - e\right) + e_f^T\left(-2e_f - Kr\right)\end{aligned}$$

Then $\dot{V}_2$ can be further bounded as

$$\dot{V}_2 \leq r^T\left(\mathbf{N}_d + \Psi - K_d sgn\left(\mathbf{E}\left(t\right)\right)\right) - \frac{1}{2}\left\|z\right\|^2 + r^T\left(\tilde{\mathbf{N}} + \mathbf{N}_{\boldsymbol{\zeta}}\right) + r^T\Phi - r^T MKr$$

where (4.32),(4.18) and (4.21) are used. From (4.23),(4.27) and (4.33), one can upper bound $\dot{V}_2$ as

$$\begin{aligned}\dot{V}_2 &\leq r^T\left(\mathbf{N}_d + C_{\boldsymbol{\zeta}} sgn\left(r\right) + \Psi - K_d sgn\left(\mathbf{E}\left(t\right)\right)\right) - \frac{1}{2}\left\|z\right\|^2 \\ &\quad + \sum_{i=1}^{2}\left|r_i\right|\rho_i\left(\left\|\mathbf{z}\right\|\right)\left\|\mathbf{z}\right\| + k_3\left|U_2\right| r_1\left\|\mathbf{z}\right\| - r^T MKr\end{aligned}$$

where $\rho_i\left(\left\|\mathbf{z}\right\|\right)\left\|\mathbf{z}\right\| = \sum_{j=1}^{2}\rho_{j,i}\left(\left\|\mathbf{z}\right\|\right)\left\|\mathbf{z}\right\|, i = 1, 2$ and

$$C_{\boldsymbol{\zeta}} sgn\left(r\right) = \left[\begin{array}{cc} C_{\boldsymbol{\zeta},1} sgn\left(r_1\right) & C_{\boldsymbol{\zeta},2} sgn\left(r2\right)\end{array}\right]^T$$

As we known that the matrices $\bar{K} \triangleq -K$ is Hurwitz and can be picked arbitrarily in the form of a low triangular matrix. By utilizing the fact M is a positive definite (P.D.) matrix, there exists a a diagonal P.D. matrix Q ensuring the following equation

$$M\bar{K} + \bar{K}^T M = -Q \tag{4.39}$$

where Q is defined as

$$Q = \left[\begin{array}{cc} 2q_1 & \\ & 2q_2\end{array}\right] \tag{4.40}$$

and $q_1 > 0, q_2 > 0$. Substituting the matrix definitions (4.30)(4.40) into (4.39), we can get

$$k_3 = \frac{q_2}{2m_3}. \tag{4.41}$$

where m_3 is a positive diagonal component of M. Readers can refer to Appendix for more details.

By utilizing (4.39) and (4.41) $\dot{V}_2$ can be further bounded as

$$\begin{aligned}\dot{V}_2 \leq r^T \left(\mathbf{N}_d + C_{\boldsymbol{\zeta}} sgn\left(r\right) + \Psi - K_d sgn\left(\mathbf{E}\left(t\right)\right)\right) - \tfrac{1}{2}\left\|z\right\|^2 \\ + \sum_{i=1}^{2} \left|r_i\right| \rho_i\left(\left\|\mathbf{z}\right\|\right)\left\|\mathbf{z}\right\| + r_1 \left|\tfrac{q_2 U_2}{2m_3}\right| \left\|\mathbf{z}\right\| - q_1 r_1^2 - q_2 r_2^2\end{aligned} \tag{4.42}$$

Choosing

$$q_1 = q_2 + q_3, q_3 > 0 \tag{4.43}$$

yields

$$\dot{V}_2 \leq L\left(t\right) - \left(\frac{1}{2} - \sum_{i=1}^{2} \frac{\rho_i^2\left(\left\|\mathbf{z}\right\|\right)}{4q_2} - \frac{q_2^2 U_2^2}{16 m_3^2 q_3}\right)\left\|\mathbf{z}\right\|^2 \tag{4.44}$$

To render the second terms in the right side of the inequality (4.44) to be negative, the q_2, q_3 can be chosen as

$$q_3 > \frac{q_2^2 U_2^2}{4m_3^2}, q_2 > 2\max\left\{\rho_1^2\left(\left\|\mathbf{z}\right\|\right), \rho_1^2\left(\left\|\mathbf{z}\right\|\right)\right\}. \tag{4.45}$$

Thus on the set of

$$\mathcal{S} = \left\{\mathbf{z} \in \mathbb{R}^3 \middle| \left\|\mathbf{z}\right\| \leq \min\left(\rho_1^{-1}\left(\sqrt{\frac{q_2}{2}}\right), \rho_2^{-1}\left(\sqrt{\frac{q_2}{2}}\right)\right)\right\} \tag{4.46}$$

$\dot{V}$ can be further bounded as

$$\dot{V}_2 \leq -C_2\left\|\mathbf{z}\right\|^2 + C_1\left\|\mathbf{z}\right\| \tag{4.47}$$

where $\left|L\left(t\right)\right| \leq C_1\left\|\mathbf{z}\right\|$ is utilized and

$$C_1 = \left|r^T\left(\mathbf{N}_d + C_{\boldsymbol{\zeta}} sgn\left(r\right) + \boldsymbol{\Phi} - K_d sgn\left(\mathbf{E}\left(t\right)\right)\right)\right|_{\mathcal{L}_\infty}$$

One can find from (4.46) that the bounds of $\left\|\mathbf{z}\right\|$ depends on the auxiliary control gain q_2. By choosing q_1, q_2, q_3 as shown in (4.43)(4.45), one can bound $\dot{V}_2$ as shown in (4.47) From (4.38) and (4.47), one can conclude that V_2 are uniformly ultimately bounded. Thus, we have $e_1, e_2, r \in \mathcal{L}_\infty$.

Therefore we can applied Lemma 6 to the next step to prove the system to be asymptotically stable. Thus there exists two diagonal constants matrix ε_1 and ε_2 such that (4.34) hold, make the inequality (4.37) hold. Then one can pick a nonnegative function $P(t) \triangleq C_d - \int_0^t L(t)d\tau$ according to Lemma 7 and build the following Lyapunov function candidate■

$$V_3 = V_2 + P \tag{4.48}$$

Taking the derivative of V_0 with respect to t and following same procedure of bounding $\dot{V}_2$, one can have the bounds of $\dot{V}_3$ as following

$$\begin{aligned} \dot{V}_3 \;\leq\; & \left[r^T\left(\mathbf{N}_d + C_{\boldsymbol{\zeta}} sgn(r) + \boldsymbol{\Phi} - K_d sgn(\mathbf{E}(t))\right) - \dot{P}(t)\right] \\ & - \left(\frac{1}{2} - \sum_{i=1}^{2} \frac{\rho_i^2(\|\mathbf{z}\|)}{4q_2} - \frac{q_2^2 U_2^2}{16 m_3^2 q_3}\right)\|\mathbf{z}\|^2 \end{aligned}$$

With canceling out the bracketed terms, $\dot{V}_3$ is further bounded as

$$\dot{V}_3 \leq -C_2 \|\mathbf{z}\|^2 \tag{4.49}$$

The inequality of (4.49) implies that $\dot{V}$ is negative semi-definite on the set of $\mathcal{S}$ given in (4.46). Thus $\dot{V}_3$ could be upper bounded as

$$\dot{V}_3 \leq -W_1(\mathbf{q}), \tag{4.50}$$

where $\mathbf{q} = \begin{bmatrix} \mathbf{z}^T & \sqrt{P} \end{bmatrix}^T$ the upper bounded function is given as

$$W_1(\mathbf{q}) = c_y \|\mathbf{z}\|, \tag{4.51}$$

and c_y is some positive constant. By properly choosing K, Q, one can ensure $W_1(\mathbf{e})$ is a positive definite function. Note here that the control gains K, Q are chosen to satisfy (4.39) and (4.45).

Then $\dot{V}$ is guaranteed to be negative definite in the region of $\mathcal{S}$. Noticed that attraction region $\mathcal{S}$ could be made arbitrarily large by increasing the control gain K. From (4.48) and (4.50), we know $V_3(\mathbf{q},t)$ are bounded; hence $e, e_f, r(t) \in \mathcal{L}_\infty$, which also results in the boundedness of control input u for all time. By taking advantage of aforementioned boundedness statements, we can state $\dot{W}_1(\mathbf{q}) \in \mathcal{L}_\infty$ from (4.12)(4.31)(4.51). Then one can have $W_1(\mathbf{y})$ is uniformly continuous.Thus, Barbalat's Lemma can be used to show that $r(t) \to 0$ as $t \to 0$. From Eq. (4.11), it is clear that $e(t), e_f(t) \to 0$ as $t \to 0$. Furthermore, from the asymptotic stability of the zero dynamics, all system states are guaranteed to asymptotically converge to the origin.

Simulation Results and Discussions

Since the nominal wing section model used in this chapter is the same as the one in the section MIMO system extension of chapter 2, The model parameters setting is the same as that shown in Table 2.2. The wing section model is built based on structural and aerodynamic equations of (2.42) and (2.43). The initial states and desired trajectory variables are set as the same as those in section MIMO system extension of chapter 2. The output feedback controller is implemented vis filter errors defined in (4.8)(4.9). To avoid chattering problem caused by signum function, we use tangent hyperbolic function to approximate it, while a gain constant $K_{\tanh} = 1000$ was add to the tangent hyperbolic function and the control law becomes (4.52)

$$\mathbf{u} = D\left[-K^T\mathbf{e}_f + K_d \tanh\left(K_{\tanh}\mathbf{E}(t)\right)\right]. \tag{4.52}$$

The parameters for the controller are listed in Table 4.1.

Table 4.1: Controller parameters

	No disturbance		Triangular	
V_∞	$0.9V_f$	$1.1V_f$	$0.9V_f$	$1.1V_f$
Q	$\begin{bmatrix} 1 & \\ & 0.8 \end{bmatrix}$	$\begin{bmatrix} 1 & \\ & 0.8 \end{bmatrix}$	$\begin{bmatrix} 1 & \\ & 0.8 \end{bmatrix}$	$\begin{bmatrix} 2 & \\ & 1.6 \end{bmatrix}$
Kd	$\begin{bmatrix} 1 & \\ & 0.5 \end{bmatrix}$	$\begin{bmatrix} 2 & \\ & 1 \end{bmatrix}$	$\begin{bmatrix} 1 & \\ & 0.5 \end{bmatrix}$	$\begin{bmatrix} 2 & \\ & 1.5 \end{bmatrix}$
K	$\begin{bmatrix} 148.45 & 0 \\ -22.90 & 0.34 \end{bmatrix}$	$\begin{bmatrix} 148.45 & 0 \\ -22.90 & 0.34 \end{bmatrix}$	$\begin{bmatrix} 148.45 & 0 \\ -22.90 & 0.34 \end{bmatrix}$	$\begin{bmatrix} 296.89 & 0 \\ -45.80 & 0.69 \end{bmatrix}$
	Graded		Sinusoidal	
V_∞	$0.9V_f$	$1.1V_f$	$0.9V_f$	$1.1V_f$
Q	$\begin{bmatrix} 1 & \\ & 0.8 \end{bmatrix}$	$\begin{bmatrix} 2 & \\ & 1.6 \end{bmatrix}$	$\begin{bmatrix} 1 & \\ & 0.8 \end{bmatrix}$	$\begin{bmatrix} 1 & \\ & 0.8 \end{bmatrix}$
Kd	$\begin{bmatrix} 2 & \\ & 1.5 \end{bmatrix}$	$\begin{bmatrix} 2 & \\ & 1.5 \end{bmatrix}$	$\begin{bmatrix} 2 & \\ & 1.6 \end{bmatrix}$	$\begin{bmatrix} 3 & \\ & 2.5 \end{bmatrix}$
K	$\begin{bmatrix} 148.45 & 0 \\ -22.90 & 0.34 \end{bmatrix}$	$\begin{bmatrix} 296.89 & 0 \\ -45.80 & 0.69 \end{bmatrix}$	$\begin{bmatrix} 148.45 & 0 \\ -22.90 & 0.34 \end{bmatrix}$	$\begin{bmatrix} 148.45 & 0 \\ -22.90 & 0.34 \end{bmatrix}$

Three types of external disturbance are considered as demonstration. They are triangular gust, graded gust and sinusoidal gust. The velocity distribution function $w_G(\tau)$ can be found in Eqs. (3.45-3.47). Various simulations is run to test the nominal system response as well as that the external disturbances. Figure (4.1) shows the open- and closed-loop system response at pre-flutter speed $V = 0.9V_f$ without disturbance. The controller was turned on at $t = 0.5[s]$. Even at pre-flutter speed the plunging and pitching displacement can converge in finite time at open-loop system without disturbance, however, in the closed-loop, the control has decrease the converge time obviously as shown in Figure (4.1). Figure (4.3) shows open- and closed-loop system response without gust disturbance at post-flutter speed $V = 1.1V_f$. As we can see, the controller has stabilized plunging and pitching displacement in 1 second. Figure (4.2) shows the control input of closed-loop system without gust disturbance at post-flutter speed $V = 0.9V_f$.

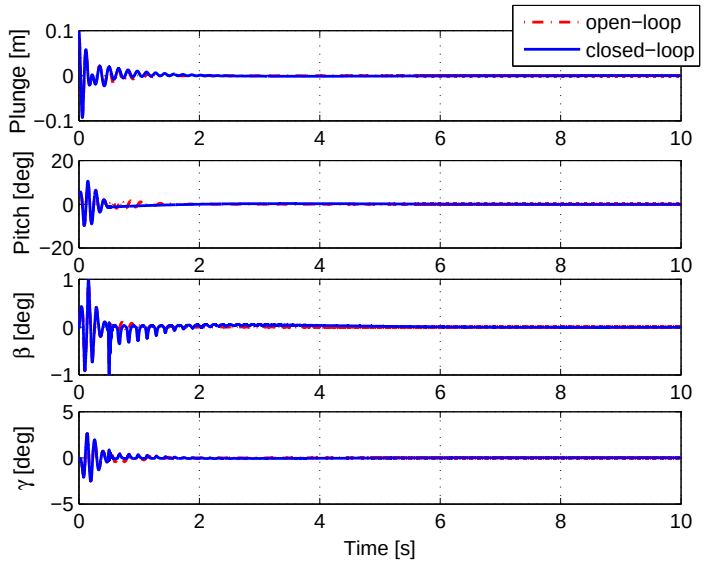

Figure 4.1: Open- and closed-loop system respone without gust disturbance at pre-flutter speed $V = 0.9V_f$

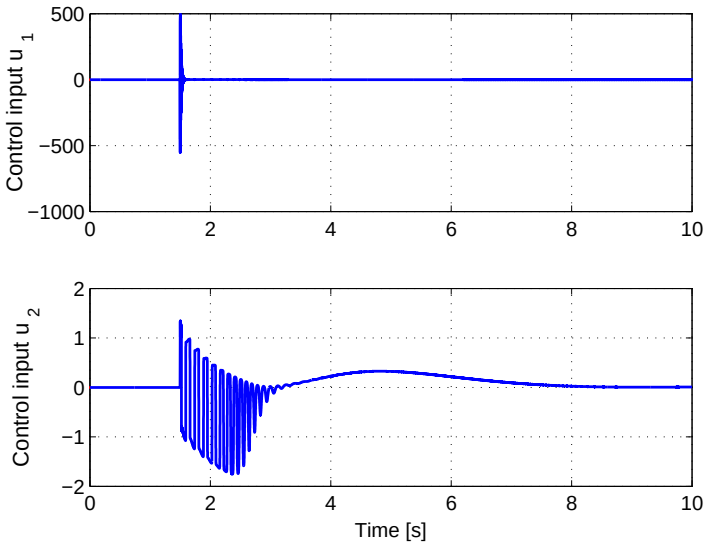

Figure 4.2: Control input of closed-loop system without gust disturbance at post-flutter speed $V = 0.9V_f$

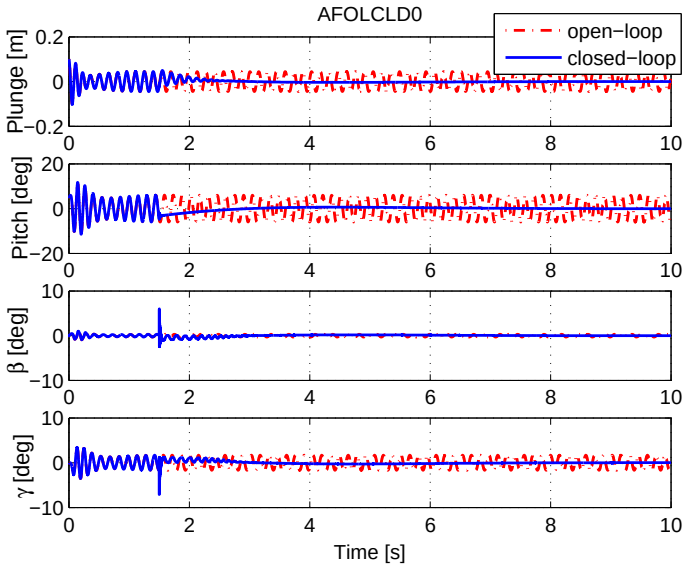

Figure 4.3: Open- and closed-loop system respone without gust disturbance at post-flutter speed $V = 1.1V_f$

Since different kinds of gust disturbance can have remarkable impact on the aerodynamics in terms of gust loading $L_g(t)$ as shown in 4.2, it will be intuitive to present the response of the wing section model with the corresponding plot of gust load. Due to the fact that I_{MG} is a linear functions of I_{LG} as shown in (3.2) and (3.3), we only present the plot of $I_{LG.}$.Figure (4.4) shows the triangular gust starts at $1.5[s]$ and last for $0.5[s]$. As we can seen after filtering by Kussner's function (3.4), the loading produced by the gust becomes smoother and longer-lasting than the gust itself. Figures 4.6 and 4.8 are system responses under triangular disturbance at pre- and post flutter speed. In these two sets of simulations, the disturbance is turned on at $t = 1[s]$ while the controller is turned on at $t = 1.5[s]$ .The controller plots are shown in figures (4.5) and (4.7). At pre-flutter speed, the system converging time decreased from $4[s]$ to $2[s]$ and steady-state errors caused by the remnant of the disturbance was eliminated. In figure (4.8), one can see the controller has effectively suppressed the oscillation of pitching and plunging displacement in about $2.5[s]$.

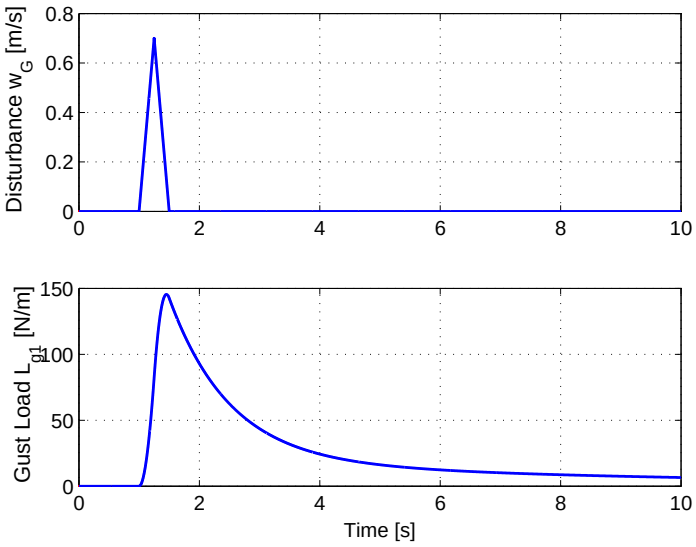

Figure 4.4: Triangular gust disturbance and corresponding gust loading

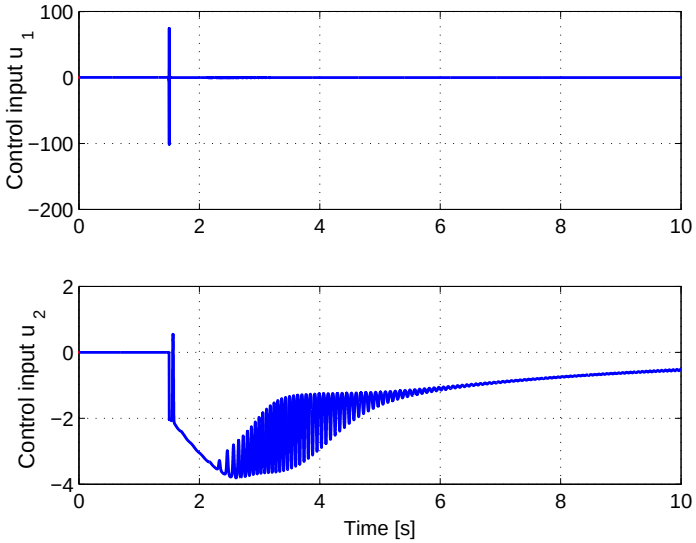

Figure 4.5: Control input of closed-loop system under triangular disturbance at pre-flutter speed $V = 0.9V_f$

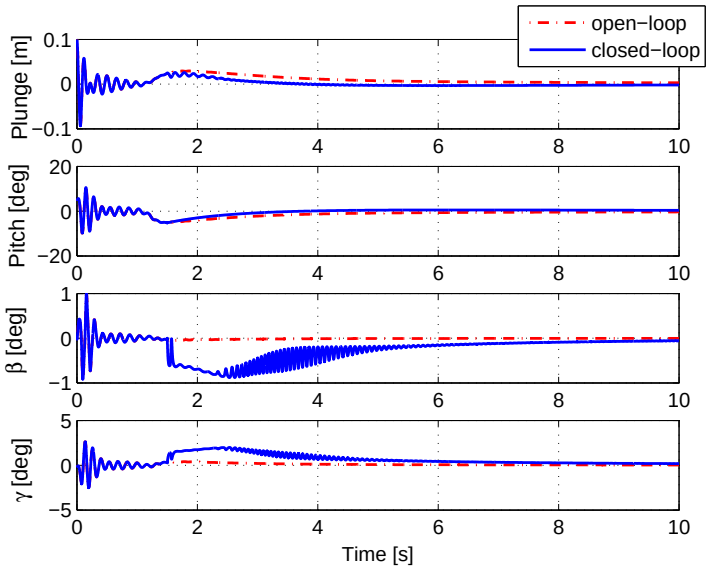

Figure 4.6: Open- and closed-loop system response under triangular gust at pre-flutter speed $V = 0.9V_f$

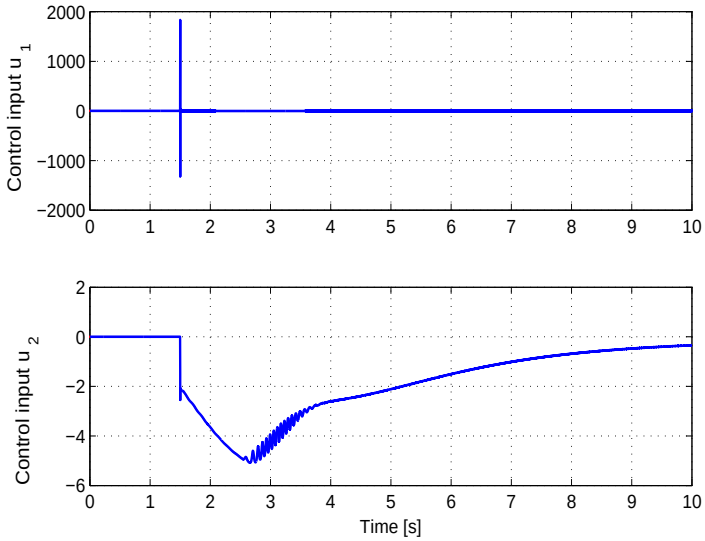

Figure 4.7: Control input of closed-loop system under triangular disturbance at post-flutter speed $V = 1.1V_f$

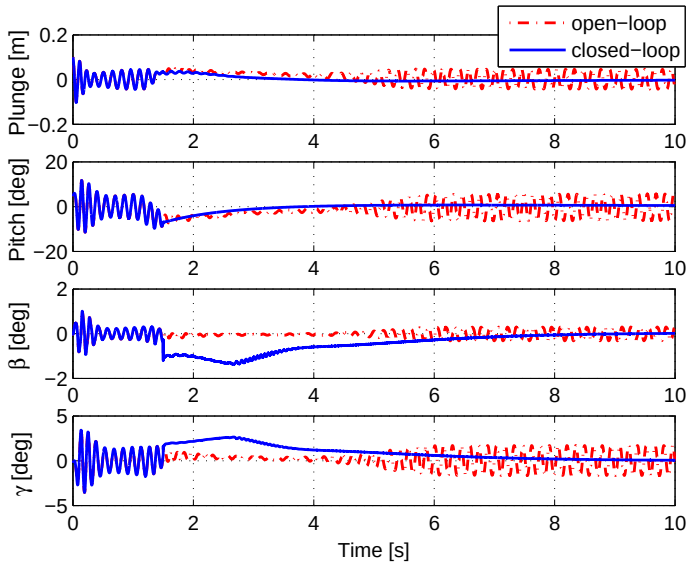

Figure 4.8: Open- and closed-loop system response under triangular gust at post-flutter speed $V = 1.1V_f$

The system responses under graded disturbance are shown in Figures (4.11) and (4.13). The disturbance starts from $t = 1[s]$ and controller is turned on at $t = 1.5[s]$. As seen in figure (4.11), due to the persistence of graded disturbance, the open-loop system can not converged at pre-flutter speed. The closed-loop system response at pre- and post-flutter speed as observed from figures (4.11) and (4.13) have the capability of the controller to suppress the persistent disturbance and stabilize the outputs. The controller plots is shown in figures (4.10) and (4.12). As expected, the persistent disturbance causes the control signal not to converge to zero along with output.

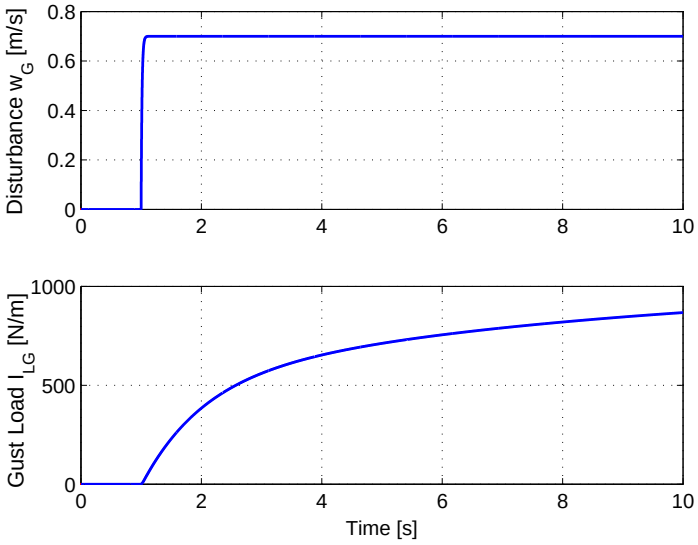

Figure 4.9: Graded gust disturbance and corresponding gust loading

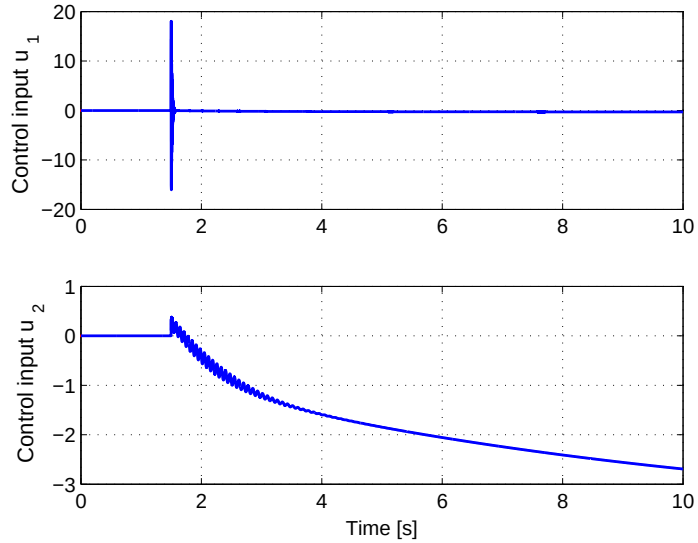

Figure 4.10: Control input of closed-loop system under graded disturbance at pre-flutter speed $V = 0.9V_f$

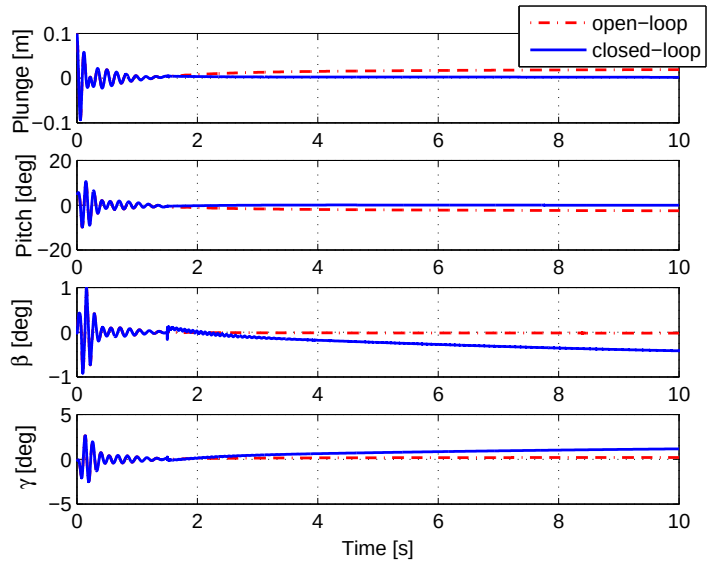

Figure 4.11: Open- and closed-loop system response under graded gust at pre-flutter speed $V = 0.9V_f$

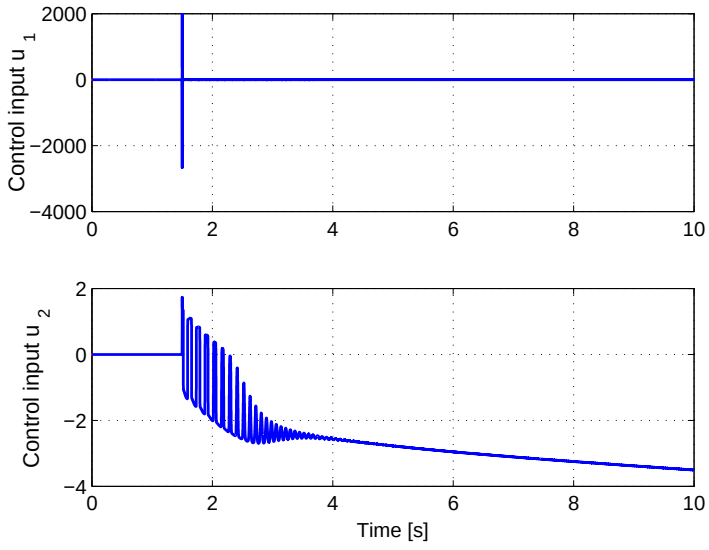

Figure 4.12: Control input of closed-loop system under graded disturbance at post-flutter speed $V = 1.1V_f$

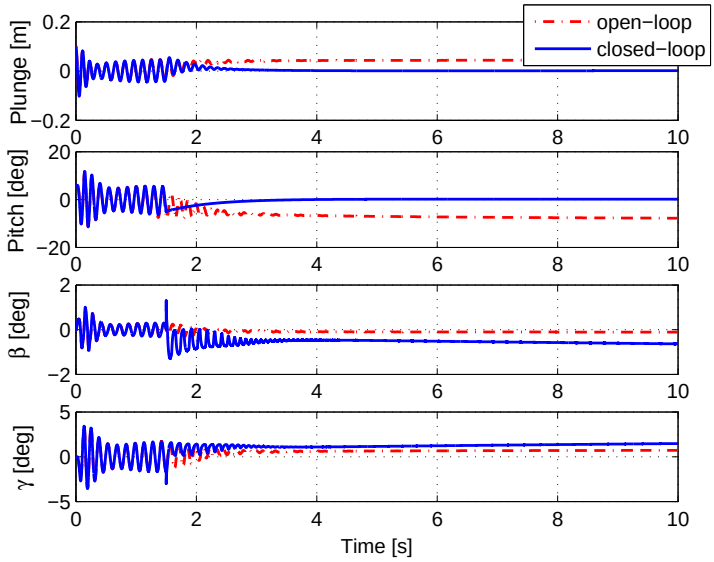

Figure 4.13: Open- and closed-loop system response under graded gust at post-flutter speed $V = 1.1V_f$

The last simulation set is for system response under sinusoidal disturbance. Figures 4.16 and 4.18 show the open- and closed-loop system response at both pre- and post-flutter speed under sinusoidal disturbance. The disturbance starts from $t = 1[s]$ shown in 4.14 and the controller is turned on at $t = 1.5[s]$.From (4.16), one can see system keeps oscillating even at pre-flutter speed because of sinusoidal disturbance the open-loop. After the turning on of controller the outputs h and α are stabilized in $1[s]$.While at post-flutter speed as shown in (4.18), the open-loop system response are obviously coupled with the sinusoidal disturbance. However, the controller still can effectively stabilize the system in $1[s]$. As shown in (4.16) and (4.18), due to the persistence of sinusoidal disturbance, there are still small small residual oscillations in the response of β and γ.

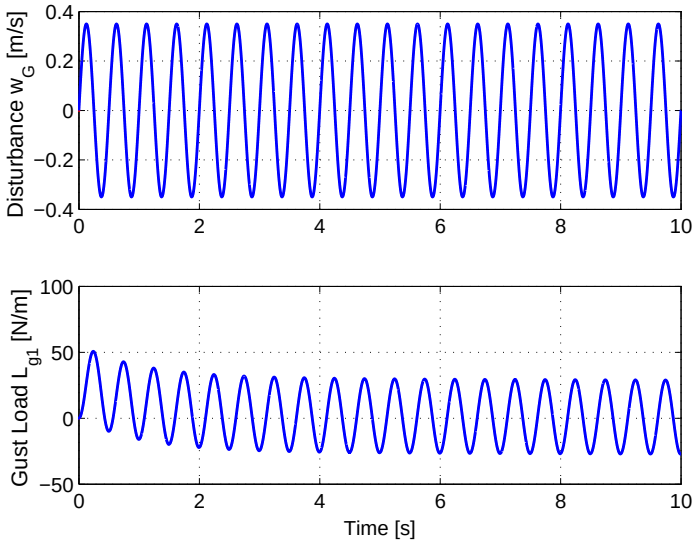

Figure 4.14: Sinusoidal gust disturbance and corresponding gust loading

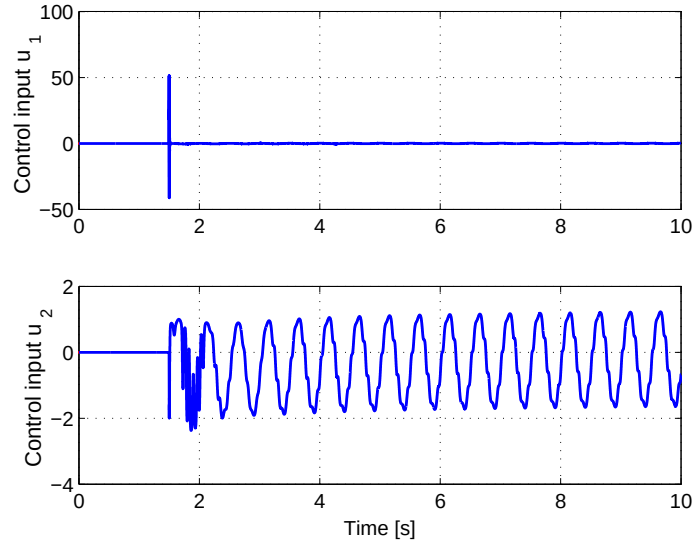

Figure 4.15: Control input of closed-loop system under sinusoidal disturbance at pre-flutter speed $V = 0.9V_f$

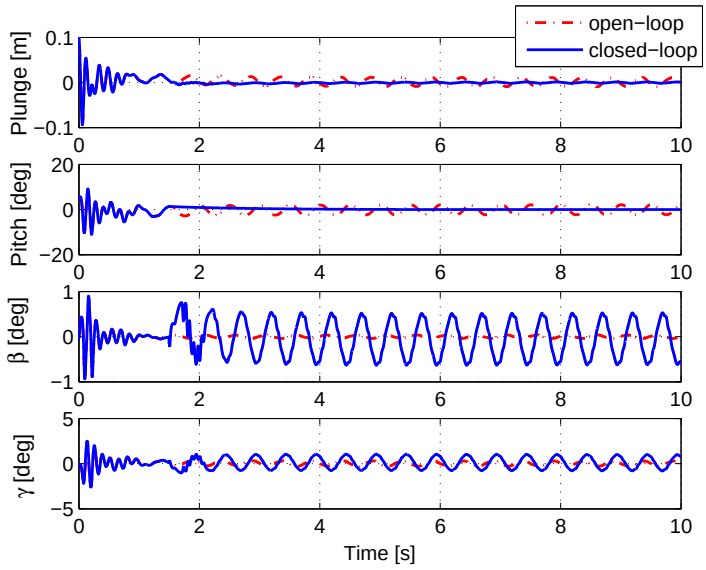

Figure 4.16: Open- and closed-loop system response under sinusoidal gust at pre-flutter speed $V = 0.9V_f$

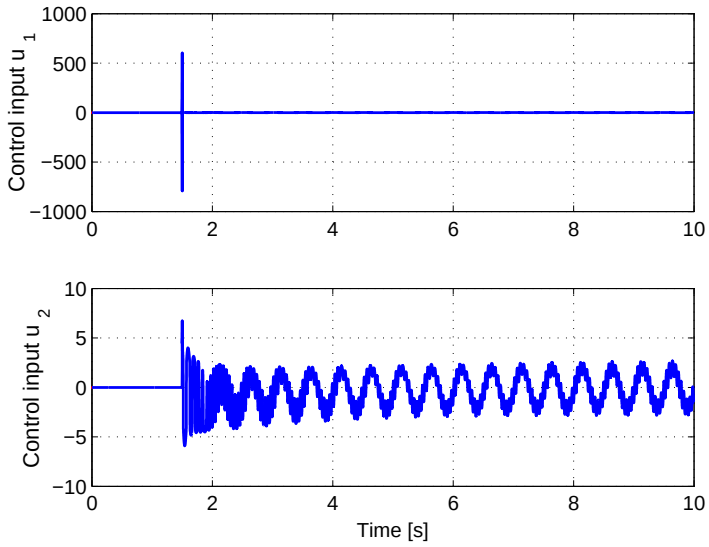

Figure 4.17: Control input of closed-loop system under sinusoidal disturbance at post-flutter speed $V = 1.1V_f$

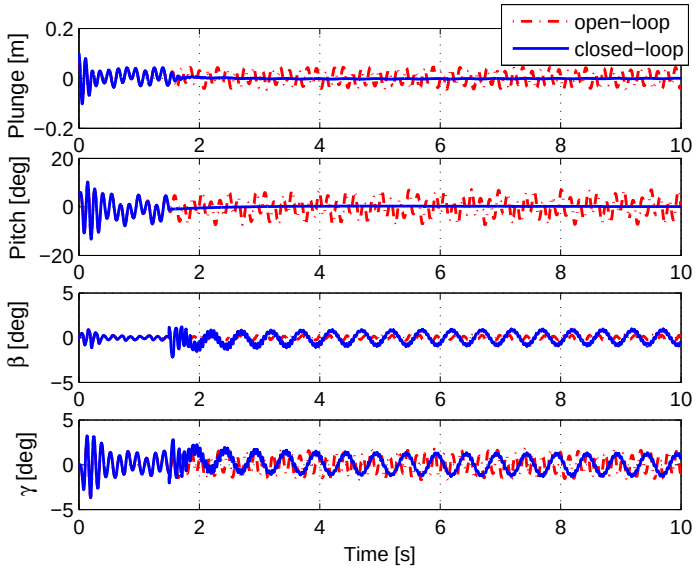

Figure 4.18: Open- and closed-loop system respone under sinusoidal gust at post-flutter speed $V = 0.9V_f$

Conclusion

A two-dimensional aeroelastic model operating in an incompressible flowfield is modeled which is exposed to three different kinds of external gust loads. The leading edge (LE) and trailing edge (TE) control surfaces was taken as the control input. An robust output feedback controller was proposed by utilizing the measurements of the pitching and plunging displacement to suppress the aeroelastic vibration subject to external disturbance on a nonlinear plunging and pitching wing section subject to unsteady aerodynamics. The control strategy was implemented with a filter mechanism to build a special siding surface without the measurements of velocity of the output. A semi-global asymptotic stability result on the pitching and plunging displacement was provided by Lyapunov stability analysis.

The robustness and efficacy of the controller is validated by simulation results under different operating conditions and disturbances. Several most common disturbance were covered in this paper. Since it is impossible to present the system response under all possible kinds of disturbance, but satisfactory simulation results can be expected based on the the the rigorous stability analysis presented in this chapter.

CHAPTER 5: MODEL FREE NONLINEAR CONTROL FOR AEROELASTIC SYSTEM

Introduction

Motivated by our previous work in [21], [22], [23],[24] and [15], a novel neural network (NN) based robust controller is designed to asymptotically stabilize a supersonic aeroelastic system with unstructured nonlinear uncertainties. In contrast to existing NN-based controllers that only achieve practical stability, the novel continuous control design in this paper is able to achieve asymptotic stability of the origin. A three-layer neural network is implemented to approximate the unknown nonlinearity of the system. While adaptive control relies on linear parameterization of the system nonlinearity and the determination of a regression matrix, the universal approximation property of the NN controller enables approximation of the unstructured nonlinear system in a more suitable way. To compensate for the inevitable NN functional approximation error, an integral of a sliding mode term is introduced. Through a Lyapunov analysis, global asymptotic stability can be obtained for the tracking error in the pitching degree of freedom. Then, based on the fact that the system is minimum phase, the asymptotic stability of the plunging degree of freedom is also guaranteed for the numerical system. Simulation results show that this NN-based robust continuous control design can rapidly suppress the flutter and limit cycle oscillations of the aeroelastic system.

Dynamic Model Development

The model of A non-linear 2-D wing-flap system operating in supersonic flight speed regimes is developed in this part. The aeroelastic governing equations of a supersonic wing section with plunging and twisting degrees-of-freedom (graphically represented in Fig. 5.1), accounting for

flap deflections, and constrained by a linear translational spring and a non-linear torsional spring, are given as follows

$$\begin{bmatrix} 1 & \varkappa_\alpha \\ \frac{\varkappa_\alpha}{r_\alpha^2} & 1 \end{bmatrix} \begin{bmatrix} \ddot{\xi} \\ \ddot{\alpha} \end{bmatrix} + \begin{bmatrix} 2\zeta_h(\frac{\bar{\omega}}{V}) & 0 \\ 0 & \frac{2\zeta_\alpha}{V} \end{bmatrix} \begin{bmatrix} \dot{\xi} \\ \dot{\alpha} \end{bmatrix} + \begin{bmatrix} (\frac{\bar{\omega}}{V})^2 & 0 \\ 0 & \frac{1}{V^2} + \frac{B\alpha^2}{V^2} \end{bmatrix} \begin{bmatrix} \xi \\ \alpha \end{bmatrix} = \begin{bmatrix} l_a \\ -m_a \end{bmatrix}. \tag{5.1}$$

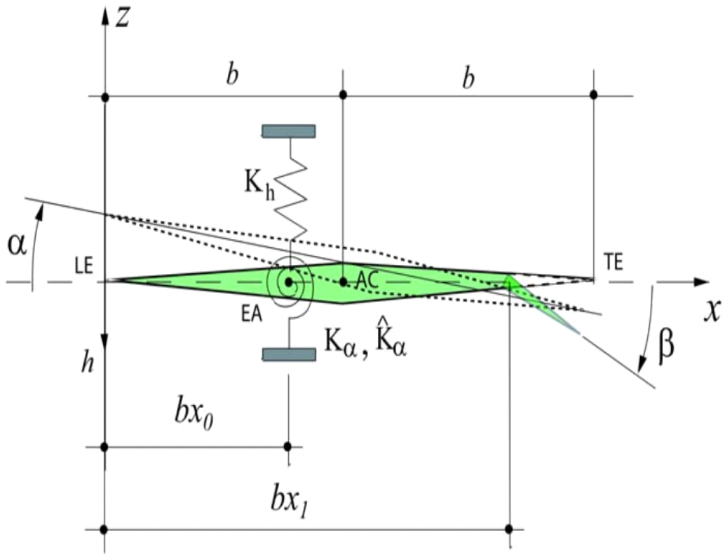

Figure 5.1: Supersonic wing section with flap

The dimensionless plunging distance (positive downward) is expressed as $\xi(\equiv h/b)$, while α is the pitch angle (positive nose up), $\dot{\alpha}$ and $\dot{\xi}$ are derivatives with respect to dimensionless time $\tau = Ut/b$, and $V = U/b\omega_\alpha$ is the dimensionless flight speed. The parameter B represents the non-linear restoring moment, and is defined as the ratio between the linear and non-linear stiffness coefficients, thus it measures of the degree of non-linearity of the system; $B > 0$ corresponds to hard structural nonlinearities, $B = 0$ corresponds to a linear model, while $B < 0$ correspond to soft structural nonlinearities. In addition, l_α and m_α represent the dimensionless aerodynamic lift

and moment with respect to the elastic axis.

In order to account for flap deflections, some modifications need to be made to the non-linear Piston Theory Aerodynamics (PTA) which is used here to produce the aerodynamic loads on the lifting surface. To keep the paper self-contained, a short description of the PTA modified to account for the flap deflection is presented next. Within the PTA, the unsteady pressure can be defined as follows

$$p(y,t) = p_\infty(1 + \frac{\gamma-1}{2}\frac{v_z}{a_\infty})^{2\gamma/(\gamma-1)} \tag{5.2}$$

where $v_z(t)$ and a_∞ represent the downwash velocity normal to the airfoil surface and the undisturbed speed of sound respectively, and are defined as follows

$$v_z = \mp(w_t + U_\infty w_x); \qquad a_\infty^2 = \gamma p_\infty/\rho_\infty \tag{5.3}$$

In the definition of $v_z(t)$, $\mp$ denotes the upper and lower surfaces, respectively, while U_∞ denotes the air speed of the undisturbed flow. In the expression for a_∞, p_∞ and ρ_∞ denote the pressure and air density of the undisturbed flow, respectively, while γ is the isentropic gas coefficient ($\gamma = 1.4$ for dry-air). The transverse deflection $w(t)$ in (5.3) can be expressed as [25]

$$w(t) = \begin{cases} h(t) + (x - bx_0)\alpha(t) & \text{for } x < bx_1, \\ h(t) + (x - bx_0)\alpha(t) + (x + bx_1)\beta(t) & \text{for } x \geq bx_1 \end{cases} \tag{5.4}$$

where x_0 and x_1 denote the dimensionless location of the elastic axis and of the torsional spring of the flap from the leading edge respectively, while $\beta(t)$ represents the flap displacement. In the binomial expansion of (5.2), the pressure formula for PTA in the third-order approximation can be obtained by retaining the terms up to and including $(v_z/a_\infty)^3$ as follows [26],

$$\frac{p}{p_\infty} = 1 + \gamma\frac{v_z}{a_\infty}\lambda + \frac{\gamma(\gamma+1)}{4}(\frac{v_z}{a_\infty}\lambda)^2 + \frac{\gamma(\gamma+1)}{12}(\frac{v_z}{a_\infty}\lambda)^3 \tag{5.5}$$

The aerodynamic correction factor, $\lambda = M/\sqrt{M^2-1}$, is used to correct the PTA to better approximate the pressure at low supersonic flight speed regime. It is important to note that (5.2) and (5.5) are only applicable as long as the transformation through contraction and expansion can be consider isentropic, *i.e.,* as long as the induced show losses are negligible (low-intensity waves). For more details, see [27, 28, 29].

PTA provides results in excellent accordance with those based on the Euler solution and the CFL3D code [30]. Considering that flow takes place on both the upper and lower surfaces of the airfoil, $U_\infty^+ = U_\infty^- = U$; from (5.3)-(5.5), the aerodynamic pressure $\delta p \triangleq p - p_\infty$difference can be expressed as

$$\delta p = -\frac{4q_\infty}{M}\lambda\left[\frac{1}{U_\infty}w_t + w_x + \frac{1+\gamma}{12}\lambda^2 M^2\left(\frac{1}{U_\infty}w_t + w_x\right)^3\right] \tag{5.6}$$

Notice that δp also account for the deflection of the flap β. Here, $M = U_\infty/\alpha_\infty$ is the undisturbed flight Mach number, while $q_\infty = \rho_\infty U_\infty^2/2$ is the undisturbed dynamic pressure as presented in [27] and [31]. The model can be simplified to account only for the nonlinearities associated with α and discarding those associated with β. Even though this is an approximation, the magnitude of the nonlinearities associated with β is much smaller than those associated with α and will thus be omitted in this paper. In addition, it is assumed in the following development that the nonlinear aerodynamic damping in (5.6), *i.e.,* the terms w_t^3, $w_t^2 w_x$, and $w_t w_x^2$ will be discarded and consequently, the cubic nonlinear aerodynamic term reduces to w_x^3 only. Although nonlinear damping can be included in the model, this paper only considers linear damping, and thus conservative estimates of the flutter speed are expected.

Finally, the nonlinear aerodynamic lift and moment can be obtained from the integration of the

difference of pressure on the upper and lower surfaces of the airfoil

$$L_a(t) = \int_0^{bx_1} \delta p|_{x<bx_1} dx + \int_{bx_1}^{2b} \delta p|_{x\geq bx_1} dx \tag{5.7}$$

$$M_a(t) = \int_0^{bx_1} \delta p|_{x<bx_1}(x - bx_0) dx - \int_{bx_1}^{2b} \delta p|_{x\geq bx_1 x - bx_0} dx \tag{5.8}$$

where $\delta p|_{x<bx_1}$ and $\delta p|_{x\gg bx_1}$ are the aerodynamic pressure difference on the clean airfoil and on the flap. In the governing EOM presented in (5.1), l_a and m_a denote the counterpart of (5.7) and (5.8), and are defined as

$$\begin{aligned} l_a &= -\frac{\lambda}{12M\mu}\{12\alpha(t) + M^2(1+\gamma)\lambda^2\alpha(t)^3 - 3[2(2-x_1)\beta(t) + 4(-1+x_0)\dot{\alpha}(t) \\ &\quad -(-2+x_1)^2\dot{\beta}(t) - 4\dot{\xi}(t)]\} \end{aligned} \tag{5.9}$$

$$\begin{aligned} m_a &= -\frac{\lambda}{12M\mu r_\infty^2}\{12(1-x_0)\alpha(t) + M^2(1+\gamma)\lambda^2(1-x_0)\alpha(t)^3 \\ &\quad -3(-2-x_1)(2-2x_0+x_1)\beta(t) + (-2+x_1)^2(4-3x_0+x_1) \\ &\quad +4[(4-6x_0+3x_0^2)\dot{\alpha}(t) - 3(-1+x_0)\dot{\xi}(t)]\} \end{aligned} \tag{5.10}$$

Here, μ represent a the dimensionless mass ratio defined as $m/4\rho b^2$. Given the definitions above, the governing EOM can be transformed into the following form

$$\dot{\mathbf{x}} = \mathbf{A}\mathbf{x} + \mathbf{\Phi}(y) + \mathbf{G}\beta + \mathbf{G}_d\dot{\beta} \tag{5.11}$$

where $\mathbf{x} = \begin{bmatrix} \alpha & \dot{\alpha} & \xi & \dot{\xi} \end{bmatrix}^T \in \Re^4$ is a vector of systems states, $\beta(t)$ is a flap deflection control

input, while $\mathbf{A}, \mathbf{G}(\mathbf{z}), \mathbf{G}_d(z)$, and $\mathbf{\Phi}(y)$ are defined as follows

$$\begin{aligned}
\mathbf{A} &= \begin{bmatrix} 0 & 1 & 0 & 0 \\ c_1 & c_2 & c_3 & c_4 \\ 0 & 0 & 0 & 1 \\ k_1 & k_2 & k_3 & k_4 \end{bmatrix}, \mathbf{\Phi}(y) = \begin{bmatrix} 0 \\ p_2\Phi(y) \\ 0 \\ p_4\Phi(y) \end{bmatrix}, \\
\mathbf{G} &= \begin{bmatrix} 0 \\ g_1 \\ 0 \\ g_2 \end{bmatrix}, \mathbf{G}_d = \begin{bmatrix} 0 \\ g_3 \\ 0 \\ g_4 \end{bmatrix}, \\
y &= x_1, \ \mathbf{x} = \begin{bmatrix} \alpha \\ \dot{\alpha} \\ \xi \\ \dot{\xi} \end{bmatrix}.
\end{aligned} \tag{5.12}$$

where the explicit definitions for the constants $c_i, k_i, \forall i = 1, ..., 4$ as well as p_2 and p_4 are reported in the Appendix B.

Open-Loop Error System Development

The explicit control objective of this paper is to design a model-free aeroelastic vibration suppression strategy to guarantee the asymptotic convergence of the pitch angle α using the flap deflection β as a control input. The secondary objective is to ensure that all system states remain bounded at all times during closed-loop operation. One prove the zero dynamics of (5.11) are stable by checking the poles of the system (5.11) when setting outputs to zero. Given the definitions of (5.11) and

(5.12), $\ddot{\alpha}$ can be expressed as follows

$$\ddot{\alpha} = c_1\alpha + c_2\dot{\alpha} + p_2\Phi(\alpha) + c_3\xi + c_4\dot{\xi} + g_1\beta + g_3\dot{\beta}. \tag{5.13}$$

The tracking error $e_1 \triangleq \alpha_d - \alpha$ is defined where $\alpha_d \in \Re$ denotes the desired output vector which needs to be smooth in deference to the requirements of the subsequent control design. For the control objective, one can simply choose α_d to be zero all the time or use another desirable smooth time-varying trajectory $\alpha_d(t)$ along which the actual pitching variable α can be driven towards the origin. In order to facilitate the ensuing control design and stability analysis, we also define the tracking error $e_2(t) \in \Re$ and the filtered tracking error signal $r(t) \in \Re$ as follows

$$e_2 = \dot{e}_1 + \lambda_1 e_1 \tag{5.14}$$

$$r = e_2 + \lambda_2 e_1 \tag{5.15}$$

where $\lambda_{1,}\lambda_2$ are positive constants. By utilizing the definitions above, one can obtain

$$\dot{r} = \ddot{\alpha}_d - \ddot{\alpha} + \lambda_1\dot{e}_1 + \lambda_2\dot{e}_1.$$

By substituting (5.13) for $\ddot{\alpha}$ in the above expression, the open-loop dynamics for r can be obtained as follows

$$\dot{r} = \ddot{\alpha}_d - c_1\alpha - c_2\dot{\alpha} - p_2\Phi(\alpha) - c_3 z - c_4\dot{z} - g_1\beta - g_3\dot{\beta} + \lambda_1\dot{e}_1 + \lambda_2\dot{e}_1 \tag{5.16}$$

After a convenient rearrangement of terms, the open-loop dynamics can be rewritten as follows

$$\frac{\dot{r}}{|g_3|} = \frac{1}{|g_3|}\left(\ddot{\alpha}_d - c_1\alpha - c_2\dot{\alpha} - p_2\Phi(\alpha) + \lambda_1\dot{e}_1 + \lambda_2 e_2 - c_3 z - c_4\dot{z}\right) - \frac{g_1}{|g_3|}\beta - \text{sgn}(g_3)\,\dot{\beta}. \tag{5.17}$$

In order to design a model-free controller, we define an auxiliary nonlinear signal $N(\cdot)$ as follows

$$N(\alpha_d, \dot{\alpha}_d, \ddot{\alpha}_d, x_1, x_2, x_3, x_4) \triangleq \frac{1}{|g_3|}\left(\ddot{x}_{1d} - c_1\alpha - c_2\dot{\alpha} - p_2\Phi(\alpha) + \lambda_1\dot{e}_1 + \lambda_2 e_2 - c_3 z - c_4\dot{z}\right) \tag{5.18}$$

By utilizing the definition of (5.18) above, the open-loop dynamics of the system can be compactly rewritten as follows

$$\frac{\dot{r}}{|g_3|} = N(x_{1d}, \dot{x}_{1d}, \ddot{x}_{1d}, x_1, x_2, x_3, x_4) - \frac{g_1}{|g_3|}\beta - \text{sgn}(g_3)\,\dot{\beta}. \tag{5.19}$$

Control Design and Closed-Loop Error System

Since the structure of the model is assumed to be unknown in the control design, standard adaptive control cannot be applied. In its lieu, a neural network feedforward compensator $\hat{N}$ along with a robustifying term is proposed to compensate for the function N as defined above in (5.18). By the universal function approximation property [32], the nonlinear function of the system N can be approximated as a three-layer network target function as follows

$$N(x_{1d}, \dot{x}_{1d}, \ddot{x}_{1d}, x_1, x_2, x_3, x_4) = \mathbf{W}^T\sigma\left(\mathbf{V}^T\bar{\mathbf{x}}\right) + \epsilon \tag{5.20}$$

as long as N is a general smooth function from $\Re^7$ to $\Re^1$, and the set of inputs to the function is restricted to a compact set S of $\Re^7$. In (5.20), $\bar{\mathbf{x}} = [\mathbf{1}\ \alpha_d\ \dot{\alpha}_d\ \ddot{\alpha}_d\ x_1\ x_2\ x_3\ x_4]^T \in \Re^{8\times 1}$ denotes the augmented input vector, vector $\mathbf{V}^T \in \Re^{10\times 8}$ is the ideal first layer interconnection weight matrix between input layer and hidden layer, $\sigma(\cdot) \in \Re^{11\times 1}$ denotes the sigmoidal activation function, while $\mathbf{W}^T \in \Re^{1\times 11}$ denotes the ideal second layer interconnection weight matrix. In this work, the weight matrices $\mathbf{W}$ and $\mathbf{V}$ are assumed to be constant and bounded as $\|\mathbf{W}\|_F \leq \mathbf{W}_B$ and $\|\mathbf{V}\|_F \leq \mathbf{V}_B$, where $\mathbf{W}_B$ and $\mathbf{V}_B$ are positive constants. The approximation error is assumed

to be bounded in compact set $\|\epsilon\| < \epsilon_N$ where ϵ_N is an unknown positive constant related to the number of nodes in the hidden layer.

After substituting the approximation from (5.20) into (5.19) , one can rewrite the open-loop dynamics as follows

$$\frac{\dot{r}}{|g_3|} = \mathbf{W}^T \boldsymbol{\sigma}\left(\mathbf{V}^T \bar{\mathbf{x}}\right) + \epsilon - g\beta - \text{sgn}\left(g_3\right)\dot{\beta} \tag{5.21}$$

where $g \triangleq \frac{g_1}{|g_3|}$. Motivated by the open-loop dynamics and the ensuing stability analysis, the control law is designed as follows

$$\dot{\beta} = -\text{sgn}\left(g_3\right)\hat{g}\beta + \text{sgn}\left(g_3\right)\left[\hat{N} + K_v r - v + K_d \text{sgn}\left(r\right)\right]. \tag{5.22}$$

where K_v, $K_d > 0$ are constant control gains, $\hat{N}$ is a typical three-level neural network compensator for target function $N(\bar{\mathbf{x}})$, defined as follows

$$\hat{N}(\bar{\mathbf{x}}) = \hat{\mathbf{W}}^T \boldsymbol{\sigma}\left(\hat{\mathbf{V}}^T \bar{\mathbf{x}}\right), \tag{5.23}$$

v is a robustifying term which will be defined later while $\hat{g}$ is an adaptive estimate for g. The dynamic update law for $\hat{g}$ is designed as follows

$$\dot{\hat{g}} = proj\left\{-\Gamma\beta r\right\} \tag{5.24}$$

where the parameter projection operator $proj\{\cdot\}$ is designed to bound $\hat{g}$ in a known compact set Ω such that $sgn(g_3)\hat{g}\left(t\right) \geq \varepsilon > 0$ for all time. The projection operator defined here is meaningful because the minimum-phase nature of the system ensures that $sgn(g_3)g\left(t\right) = g_3^{-1}g_1$ is always positive. In (5.23), $\hat{\mathbf{W}}$ and $\hat{\mathbf{V}}$ are estimates for the neural network interconnection weight matrices

that are dynamically generated as follows

$$\begin{aligned} \dot{\hat{\mathbf{W}}} = & \left(\mathbf{F}\hat{\boldsymbol{\sigma}} - \mathbf{F}\hat{\boldsymbol{\sigma}}'\hat{\mathbf{V}}^T\bar{\mathbf{x}}\right) r^T - \kappa\mathbf{F}\left\|r\right\|\hat{\mathbf{W}} \\ \dot{\hat{\mathbf{V}}} = & \mathbf{G}\bar{\mathbf{x}}\left(\hat{\boldsymbol{\sigma}}'^T\hat{\mathbf{W}}r\right)^T - \kappa\mathbf{G}\left\|r\right\|\hat{\mathbf{V}} \end{aligned} \tag{5.25}$$

where $\hat{\boldsymbol{\sigma}} \triangleq \boldsymbol{\sigma}(\hat{\mathbf{V}}^T\bar{\mathbf{x}})$, $\hat{\boldsymbol{\sigma}}' \triangleq d\sigma(\hat{\mathbf{V}}^T\bar{\mathbf{x}})/d(\hat{\mathbf{V}}^T\bar{\mathbf{x}})$, $\mathbf{F} \in \Re^{11\times 11}$ and $G \in \Re^{8\times 8}$ are positive definite diagonal gain matrices, while $\kappa > 0$ is a scalar design parameter. By substituting the expression for the control law in (5.22) into the open-loop dynamics of (5.21) and conveniently rearranging the terms, one can obtain the closed-loop system dynamics as follows

$$\frac{\dot{r}}{|g_3|} = -K_v r + N - \hat{N} + v - K_d \text{sgn}\,(r) + \tilde{g}\beta$$

where $\tilde{g} \triangleq \hat{g} - g$ is a parameter estimation error. Also note that we can write

$$\mathbf{W}^T\boldsymbol{\sigma}\left(\mathbf{V}^T\bar{\mathbf{x}}\right) + \epsilon - \hat{\mathbf{W}}^T\boldsymbol{\sigma}\left(\hat{\mathbf{V}}^T\bar{\mathbf{x}}\right) = \tilde{\mathbf{W}}^T\left[\hat{\boldsymbol{\sigma}} - \hat{\boldsymbol{\sigma}}'\hat{\mathbf{V}}^T\bar{\mathbf{x}}\right] + \hat{\mathbf{W}}^T\hat{\boldsymbol{\sigma}}'\tilde{\mathbf{V}}^T\bar{\mathbf{x}} + w$$

where the weight estimation errors are defined as $\tilde{\mathbf{W}} \triangleq \mathbf{W} - \hat{\mathbf{W}}$, $\tilde{\mathbf{V}} \triangleq \mathbf{V} - \hat{\mathbf{V}}$ while w is defined as follows

$$w = \tilde{\mathbf{W}}^T\hat{\boldsymbol{\sigma}}'\mathbf{V}^T\bar{\mathbf{x}} + \tilde{\mathbf{W}}^T O\left(\tilde{\mathbf{V}}^T\bar{\mathbf{x}}\right)^2 + \epsilon\left(\bar{\mathbf{x}}\right).$$

To facilitate the subsequent analysis, one can also obtain a compact form representation for $\|\mathbf{w}\|$ as follows

$$\left\|w\right\| \quad = C_0 + C_1\left\|\tilde{\mathbf{Z}}\right\|_F + C_2\left\|\tilde{\mathbf{Z}}\right\|_F\left\|r\right\| \tag{5.26}$$

where C_0, C_1, and C_2 are all positive constants while the ideal composite weight matrix $\mathbf{Z}$, estimated composite weight matrix $\hat{\mathbf{Z}}$, and the composite weight mismatch matrix $\tilde{\mathbf{Z}} \triangleq \mathbf{Z} - \hat{\mathbf{Z}}$ are

given as follows

$$\mathbf{Z}=\begin{bmatrix}\mathbf{W} & \mathbf{0}\\ \mathbf{0} & \mathbf{V}\end{bmatrix},\quad \hat{\mathbf{Z}}\equiv\begin{bmatrix}\hat{\mathbf{W}} & \mathbf{0}\\ \mathbf{0} & \hat{\mathbf{V}}\end{bmatrix},\quad \tilde{\mathbf{Z}}\equiv\begin{bmatrix}\tilde{\mathbf{W}} & \mathbf{0}\\ \mathbf{0} & \tilde{\mathbf{V}}\end{bmatrix}. \tag{5.27}$$

Per the boundedness property for $\|\mathbf{W}\|_F$ and $\|\mathbf{V}\|_F$ as described above, there exists a constant Z_B such that $Z_B > \|\mathbf{Z}\|_F$. Based on the definition of Z_B, the robustifying term v can be designed as follows

$$v=-K_z\left(\left\|\hat{\mathbf{Z}}\right\|_F+Z_B\right)r \tag{5.28}$$

where K_z is a positive constant. Finally, it is noted that the functional reconstruction error $\epsilon\left(\bar{\mathbf{x}}\right)$ is assumed to be bounded. Thus, the closed-loop dynamics can be finally written as follows

$$\frac{\dot{r}}{|g_3|}=-K_v r+\tilde{\mathbf{W}}^T\left[\hat{\boldsymbol{\sigma}}-\hat{\boldsymbol{\sigma}}'\hat{\mathbf{V}}^T\bar{\mathbf{x}}\right]+\hat{\mathbf{W}}^T\hat{\boldsymbol{\sigma}}'\tilde{\mathbf{V}}^T\bar{\mathbf{x}}+w+v-K_d\text{sgn}\left(r\right)+\tilde{g}\beta. \tag{5.29}$$

Stability Analysis

In this part, we provide the stability analysis for the proposed model-free controller. We begin by defining a non-negative Lyapunov function candidate V_2 as follows

$$V_2=\frac{1}{2\left|g_3\right|}r^2+\frac{1}{2}tr\left\{\tilde{W}^T F^{-1}\tilde{W}\right\}+\frac{1}{2}tr\left\{\tilde{V}^T G^{-1}\tilde{V}\right\}+\frac{1}{2}\Gamma^{-1}\tilde{g}^2. \tag{5.30}$$

After differentiating V_2 along the dynamics of (5.24) and (5.29), one can obtain the following expression for $\dot{V}_2$

$$\begin{aligned}\dot{V}_2=\;& r\left[-K_v r+\tilde{\mathbf{W}}^T\left[\hat{\boldsymbol{\sigma}}-\hat{\boldsymbol{\sigma}}'\hat{\mathbf{V}}^T\bar{\mathbf{x}}\right]+\hat{\mathbf{W}}^T\hat{\boldsymbol{\sigma}}'\tilde{\mathbf{V}}^T\bar{\mathbf{x}}+w+v-K_d\text{sgn}\left(r\right)\right]\\ &+tr\left\{\tilde{\mathbf{W}}^T\mathbf{F}^{-1}\dot{\tilde{\mathbf{W}}}\right\}+tr\left\{\tilde{\mathbf{V}}^T\mathbf{G}^{-1}\dot{\tilde{\mathbf{V}}}\right\}\end{aligned} \tag{5.31}$$

After applying the neural network weight update laws designed in (5.25), canceling out the matched terms, and utilizing the definitions of (5.27), (5.31) can be upperbounded as follows

$$\dot{V}_2 \leq -K_v r^2 + \kappa \|r\| \, tr\left\{\tilde{\mathbf{Z}}^T\left(\mathbf{Z} - \tilde{\mathbf{Z}}\right)\right\} + \|r\| \|\mathbf{w}\| + rv - r\kappa \text{sgn}(r). \tag{5.32}$$

By substituting (5.26) and (5.28) into (5.32), it is possible to further upperbound $\dot{V}_2$ as follows

$$\begin{aligned} \dot{V}_2 \leq \; & -\|r\| \left[K_v \|r\| - \kappa \left\|\tilde{\mathbf{Z}}\right\|_F \left(Z_B - \left\|\tilde{\mathbf{Z}}\right\|_F\right) - C_0 - C_1 \left\|\tilde{\mathbf{Z}}\right\|_F \right. \\ & \left. -C_2 \left\|\tilde{\mathbf{Z}}\right\|_F \|r\| + K_z \left(\left\|\hat{\mathbf{Z}}\right\|_F + Z_B\right) \|r\| - K_d \text{sgn}(r)\right] \end{aligned} \tag{5.33}$$

where the following relation has been used to derive (5.33)

$$\begin{aligned} tr\left\{\tilde{\mathbf{Z}}^T\left(\mathbf{Z} - \tilde{\mathbf{Z}}\right)\right\} &= \left\langle \tilde{\mathbf{Z}}, \, \mathbf{Z} \right\rangle - \left\|\tilde{\mathbf{Z}}\right\|_F^2 \leq \left\|\tilde{\mathbf{Z}}\right\|_F \|\mathbf{Z}\|_F - \left\|\tilde{\mathbf{Z}}\right\|_F^2 \\ &\leq \left\|\tilde{\mathbf{Z}}\right\|_F Z_B - \left\|\tilde{\mathbf{Z}}\right\|_F^2. \end{aligned} \tag{5.34}$$

Based on the fact that $\left\|\hat{\mathbf{Z}}\right\|_F + Z_B > \left\|\tilde{\mathbf{Z}}\right\|_F$, one can choose $K_z > C_2$ such that (5.33) can be rewritten as

$$\dot{V}_2 \leq -\|r\| \left[\mathbf{K}_v \|r\| - \kappa \left\|\tilde{\mathbf{Z}}\right\|_F \left(Z_B - \left\|\tilde{\mathbf{Z}}\right\|_F\right) - C_0 - C_1 \left\|\tilde{\mathbf{Z}}\right\|_F\right] - rK_d \text{sgn}(r). \tag{5.35}$$

By defining $C_3 = Z_B + C_1/\kappa$ and conveniently rearranging the terms, (5.35) can be rewritten as follows

$$\dot{V}_2 \leq -\|r\| \left[\mathbf{K}_v \|r\| + \kappa \left(\left\|\tilde{\mathbf{Z}}\right\|_F - C_3/2\right)^2\right] + \|r\| \left[C_0 - \kappa C_3^2/4\right] - rK_d \text{sgn}(r).$$

By choosing $K_d > [C_0 - \kappa C_3^2/4]$, one can obtain the following upperbound on $\dot{V}_2$

$$\dot{V}_2 \leq -\|r\| \left[\mathbf{K}_v \|r\| + \kappa \left(\left\|\tilde{\mathbf{Z}}\right\|_F - C_3/2\right)^2\right] \tag{5.36}$$

From (5.30) and (5.36), it is easy to see that $r \in \mathcal{L}_2 \cap \mathcal{L}_\infty$ while $\hat{g}, \tilde{\mathbf{W}}, \tilde{\mathbf{V}} \in \mathcal{L}_\infty$. The boundedness of r implies that $\alpha, \dot{\alpha}$ are bounded by virtue of the definitions of (5.14) and (5.15). Since the system is minimum phase and relative degree one, the boundedness of the output guarantees that any first order stable filtering of the input will remain bounded. This implies that all system states remain bounded in closed-loop operation which further implies that $N\left(x_{1d}, \dot{x}_{1d}, \ddot{x}_{1d}, x_1, x_2, x_3, x_4\right)$ stays bounded. Since (5.22) defines a stable filter acting on a bounded input, it is easy to see that β and $\dot{\beta}$ stay bounded; furthermore, the flap deflection control input β is continuous at all times. The boundedness of β implies in turn that $\dot{r} \in \mathcal{L}_\infty$ by virtue of (5.29). Thus, using previous assertions, one can utilize Barbalat's Lemma [4] to conclude that $r \to 0$ as $t \to \infty$ which further implies that $e_1, \dot{e}_1 \to 0$ as $t \to \infty$. From the asymptotic stability of the zero dynamics, we can further guarantee that $x_3, x_4 \to 0$ as $t \to \infty$. Thus, both the pitching and plunging variables show asymptotic convergence to the origin.

Simulation Results

In this section, simulation results are presented for a aeroelastic system controlled by the proposed continuous robust controller. The nonlinear aerodynamic model is simulated using the dynamics of (5.1) , (5.7) and (5.10). The flap deflection is constrained to lie between $\pm 15[\mathrm{deg}]$.The nominal model parameters are listed as follows and the controller parameters are listed in Table 5.2.

Table 5.1: Model parameters

$\chi_\alpha = 0.25,$	$\zeta_h = 0.01,$	$x_0 = 0.5,$
$r_\alpha = 0.5,$	$\zeta_\alpha = 0.01,$	$x_1 = 0.75,$
$b = 1.5$ [m],	$\gamma = 1.4,$	$\overline{\omega} = 1,$
$\lambda = 1,$	$M = 2,$	$V = 7.556,$
$\mu = 50,$	$B = 5,$	$\omega_h = \omega_\alpha = 60$ [Hz],

Table 5.2: Controller parameters

Parameter	Value	Parameter	Value
K_z	0.1	Z_b	0.1
κ	2	K_v	100
K_d	$1e-4$	Γ	$1e-5$
$\mathbf{F}$	0.1	$\mathbf{G}$	2

The desired trajectory variables $\alpha_d, \dot{\alpha}_d$,and $\ddot{\alpha}_d$ are simply selected as zero. The initial conditions for pitching displacement $\alpha(t)$ and plunging displacement $\xi(t)$ are chosen as $\alpha(0) = 5.729\,\mathrm{deg}$ $(\mathrm{about}\ 0.1$ radians) and $\xi(0) = 0$ m, while all other state variables are initialized to zero. The initial parameter estimate $\hat{g}(0)$ is set to be -1.20, which is a 10% shift from its nominal value. The flap deflection $\beta\,(t)$ is constrained to vary between ± 15 deg.

The effect of structural nonlinearities on LCO amplitude was analyzed before applying any control. As shown in [33], increase in structural stiffness factor denoted by B led to decrease in LCO amplitude provided the flutter speed remains constant. Furthermore, we also explored the effect of the location of the elastic axis from the leading edge. It was shown in [33] that a decrease in x_0 leads to decrease in LCO amplitude while the flutter speed increases. It was also shown that increasing the damping ratios, ζ_h and ζ_α resulted in decrease of the amplitude of the LCO.

Fig (5.2) shows the dynamics of open-loop pitching displacement α and plunging displacement ξ at pre-flutter speed. The simulation is carried out in subcritical flight speed regime, $M = 2$, below the flutter speed of $M_{flutter} = 2.15$.

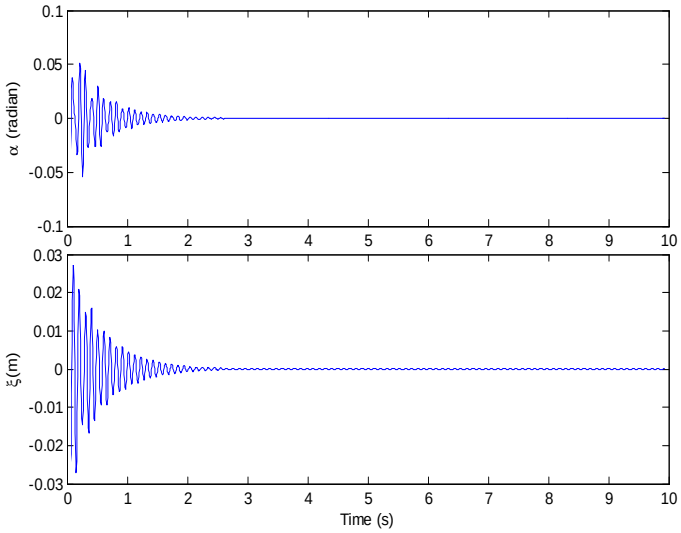

Figure 5.2: Open-loop dynamics of the aeroelastic system at pre-flutter speed $M = 2 < M_{flutter} = 2.15$

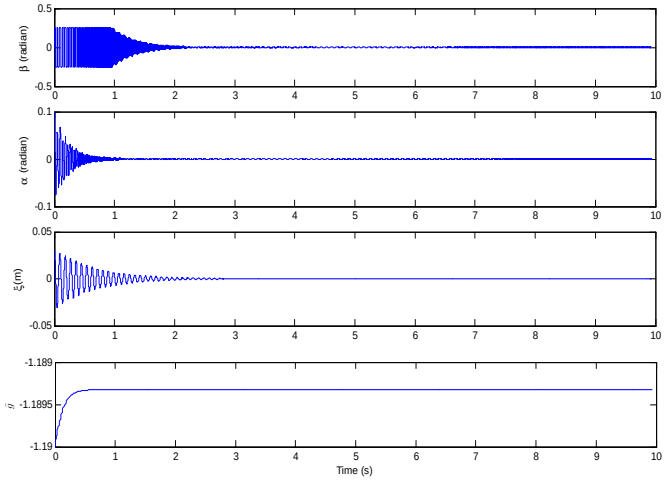

Figure 5.3: Closed-loop plunging, pitching, control deflection and parameter estimation at pre-flutter speed, $M = 2 < M_{flutter} = 2.15$

Without the controller, it is obvious that the oscillation of pitching degree-of-freedom α will converge within 3[s] while the plunging displacement are lightly damped and it takes over 3[s] to converge. In Fig (5.3), it is shown that the proposed robust controller suppresses the oscillation of α in less than 1.5[s] while the plunging displacement ξ is suppressed in 2.5[s] . The parameter estimate $\hat{g}$ is seen to converge to a constant value within less than 0.5[s].

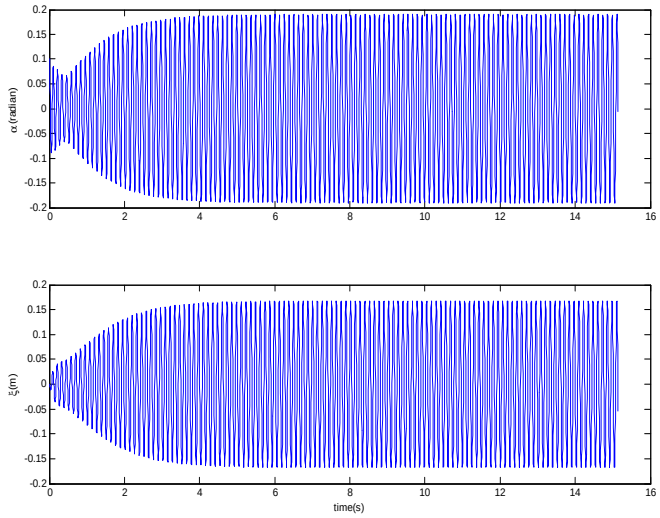

Figure 5.4: Open-loop dynamics of the aeroelastic system at post-flutter speed $M = 3 > M_{flutter} = 2.15$

As shown in Fig (5.4), in post-flutter regime, the system dynamics show sustained limit cycle oscillations in open-loop operation. From Fig(5.5), it is shown that the control is very effective when it is turned on at t=0[s] and the oscillation of α is suppressed within 1.5[s]. The dynamic oscillatory behavior of the plunging displacement ξ is suppressed within 2.5[s].

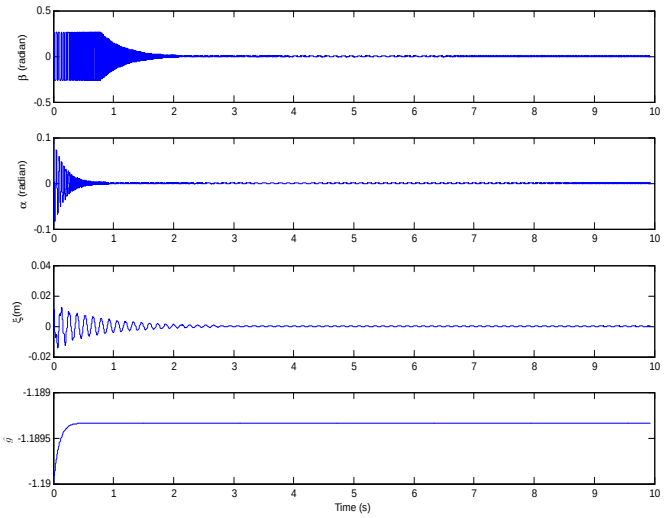

Figure 5.5: Closed loop plunging,pitching,control deflections and parameter estimation at post-flutter speed, $M = 3 > M_{flutter} = 2.15$

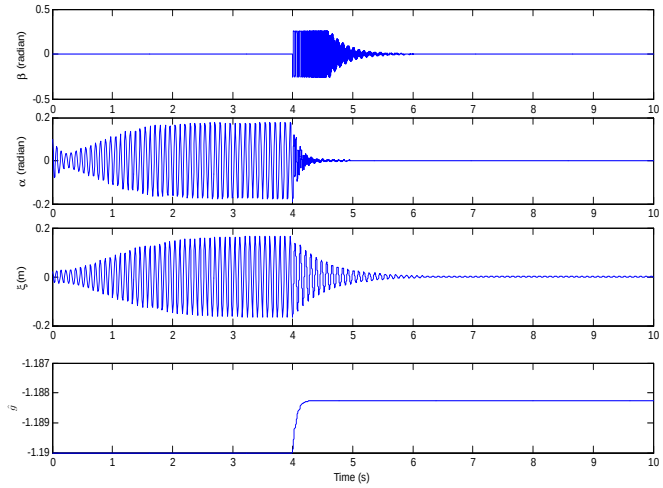

Figure 5.6: Closed-loop plunging, pitching, control deflection and parameter estimation at post-flutter speed, $M = 3 > M_{flutter} = 2.15$; control applied at $t = 4$ s.

In Fig (5.6), control was turned on at $t = 4$[s] after the system had gone into an LCO. It is seen that the oscillations of the pitching degree α and plunging displacement ξ are suppressed respectively in 1.5[s] and 3[s]. The parameter estimate $\hat{g}$ also converges to a constant in less than 0.5[s]. These simulation results show that the proposed novel robust controller can effectively suppress the oscillation of both pitching and plunging degrees-of-freedom of the airfoil at both pre-flutter and post-flutter flight speed regimes.

Conclusions

A modular model-free continuous robust controller was proposed to suppress the aeroelastic vibration characteristics (including flutter and limit cycle oscillations in pre- and post-flutter condition) of a supersonic 2-DOF lifting surface with flap. Differently from traditional adaptive control strategies, which strictly require the linear parameterization of the system, no prior knowledge of the system model is required for the method presented in this paper. A Lyapunov method based analysis was provided to obtain the global asymptotic stability result. Finally, the simulation results showed that this control strategy can rapidly suppress any aeroelastic vibration in pre- and post-flutter flight speed regimes.

CHAPTER 6: CONCLUSION AND FUTURE WORK

In this dissertation, we have investigated several Lyapunov-based control schemes for aeroelastic systems operating under different conditions. Specifically, the following subjects have been discussed in the dissertation.

1. Lyapunov-based Adaptive Control Design. This topic is discussed in Chapter 2. Here, the structure of the system is assumed to be known which is utilized to parameterize the system for adaptive control design. This design is unique because it has designed a convolution-based filter to estimate the immeasurable internal states.

2. Robust Control Design. There are two chapters is about this topic: Chapter 3 and Chapter 4. The first is an extension of robust integral of the sign of error (RISE) to system with zero dynamics. An Input-to-State Stability like Lemma is provided to get the boundedness of internal dynamics in terms of output for minimum-phase system. The second part is a robust output feedback control design for a MIMO system. A specific filter error based on output errors is built to avoid using velocity sensor to measure the rates of output variables and actuator deflection. Lyapunov function based stability proofs are provided to guarantee robustness of the system to external disturbance.

3. Model Free Control Design. In Chapter 5, a novel neural network (NN) based robust controller is designed to asymptotically stabilize a supersonic aeroelastic system with unstructured nonlinear uncertainties. The merit of this design is there is no need for the system structure information and parameters are tuned online.

Future research directions can be expected to focus on developing robust controls with only output feedback for MIMO system with arbitrarily DOF and order under external disturbances and system uncertainties. Applications to other real systems, such as robotic systems, can also be considered

in future work.

APPENDIX A: PROOF OF LEMMA

C.2 Proof of Lemma 1

From Chapter 2, $\mathbf{w}(\mathbf{0}, \boldsymbol{\zeta})$ is locally exponentially stable. Let the stability region lie in a compact set defined by $||\boldsymbol{\zeta}(\mathbf{0})|| < \gamma$ where γ is an appropriately chosen positive constant. Let us now prove that $\mathbf{w}(\boldsymbol{\mu}, \boldsymbol{\zeta})$ is locally Lipschitz. The internal dynamics of the nominal system can be denoted as

$$\dot{\boldsymbol{\zeta}} = \mathbf{w}(\mathbf{z}). \tag{A.1}$$

where $\mathbf{z} \triangleq \left(\boldsymbol{\mu}^T, \boldsymbol{\zeta}^T\right)^T = F\mathbf{x}$. After taking the derivative of (A.1) with respect to $\mathbf{z}$ and applying the chain rule, one obtains

$$\frac{\partial \mathbf{w}(\mathbf{z})}{\partial \mathbf{z}} = F_{sub} A F^{-1} + \left[F_{sub} \frac{\partial}{\partial \mathbf{x}} \mathbf{f}(x_4, x_5)\right] F^{-1} \tag{A.2}$$

where the first equation of (2.9) are utilized while F_{sub} is a submatrix of F that is defined as $\boldsymbol{\zeta} \triangleq F_{sub}\mathbf{x}$. From (2.36) and (2.37), the output $\frac{h}{b} = x_4$ stays bounded for all time, while x_5 stays bounded on a compact set $\mathcal{D}_2 = \left\{\boldsymbol{\zeta} \in \mathbf{R}^6 \;\middle|\; \|\boldsymbol{\zeta}\| \leq \gamma\right\}$, one can upperbound $\dfrac{\partial}{\partial \mathbf{x}} \mathbf{f}(x_4, x_5)$ as follows

$$\left\| \frac{\partial}{\partial \mathbf{x}} \mathbf{f}(x_4, x_5) \right\| \leq L_f \tag{A.3}$$

where the fact that the nonlinear function $\mathbf{f}(x_4, x_5)$ is a vector function composed of polynomials of x_4, x_5 (see the definitions in Appendix A) is used here.. Now, (A.3) is substituted into (A.2) to obtain the following upperbound

$$\begin{aligned} \left\| \frac{\partial \mathbf{w}(\mathbf{z})}{\partial \mathbf{z}} \right\| &\leq \left\| F_{sub} A F^{-1} \right\| + \|F_{sub}\| \left\| \left[\frac{\partial}{\partial \mathbf{x}} \mathbf{f}(x_4, x_5)\right] \right\| \left\| F^{-1} \right\| \\ &\leq \left\| F_{sub} A F^{-1} \right\| + L_f \|F_{sub}\| \left\| F^{-1} \right\| = L_0 < \infty \end{aligned}$$

Since $\dfrac{\partial \mathbf{w}(\mathbf{z})}{\partial \mathbf{z}}$ is bounded, it can be concluded that $\mathbf{w}(\mathbf{z})$ is locally Lipschitz in $\boldsymbol{\zeta}$ and globally Lipschitz in $\boldsymbol{\mu}$ (see Lemma 3.2 in [4]) which implies that

$$\|\mathbf{w}(\mathbf{z}_1) - \mathbf{w}(\mathbf{z}_2)\| \leq L_0 \|\mathbf{z}_1 - \mathbf{z}_2\|. \tag{A.4}$$

From the local exponential stability of $\mathbf{w}(\mathbf{0}, \boldsymbol{\zeta})$ and the fact that $\mathbf{w}(\mathbf{z})$ is Lipschitz in $\boldsymbol{\zeta}$, a converse theorem of Lyapunov (see [11]) implies $\exists V(\boldsymbol{\zeta}) : \mathcal{D}_2 \to \mathbf{R}$ such that

$$\begin{aligned} \alpha_1(\|\boldsymbol{\zeta}\|) \leq V(\boldsymbol{\zeta}) \leq \alpha_2(\|\boldsymbol{\zeta}\|) \\ \frac{\partial V}{\partial \boldsymbol{\zeta}} \mathbf{w}(\mathbf{0}, \boldsymbol{\zeta}) \leq -\alpha_3(\|\boldsymbol{\zeta}\|) \\ \left\| \frac{\partial V}{\partial \boldsymbol{\zeta}} \right\| \leq \alpha_4(\|\boldsymbol{\zeta}\|) \end{aligned} \tag{A.5}$$

where $\alpha_i, i = 1, 2, 3, 4$ are class $\mathcal{K}$ functions defined on $[0, \gamma]$. After taking the time derivative of $V(\boldsymbol{\zeta})$, one can obtain

$$\begin{aligned} \dot{V}(\boldsymbol{\zeta}) &= \frac{\partial V}{\partial \boldsymbol{\zeta}} \mathbf{w}(\boldsymbol{\mu}, \boldsymbol{\zeta}) \\ &\leq -\alpha_3 \|\boldsymbol{\zeta}\|^2 + \frac{\partial V}{\partial \boldsymbol{\zeta}} (\mathbf{w}(\boldsymbol{\mu}, \boldsymbol{\zeta}) - \mathbf{w}(\mathbf{0}, \boldsymbol{\zeta})) \end{aligned} \tag{A.6}$$

where (A.5) was used. After applying the boundedness of $\boldsymbol{\mu}$ from (2.39) and the Lipschitz condition of (A.4), $\dot{V}(t)$ of (A.6) can be further upperbounded as follows

$$\dot{V}(\boldsymbol{\zeta}) \leq -\alpha_3 \|\boldsymbol{\zeta}\| \left(\|\boldsymbol{\zeta}\| - \frac{\alpha_4}{\alpha_3} K(|r_0|, \Gamma^{-1}) L_0 \right).$$

Thus, it can be seen from above that

$$\dot{V}(\boldsymbol{\zeta}) \leq 0 \text{ for } \|\boldsymbol{\zeta}\| \geq \frac{\alpha_4}{\alpha_3} K\left(|r_0|, \Gamma^{-1}\right) L_0 \tag{A.7}$$

By properly choosing the adaptive gain Γ and the the size of the initial condition as encoded by $|r_0|$, one can ensure that the compact set $\mathcal{D}_3 = \left\{ \boldsymbol{\zeta} | \, \|\boldsymbol{\zeta}\| \leq \frac{\alpha_4}{\alpha_3} K L_0 \right\}$ is a subset of the compact set $\mathcal{D}_2$. This implies that the set $\mathcal{D}_2$ is positively invariant under a proper choice of initial conditions for the plunging displacement and its time derivative. Therefore, one can conclude that the internal dynamics $\boldsymbol{\zeta}$ of the system stay bounded for all time provided that the state vector initial condition lies inside a compact set as defined above.□

C.3 Proof of Lemma 4

Using the definition of filtered error $r\,(t)$ in (3.10) and function of $L(t)$ in (3.35), we can write the integral (3.37) as

$$\begin{aligned}
\int_{t_0}^{t} L(\tau)d\tau &= \int_{t_0}^{t} \left(\dot{e}_2(\tau) + e_2(\tau)\right)\left(\bar{N}_{\mu d} - k_d sgn(e_2(\tau))\right)d\tau \\
&= \int_{t_0}^{t} \dot{e}_2(\tau)\bar{N}_{\mu d}d\tau - \int_{t_0}^{t} \dot{e}_2(\tau)k_d sgn(e_2(\tau))d\tau \\
&\quad + \int_{t_0}^{t} e_2(\tau)(\bar{N}_{\mu d} - k_d sgn(e_2(\tau)))d\tau \\
&\leq c_{\bar{N}_{\mu d}} \int_{t_0}^{t} |\dot{e}_2(\tau)|\, d\tau - k_d \left|e_2\left(t\right)\right| + k_d \left|e_2\left(t_0\right)\right| + \int_{t_0}^{t} |e_2(\tau)|\left(c_{\bar{N}_{\mu d}} - k_d\right))d\tau
\end{aligned}$$

where $c_{\bar{N}_{\mu d}} \triangleq |\bar{N}_{\mu d}||_\infty$ and have utilized the fact that $\dot{e}_2\left(\tau\right) sgn\left(e_2\left(\tau\right)\right) = \dfrac{d\left|e_2\left(\tau\right)\right|}{d\tau}$. By using Lemma 3, the integral of $L(t)$ can be further bounded as

$$\begin{aligned}
\int_{t_0}^{t} L(\tau)d\tau &\leq \left(c_{\bar{N}_{\mu d}} + c_{\bar{N}_{\mu d}}\varepsilon_2 - k_d\right)\int_0^t |e_2|\, d\tau &\text{(A.8)} \\
&\quad + \left(c_{\bar{N}_{\mu d}} - k_d\right)\left|e_2\left(t\right)\right| + c_{\bar{N}_{\mu d}}\varepsilon_1 + k_d\left|e_2\left(t_0\right)\right| &\text{(A.9)}
\end{aligned}$$

If the control gain k_d is chosen in the manner of (3.36) and applied to (A.8), then it is easy to obtain the upperbound of (3.37). The proof is complete.

C.4 Proof of Lemma 7

Using the definition of filtered error $r(t)$ in (4.14) and function of $L(t)$ in (4.35), we can write the integral (A.10) as

$$\begin{aligned}\int_{t_0}^{t} \mathbf{L}(\tau)d\tau &= \int_0^t \left(\mathbf{E}(\tau) + \dot{\mathbf{E}}(\tau)\right)^T \left(\bar{\mathbf{N}}_d - K_d sgn\left(\mathbf{E}(t)\right)\right) d\tau \\ &= \int_0^t \mathbf{E}(\tau)^T \left(\bar{\mathbf{N}}_d - K_d sgn\left(\mathbf{E}(\tau)\right)\right) d\tau + \tfrac{1}{2}\int_0^t \dot{\mathbf{E}}(\tau)^T \bar{\mathbf{N}}_d d\tau \\ &\quad -\tfrac{1}{2}\int_0^t \dot{\mathbf{E}}(\tau)^T K_d sgn\left(\mathbf{E}(\tau)\right) d\tau.\end{aligned} \tag{A.10}$$

The first term of (A.10) can be evaluated as follows

$$\begin{aligned}\int_{t_0}^{t} \mathbf{E}(\tau)^T \left(\bar{\mathbf{N}}_d - K_d sgn\left(\mathbf{E}(\tau)\right)\right) d\tau &= \int_{t_0}^{t} \sum_{i=1}^{2} |E_i(\tau)| \left(\bar{N}_{d,i} sgn\left(E_i(\tau)\right) - k_{d,i}\right) d\tau \\ &\leq \sum_{i=1}^{2} \left(c_{\bar{N}_{d,i}} - k_{d,i}\right) \int_{t_0}^{t} |E_i(\tau)| d\tau\end{aligned}$$

By applying Lemma 1, the second term can be written as

$$\begin{aligned}\int_0^t \dot{\mathbf{E}}(\tau)^T \bar{N}_d d\tau &= \sum_{i=1}^{2} \int_0^t \dot{\mathbf{E}}_i(\tau) \bar{N}_{d,i} d\tau \\ &\leq \sum_{i=1}^{2} \int_0^t \left|\dot{\mathbf{E}}_i(\tau)\right| \left|\bar{N}_{d,i}\right| d\tau \\ &\leq \sum_{i=1}^{2} c_{\bar{N}_{d,i}} \left(\varepsilon_1 + \varepsilon_2 \int_0^t |\mathbf{E}_i| d\tau + |\mathbf{E}_i(t)|\right).\end{aligned}$$

The last term in (A.10) can be written as

$$\begin{aligned}
-\frac{1}{2}\int_0^t \dot{\mathbf{E}}\left(\tau\right)^T k_d sgn\left(\mathbf{E}\left(\tau\right)\right)d\tau &= -\frac{1}{2}\sum_{i=1}^{2} k_{d,i}\int_0^t \dot{\mathbf{E}}_i\left(\tau\right)^T sgn\left(\mathbf{E}_i\left(\tau\right)\right)d\tau \\
&= -\frac{1}{2}\sum_{i=1}^{2} k_{d,i}\left|\mathbf{E}_i\left(\tau\right)\right|_{t_0}^{t} \\
&= -\frac{1}{2}\sum_{i=1}^{2}\left(k_{d,i}\left|\mathbf{E}_i\left(t\right)\right| - k_{d,i}\left|\mathbf{E}_i\left(t_0\right)\right|\right)
\end{aligned}$$

Combining all terms, we obtain the following inequality

$$\begin{aligned}
\int_{t_0}^{t} L(\tau)d\tau &\leq \sum_{i=1}^{2}\left(c_{\bar{N}_{d,i}} - k_{d,i}\right)\int_{t_0}^{t}\left|E_i\left(\tau\right)\right|d\tau + \sum_{i=1}^{2} c_{\bar{N}_{d,i}}\left(\varepsilon_1 + \varepsilon_2\int_0^t\left|E_i\right|d\tau + \left|E_i\left(t\right)\right|\right) \\
&\quad -\sum_{i=1}^{2}\left(k_{d,i}\left|E_i\left(t\right)\right| - k_{d,i}\left|E_i\left(t_0\right)\right|\right) \\
&\leq \sum_{i=1}^{2}\left(c_{\bar{N}_{d,i}} + \frac{1}{2}c_{\bar{N}_{d,i}}\varepsilon_1 - k_{d,i}\right)\int_{t_0}^{t}\left|E_i\left(\tau\right)\right|d\tau + \sum_{i=1}^{2}\left(c_{\bar{N}_{d,i}} - k_{d,i}\right)\left|E_i\left(t\right)\right| \\
&\quad +\sum_{i=1}^{2}\left(c_{\bar{N}_{d,i}}\varepsilon_1 + k_{d,i}\left|E_i\left(t_0\right)\right|\right)
\end{aligned}$$

By selecting $k_{d,i} \geq c_{\bar{N}_{d,i}} + \frac{1}{2}c_{\bar{N}_{d,i}}\varepsilon_1$, one can bound the integral as

$$\int_{t_0}^{t} L(\tau)d\tau \leq C_d$$

where $C_d = \frac{1}{2}\sum_{i=1}^{2}\left(c_{\bar{N}_{d,i}}\varepsilon_1 + k_{d,i}\left|E_i\left(t_0\right)\right|\right)$. Then the proof is complete.

APPENDIX B: EXPRESSIONS OF EQUATIONS

C. 2 Expressions part 1

The matrices related to structural mass, stiffness, and non-circulatory load in (2.42) are given as follows

$$\Phi_1(\phi) = \pi - \phi + \sin\phi, \qquad \Phi_2(\phi) = (\pi-\phi)(1+2\cos\phi) + \sin\phi\,(2+\cos\phi),$$
$$\Phi_3(\phi) = \pi - \phi + \sin\phi\cos\phi, \quad \Phi_4(\phi) = 2(\pi-\phi)\cos\phi + \sin\phi\tfrac{2}{3}(2+\cos^2\phi)$$
$$\Phi_5(\phi) = \sin\phi(1-\cos\phi) \qquad \Phi_6(\phi) = 2(\pi-\phi) + \sin\phi\tfrac{2}{3}(2-\cos\phi)(1+2\cos\phi)$$
$$\Phi_7(\phi) = (\pi-\phi)\left(\tfrac{1}{2}+2\cos\phi\right) + \sin\phi\tfrac{1}{6}(8+5\cos\phi+4\cos^2\phi-2\cos^3\phi)$$
$$\Phi_8(\phi) = (\pi-\phi)(-1+2\cos\phi) + \sin\phi\,(2+3\cos\phi+4\cos^2\phi)$$
$$\Phi_{10}(\phi) = \Phi_{13}(\phi)\cdot\Phi_5(\phi) \qquad \Phi_{11}(\phi) = \Phi_2(\phi)\cdot\Phi_3(\phi)$$
$$\Phi_{12}(\phi) = (\pi-\phi)^2\left(\tfrac{1}{2}+4\cos^2\phi\right) + (\pi-\phi)\sin\phi\cos\phi\,(7+2\cos^2\phi) + \sin^2\phi\left(2+\tfrac{5}{2}\cos^2\phi\right)$$
$$\Phi_{13}(\phi) = \pi - \phi - \sin\phi.$$

$$\overset{8\times8}{A} = \begin{bmatrix} A_{11} & A_{12} & A_{13} \\ A_{21} & A_{22} & A_{23} \\ A_{31} & A_{32} & A_{33} \end{bmatrix}$$
$$\overset{8\times1}{B} = \begin{bmatrix} B_1^T & B_2^T & B_3^T \end{bmatrix}^T$$
$$\mathbf{C} = \begin{bmatrix} 0 & 0 & 0 & 1 & 0 & 0 & 0 & 0 \end{bmatrix}$$

$$\overset{3\times3}{\bar{M}} = -[M + \pi\rho b^2 Z_1]^{-1} \qquad \overset{3\times3}{A}_{11} = \bar{M}\pi\rho b^2 Z_2$$

$$\overset{3\times3}{A}_{12} = \bar{M}\left(\pi\rho b^2 Z_3 + K_1\right) \qquad \overset{3\times2}{A}_{13} = \bar{M}\pi\rho b^2 Z_4$$

$$\overset{3\times2}{A}_{21} = \mathbf{I},\ \overset{\mathbf{3\times2}}{\mathbf{A}}_{\mathbf{22}} = \mathbf{0} \qquad \overset{3\times3}{A}_{23} = \mathbf{0}$$

$$\overset{3\times2}{A}_{31} = \begin{bmatrix} \mathbf{r}_1 A_{11} + \mathbf{r}_2 \\ \mathbf{r}_1 A_{11} + \mathbf{r}_2 \end{bmatrix} \qquad \overset{2\times3}{A}_{32} = \begin{bmatrix} \mathbf{r}_1 A_{12} \\ \mathbf{r}_1 A_{12} \end{bmatrix}$$

$$\overset{2\times3}{A}_{33} = \begin{bmatrix} -w_1 & 0 \\ 0 & -w_2 \end{bmatrix} + \begin{bmatrix} \mathbf{r}_1 A_{13} \\ \mathbf{r}_1 A_{13} \end{bmatrix}$$

$$\overset{3\times1}{B}_1 = [\mathbf{M} + \pi\rho b^2 \mathbf{Z}_1]^{-1} \begin{bmatrix} 0_{2\times1} & 1 \end{bmatrix}^T \qquad \overset{3\times1}{B}_2 = \mathbf{0}_{3\times1}$$

$$\overset{2\times1}{B}_3 = \begin{bmatrix} \mathbf{r}_1 B_1 & \mathbf{r}_1 B_1 \end{bmatrix}^T \qquad \mathbf{C} = \begin{bmatrix} 0_{1\times3} & 1 & 0_{1\times4} \end{bmatrix}^T$$

$$K_1 = \begin{bmatrix} K_h & & \\ & K_\alpha & \\ & & K_\beta \end{bmatrix} \qquad K_2 = \begin{bmatrix} k_{n_h}(h) & & \\ & k_{n_\alpha}(\alpha) & \\ & & 0 \end{bmatrix}$$

$$\begin{aligned} \mathbf{f}(\frac{h}{b}, \alpha) &= \begin{bmatrix} \left(\bar{M}K_2\mathbf{Y}\right)^T & 0_{1\times3} & \mathbf{r}_1^T\left(\bar{M}K_2\mathbf{Y}\right)^T \end{bmatrix}^T \\ k_{n_h}(h) &= bK_h 0.09h^2 \\ k_{n_\alpha}(\alpha) &= K_\alpha\left(-22.1\alpha + 1315.5\alpha^2 + 8580\alpha^3 - 17289.7\alpha^4\right) \end{aligned}$$

$$\mathbf{Z}_1 = \begin{bmatrix} b & -ab & \frac{b}{2\pi}\Phi_4 \\ -ab^2 & b^2\left(\frac{1}{8}+a^2\right) & \frac{b^2}{4\pi}\Phi_7 \\ \frac{b^2}{2\pi}\Phi_4 & \frac{b^2}{4\pi}\Phi_7 & \frac{b^2}{4\pi}\Phi_{12} \end{bmatrix}$$

$$\mathbf{Z}_2 = \begin{bmatrix} 2V & 2V\left(1-a\right) & \frac{V}{\pi}(\Phi_3+\Phi_2) \\ -2bV\left(\frac{1}{2}+a\right) & -2Vba(\frac{1}{2}-a) & \frac{Vb}{\pi}\left\{\frac{1}{2}\Phi_6-\left(\frac{1}{2}+a\right)\Phi_2\right\} \\ \frac{Vb}{\pi}\Phi_8 & \frac{Vb}{\pi}(\frac{\Phi_9}{2}+\left(\frac{1}{2}-a\right)\Phi_8) & \frac{Vb}{2\pi^2}(\Phi_{11}+\Phi_2\Phi_8) \end{bmatrix}$$

$$\mathbf{Z}_3 = \begin{bmatrix} 0 & \frac{2V^2}{b} & \frac{2V^2}{\pi b}\Phi_1 \\ 0 & -2V^2\left(\frac{1}{2}+a\right) & \frac{V^2}{\pi}\left\{\Phi_5-2\left(\frac{1}{2}+a\right)\Phi_1\right\} \\ 0 & \frac{V^2}{\pi}\Phi_8 & \frac{V^2}{\pi^2}(\Phi_{10}+\Phi_1\Phi_8) \end{bmatrix}$$

$$\mathbf{Z}_4 = \begin{bmatrix} \frac{-2VA_1}{b} & \frac{-2VA_2}{b} \\ 2V\left(\frac{1}{2}+a\right)A_1 & 2V\left(\frac{1}{2}+a\right)A_2 \\ \frac{-V\Phi_8A_1}{\pi} & \frac{-V\Phi_8A_2}{\pi} \end{bmatrix}$$

$$\mathbf{r_1} = \begin{bmatrix} b & b\left(\frac{1}{2}-a\right) & \frac{b}{2\pi}\Phi_2 \end{bmatrix}$$

$$\mathbf{r}_2 = \begin{bmatrix} 0 & V & \frac{V}{\pi}\Phi_1 \end{bmatrix}$$

$$Z_2^{'} = \begin{bmatrix} 0 & V & \frac{V}{\pi}\Phi_3 \\ 0 & \left(\frac{1}{2}-a\right)V & \frac{V}{2\pi} \\ 0 & \frac{bV}{2\pi}\Phi_9 & \frac{bv}{2\pi^2}\Phi_{11} \end{bmatrix} \qquad Z_3^{'} = \begin{bmatrix} 0 & 0 & 0 \\ 0 & 0 & \frac{V^2}{\pi b}\Phi_5 \\ 0 & 0 & \frac{V^2}{\pi b}\Phi_{10} \end{bmatrix}$$

$$Z_4^{'} = \begin{bmatrix} \frac{2V}{b} & -2\left(\frac{1}{2}+a\right)V & \frac{V\Phi_8}{\pi} \end{bmatrix}^T \qquad \overset{3\times3}{A^{'}}_{11} = \bar{M}\pi\rho b^2 Z_2^{'}$$

$$\overset{3\times3}{A^{'}}_{12} = \bar{M}\left(\pi\rho b^2 Z_3^{'} + K_1\right) \qquad \overset{3\times2}{A^{'}}_{13} = \pi\rho b^2\bar{M}Z_4^{'} = \begin{bmatrix} g_1 & g_2 & g_3 \end{bmatrix}^T$$

$$
F = \begin{bmatrix}
0 & 0 & 0 & 1 & 0 & 0 & 0 & 0 \\
1 & 0 & 0 & 0 & 0 & 0 & 0 & 0 \\
b_2 & -b_1 & 0 & 0 & 0 & 0 & 0 & 0 \\
0 & b_3 & -b_2 & 0 & 0 & 0 & 0 & 0 \\
0 & 0 & 0 & b_2 & -b_1 & 0 & 0 & 0 \\
0 & 0 & 0 & 0 & b_3 & -b_2 & 0 & 0 \\
b_7 & 0 & 0 & 0 & 0 & 0 & 0 & -b_2 \\
0 & 0 & 0 & 0 & 0 & 0 & 1 & -1
\end{bmatrix}
$$

The definitions of parameters and expressions in (2.13) are given as following. c_2, c_4, c_6 is defined as the elements of the first row of $A_{11}^{'}$ and c_1, c_3, c_5 is defined as the elements of the first row of $A_{12}^{'}$. b_1 is the first element of the control gain vector B_1. $f_{n1}(\frac{h}{b}, \alpha)$ is the first element of aforementioned $\mathbf{f}(\frac{h}{b}, \alpha)$. The regression vector and linearized parameters of (2.13) is shown as following

$$
\begin{aligned}
\mathbf{W}_F &= \begin{bmatrix} \frac{h}{b} & \frac{\dot{h}}{b} & \alpha & \dot{\alpha} & \beta & \dot{\beta} & \mathbf{W}_\Delta(t) & h^2 & \alpha & \alpha^2 & \alpha^3 & \alpha^4 & \dot{e}_1 \end{bmatrix} \\
\boldsymbol{\theta}_F &= \begin{bmatrix} -c_1 & -c_2 & -c_3 & -c_4 & -c_5 & -c_6 \\ -g_1\boldsymbol{\theta}_\Delta & -bK_h & 22.1K_\alpha & -1315.5K_\alpha & -8580K_\alpha & 17289.7K_\alpha \end{bmatrix}^T
\end{aligned}
$$

C. 2 Expressions part 2

The matrices related to structural mass, stiffness, and non-circulatory load are given as follows

$$M_s = \begin{bmatrix} 1 & x_\alpha & x_\beta & x_\gamma \\ x_\alpha & r_\alpha^2 & \left[r_\beta^2 + x_\beta\,(c-a)\right] & \left[x_\gamma\,(d-a) - r_\gamma^2\right] \\ x_\beta & \left[r_\beta^2 + x_\beta\,(c-a)\right] & r_\beta^2 & 0 \\ x_\gamma & \left[x_\gamma(d-a) - r_\gamma^2\right] & 0 & r_\gamma^2 \end{bmatrix},$$

$$K_s = \begin{bmatrix} \omega_h^2 & 0 & 0 & 0 \\ 0 & r_\alpha^2\omega_\alpha^2 & 0 & 0 \\ 0 & 0 & r_\beta^2\omega_\beta^2 & 0 \\ 0 & 0 & 0 & r_\gamma^2\omega_\gamma^2 \end{bmatrix},$$

$$M_{nc} = P^T \bar{M}_{nc} P,\ B_{nc} = P^T \bar{B}_{nc} P,\ K_{nc} = P^T \bar{K}_{nc} P$$

$$\bar{M}_{nc} = \begin{bmatrix} -\pi & \pi a & T_1 & T_1\,(d) \\ \pi a & -\pi\left(\frac{1}{8} + a^2\right) & -2T_{13} & -2T_{13}\,(d) \\ T_1 & -2T_{13} & \frac{1}{\pi}T_3 & \frac{1}{\pi}Y_6 \\ T_1(d) & -2T_{13}\,(d) & \frac{1}{\pi}Y_6 & \frac{1}{\pi}T_3\,(d) \end{bmatrix},$$

$$\bar{B}_{nc} = \begin{bmatrix} 0 & -\pi & -T_4 & T_4\,(d) \\ 0 & \pi\left(a - \frac{1}{c}\right) & -T_{16} & -T_{16}\,(d) \\ 0 & -T_{17} & -\frac{1}{\pi}T_{19} & -\frac{1}{\pi}Y_{18} \\ 0 & -T_{17}\,(d) & -\frac{1}{\pi}Y_{10} & -\frac{1}{\pi}T_{19}\,(d) \end{bmatrix},$$

$$\bar{K}_{nc} = \begin{bmatrix} 0 & 0 & 0 & 0 \\ 0 & 0 & -T_{15} & -T_{15}(d) \\ 0 & 0 & -\frac{1}{\pi}T_{18} & -\frac{1}{\pi}Y_{17} \\ 0 & 0 & -\frac{1}{\pi}Y_9 & -\frac{1}{\pi}T_{18}(d) \end{bmatrix}, P = \begin{bmatrix} 1 & 0 & 0 & b(d-a) \\ 0 & 1 & 0 & -1 \\ 0 & 0 & 1 & 0 \\ 0 & 0 & 0 & 1 \end{bmatrix},$$

$$R = \begin{bmatrix} -2\pi & 2\pi\left(a+\frac{1}{2}\right) & -T_{12} & -T_{12}(d) \end{bmatrix}^T.$$

Explicit definitions for the constants $T_i, T_i(d)$, and Y_i can be found in Theodorsen and Garrick's report [34]. All the other variables used above are standard in aeroelastic literature; the reader is referred to [6] for definitions. The matrix definitions for the state-space description of (2.49) are given as

$$A = \begin{bmatrix} A_1 & A_2 & A_4 \\ I & 0 & 0 \\ A_{B1} & A_{B2} & A_{B4} \end{bmatrix}, \quad \bar{M} = \left(M_s - \frac{\rho}{m_s}Z_1\right),$$

$$A_1 = \bar{M}^{-1}\frac{\rho}{m_s}Z_2, \quad A_2 = \bar{M}^{-1}\left(\frac{\rho}{m_s}Z_3 - K_s\right),$$

$$A_4 = -\bar{M}^{-1}\frac{\rho}{m_s}Z_B, \quad A_3(\mathbf{y}) = -\bar{M}^{-1}K(h,\alpha),$$

$$A_{B1} = \begin{bmatrix} US_1P + bS_2PA_1 \\ US_1P + bS_2PA_1 \end{bmatrix}, \quad A_{B2} = \begin{bmatrix} bS_2PA_2 \\ bS_2PA_2 \end{bmatrix},$$

$$A_{B3}(\mathbf{y}) = \begin{bmatrix} bS_2PA_3(\mathbf{y}) \\ bS_2PA_3(\mathbf{y}) \end{bmatrix}, \quad A_{B4} = \begin{bmatrix} bS_2PA_4 + \begin{bmatrix} -w_1 & 0 \end{bmatrix} \\ bS_2PA_4 + \begin{bmatrix} 0 & -w_2 \end{bmatrix} \end{bmatrix},$$

$$Z_1 = UP^TRS_2P + b^2M_{nc}, \quad Z_2 = UP^TRS_1P + bUB_{nc},$$

$$Z_3 = U^2K_{nc}, \quad Z_B = \begin{bmatrix} UP^TRa_1 & UP^TRa_2 \end{bmatrix},$$

$$H = \left[\begin{array}{cc} \bar{M}^{-1}T & 0 \end{array} \left[\begin{array}{cc} bS_2PT & bS_2PT \end{array} \right] \right]^T, \quad S_1 = \left[\begin{array}{cccc} 0 & 1 & \frac{1}{\pi}T_{10} & \frac{1}{\pi}T_{10}(d) \end{array} \right],$$

$$S_2 = \left[\begin{array}{ccc} 1 & \frac{1}{2} - a & \frac{1}{2\pi}T_{11} & \frac{1}{2\pi}T_{11}(d) \end{array} \right], \quad \mathbf{f}(\mathbf{y}) = \left[\begin{array}{ccc} x^T A_3^T(\mathbf{y}) & 0_{1\times 4} & x^T A_{B3}^T(\mathbf{y}) \end{array} \right]^T.$$

$\Psi(\mathbf{x}, \dot{\mathbf{x}})$ in (2.50) is defined as

$$\Psi(\mathbf{x}, \dot{\mathbf{x}}) = \left[\begin{array}{cc} \bar{A}_{11} & \bar{A}_{12} \end{array} \right] \dot{x} + \left[\begin{array}{cc} \bar{A}_{21} & \bar{A}_{22} \end{array} \right] x$$

where $\bar{A}_{11}, \bar{A}_{12}, \bar{A}_{21}, \bar{A}_{22} \in \Re^{2\times 2}$ can be obtained from the following

$$\left[\begin{array}{cc} \bar{A}_{11} & \bar{A}_{12} \\ \bar{A}_{13} & \bar{A}_{14} \end{array} \right] = \frac{1}{m_s}\rho b U B_{nc} \left(M_s - \frac{1}{m_s}\rho b^2 M_{nc} \right)^{-1},$$

$$\left[\begin{array}{cc} \bar{A}_{21} & \bar{A}_{22} \\ \bar{A}_{23} & \bar{A}_{24} \end{array} \right] = \left(M_s - \frac{1}{m_s}\rho b^2 M_{nc} \right)^{-1} \left(\frac{1}{m_s}\rho U^2 K_{nc} - K_s - K(h, \alpha) \right).$$

In (2.50), the vector $\mathbf{F} \in \Re^{2\times 1}$ is obtained as the first two rows of $\mathbf{F}_0 \in \Re^{4\times 1}$ which is defined as follows

$$F_0 = \frac{1}{m_s}\rho U V^T R \left(M_s - \frac{1}{m_s}\rho b^2 M_{nc} \right)^{-1}.$$

C. 4 Expressions

$$\begin{aligned} \overline{\mathbf{\Delta}}(t) &= \left[\begin{array}{ccc} \left(\bar{M}^{-1}\mathbf{L}_g\right)^T & 0 & 0 \end{array} \right]^T \\ &= \left[\begin{array}{ccccc} d_1(t) & d_2(t) & d_3(t) & d_4(t) & 0_{1\times 6} \end{array} \right]^T \end{aligned}$$

Definitions of expressions in equations (4.6)

$$\begin{aligned}
\Phi(\boldsymbol{\mu}, \boldsymbol{\zeta}) &= \begin{bmatrix} 0 & 1 \\ 1 & 0 \end{bmatrix} \left\{ \begin{bmatrix} A_1 & A_2 & A_4 \end{bmatrix} \mathbf{X} + A_3(\mathbf{y})\,\mathbf{x} \right\} \\
\boldsymbol{\Delta}_1(t) &= \begin{bmatrix} d_2(t) & d_1(t) \end{bmatrix}^T \\
G &= \begin{bmatrix} 0_2 & \bar{I}_2 \end{bmatrix} \bar{M}^{-1} T \\
\Psi(\boldsymbol{\mu}, \boldsymbol{\zeta}) &= F_{sub} \begin{bmatrix} 0_{6\times 4} & I_6 \end{bmatrix} A\mathbf{X} + F_{sub}\mathbf{f}(\mathbf{y}) \\
\boldsymbol{\Delta}_2(t) &= F_{sub}\overline{\boldsymbol{\Delta}}(t)
\end{aligned}$$

where $\bar{I}_2 = \begin{bmatrix} 0 & 1 \\ 1 & 0 \end{bmatrix}$.

C. 5 Expressions

The auxiliary constants $k_i, c_i, g_i \forall i = 1, ..., 4$,as well as $p_{2,}$ and p_4 that were introduced in the model description of (5.12) are explicitly defined as follows

$$d = 1 - \frac{\chi_\alpha^2}{r_\alpha^2}$$

$$k_1 = \frac{-\lambda}{M\mu d} + \frac{\chi_\alpha}{V^2 d} + \frac{\chi_\alpha \lambda(1 - x_0)}{M\mu r_\alpha^2 d}$$

$$k_2 = \frac{-\lambda(1 - x_0)}{M\mu d} + \frac{2\chi_\alpha \zeta_\alpha}{Vd} + \frac{\chi_\alpha \lambda(4 - 6x_0 + 3x_0^2)}{3M\mu r_\alpha^2 d}$$

$$k_3 = \frac{-\bar{\omega}^2}{V^2 d}$$

$$k_4 = \frac{-\lambda}{M\mu d} - \frac{2\zeta_h \bar{\omega}}{Vd} + \frac{\chi_\alpha \lambda(1-x_0)}{M\mu r_\alpha^2 d}$$

$$c_1 = \frac{\chi_\alpha \lambda}{M\mu r_\alpha^2 d} - \frac{1}{V^2 d} - \frac{\lambda(1-x_0)}{M\mu r_\alpha^2 d}$$

$$c_2 = \frac{\chi_\alpha \lambda(1-x_0)}{M r_\alpha^2 d} - \frac{2\zeta_\alpha}{Vd} + \frac{\lambda b(4-6x_0+3x_0)^2}{M\mu r_\alpha^2 d}$$

$$c_3 = \frac{\chi_\alpha \bar{\omega}^2}{r_\alpha^2 V^2 d}$$

$$c_4 = \frac{\chi_\alpha \lambda}{M\mu r_\alpha^2 d} + \frac{2\chi_\alpha \zeta_h \bar{\omega}}{r_\alpha^2 V^2 d} - \frac{\lambda(1-x_0)}{M\mu r_\alpha^2 d}$$

$$g_1 = \frac{\chi_\alpha \lambda(1-x_1/2)}{M\mu r_\alpha^2 d} - \frac{\lambda(1-x_1/2)(1-x_0+x_1/2)}{M\mu r_\alpha^2 d}$$

$$g_2 = \frac{-\lambda(1-x_1/2)}{M\mu d} + \frac{\chi_\alpha \lambda(1-x_1/2)(1-x_0+x_1/2)}{M\mu r_\alpha^2 d}$$

$$g_3 = \frac{\chi_\alpha \lambda(-1+x_1/2)^2}{M\mu r_\alpha^2 d} - \frac{\lambda(-1+x_1/2)^2(4-3x_0+x_1)}{3M\mu r_\alpha^2 d}$$

$$g_4 = \frac{-\lambda(-1+x_1/2)^2}{M\mu d} + \frac{\chi_\alpha \lambda(-1+x_1/2)^2(4-3x_0+x_1)}{3M\mu r_\alpha^2 d}$$

$$p_2 = \frac{\chi_\alpha \lambda^2 M(1+\gamma)}{12\mu r_\alpha^2 d} - \frac{\lambda^2 M(1+\gamma)(1-x_0)}{12\mu r_\alpha^2 d} + \frac{B}{V^2 d}$$

$$p_4 = -\frac{\lambda^2 M(1+\gamma)}{12\mu d} + \frac{\chi_\alpha \lambda^2 M(1+\gamma)(1-x_0)}{12\mu r_\alpha^2 d} + \frac{\chi_\alpha B}{V^2 d}$$

LIST OF REFERENCES

[1] Behal, A., Rao, V.M., and Marzocca, P., "Adaptive Control for a Nonlinear Wing Section with Multiple Flaps," *Journal of Guidance, Control, and Dynamics*, Vol. 29, No. 5, 2006, pp. 744-748.

[2] Zhang, K., and Behal, A., Continuous robust control for aeroelastic vibration control of a 2-D airfoil under unsteady flow, Journal of Vibration and Control,2014, DOI :10.1177/1077546314554821

[3] York, D.L., "Analysis of Flutter and Flutter Suppression via an Energy Method, MS Thesis," Department of Aerospace and Ocean Enginerring, Virginia Polytechnic Institute and State University, Blacksburg, VA, May 1980.

[4] Khalil, Hassan K., *Nonlinear Systems,* Prentice Hall, Third Edition, pp. 323-324, 1996.

[5] Librescu, L., Na S., Marzocca, P., Chung, C. and Kwak, M. K., "Active aeroelastic control of 2-D wing-flap systems operating in →an incompressible flowfield and impacted by a blast pulse," *Journal of Sound and Vibration*, Vol. 283, pp. 685-706, 2005.

[6] Edwards, J.W., "Unsteady aerodynamic modeling and active aeroelastic control", SUDARR 504 (NASA Grant ngl-05-020-007), Stanford University, February 1977. Also available as NASA CR-148019.

[7] Kussner, H.G., Schwarz, I., "The oscillating wing with aerodynamically balanced elevator", NACA-TM991, October 1941.

[8] Rodden, W.P., and Stahl, B., "A strip method for prediction of damping in subsonic wind tunnel and flight flutter tests," *Journal of Aircraft,* Vol. 6, No. 1, pp. 9-17, 1969. doi: 10.2514/3.43994

[9] Chen, J., Behal, A. and Dawson, D. M., "Robust Feedback Control for a Class of Uncertain MIMO Nonlinear Systems," *IEEE Trans. Autom. Control*, Vol. 53, No. 2, pp. 591-596, Mar. 2008.

[10] Pomet, J. B. and Praly, L., "Adaptive Nonlinear Regulation: Estimation from the Lyapunov Equation," *IEEE Trans. Automatic Control*, Vol. 37, pp. 729-740, 1992.

[11] Sastry, S. Shankar and Isidori, Alberto, "Adaptive Control of Linearizable Systems," *IEEE Transactions on Automatic Control*, vol. 34, No. 11, Nov. 1989.

[12] Bhoir, N. and Singh, Sahjendra N., "Output feedback nonlinear control of an aeroelastic system with unsteady aerodynamics," *Aerospace Science and Technology*, Vol. 8, pp. 195-205, 2004,

[13] Zhang, K., Wang, Z., Behal, A., and Marzocca, P., "Novel Nonlinear Control Design for a Two-Dimensional foil Under Unsteady Flow," *Journal of Guidance Control Dynamics*, Vol. 36, No. 6, pp. 1681-1694. 2013.

[14] Wang, Z., Behal, A., and Marzocca, P., "Adaptive and Robust Aeroelastic Control of Nonlinear Lifting Surfaces with Single/Multiple Control Surfaces: A Review," *International Journal of Aeronautical and Space Science*, Vol. 11, No. 4, pp.285302, 2010.

[15] Xian, B., Dawson, D. M., de Queiroz, M. S., and Chen, J., "A Continuous Asymptotic Tracking Control Strategy for Uncertain Nonlinear Systems," *IEEE Transactions on Automatic Control*, vol. 49, no. 7, Jul., pp. 1206-1211, 2004.

[16] Marzocca, P., Librescu, L., and Chiocchia, G., "Aeroelastic Response of 2-D Lifting Surfaces to Gust and Arbitrary Explosive Loading Signatures," *International Journal of Impact Engineering*, Vol. 25, No. 1, pp. 41-65, 2001.

[17] Sadegh, N. and Horowitz, R., "Stability and Robustness Analysis of a Class of Adaptive Controllers for Robotic Manipulators," *International Journal of Robotic Research*, Vol. 9, No. 3, pp. 74–92, June 1990.

[18] Strang, G., *Linear Algebra and its Applications,* 2^{nd} *ed.*, New York: Academic Press, Inc., 1980.

[19] Morse, A.S., "A Gain Matrix Decomposition and Some of Its Applications," *Systems and Control Letters*, vol. 21, pp. 1-10, 1993.

[20] Zhang, K., Talebi, S. and A. Behal, "Robust Output Feedback Control for Aeroelastic Vibration Supression of a 4-DOF Airfoil under Unsteady Flow," Submitted to IEEE Trans. on Control Systems Technology.

[21] Wang, Z., Behal, A. and Marzocca, P., "Continuous Robust Control for Two-Dimensional Airfoils with Leading- and Trailing-Edge Flaps," AIAA Journal of Guidance, Control, and Dynamics, vol. 35, no. 2, pp. 510-519, March-April 2012.

[22] Wang, Z., Behal, A. and Marzocca, P., "Model-Free Control Design for MIMO Aeroelastic System Subject to External Disturbance," *J. of Guidance Control and Dynamics*, vol. 34, pp. 446-458, 2011.

[23] Zhang, X., Behal, A., Dawson, D.M. and Xian, B., "Output Feedback Control for a Class of Uncertain MIMO Nonlinear Systems With Non-Symmetric Input Gain Matrix," in *Proc. of IEEE Conference on Decision and Control*, Seville, Spain, pp. 7762-7767, 2005.

[24] Wang, Z. and Behal, A., Continuous robust control for a class of uncertain MIMO nonlinear systems, *In Decision and Control and European Control Conference (CDC-ECC)*, 2011 50th IEEE Conference on, pp. 7561-7566, 2011.

[25] Ashley, H. and Zartarian, G., "Piston Theory - A New Aerodynamic Tool for the Aeroelastician," *Journal of the Aerospace Sciences*, vol. 23, no. 10, pp. 1109-1118, 1956.

[26] Librescu, L., "Aeroelastic Stability of Orthotropic Heterogeneous Thin Panels in the Vicinity of the Flutter Critical Boundary, Part One: Simply supported panels" *Journal de Mécanique*, Part I, vol. 4, no. 1, pp. 51-76, 1965.

[27] Librescu, L., Marzocca, P. and Silva, W.A., Supersonic/hypersonic flutter and postflutter of geometrically imperfect circular cylindrical panels, *Journal of Spacecraft and Rockets*, 39(5), pp. 802-812, September-October 2002.

[28] Librescu, L., *Elastostatics and Kinetics of Anisotropic and Heterogeneous Shell-Type Structures, Aeroelastic Stability of Anisotropic Multilayered Thin Panels*, 1st ed., Book series: Mechanics of Elastic Stability, edited by H. Leipholz, Noordhoff International Publishing, Leyden, The Netherlands, 1975, Chapter 1, pp. 53-63, 106-158, Appendix A, pp. 543-550.

[29] Librescu, L., Chiocchia, G. and Marzocca, P., "Implications of cubic physical/aerodynamic nonlinearities on the character of the flutter instability boundary," *International Journal of Nonlinear Mechanics,* 38, pp. 173-199, March 2003.

[30] Thuruthimattam, B.J., Friedmann, P.P., McNamara, J.J. and Powell, K.G., "Aeroelasticity of a Generic Hypersonic Vehicle," *43rd AIAA/ASME/ASCE/AHS/ASC Structures, Structural Dynamics, and Materials Conference,* AIAA Paper no. 2002-1209, April 2002.

[31] Marzocca, P., Librescu, L. and Silva, W.A., "Flutter, Post-Flutter and Control of a Supersonic 2-D Lifting Surface," *Journal of Guidance, Control, and Dynamics*, vol. 25, no. 5, pp. 962-970, September - October 2002.

[32] Hornik, K., Stinchombe, M. and White, H.,"Multilayer Feedforward Networks are Universal Approximators," *J. Neural Networks*, vol. 2, pp. 359-366, March 1989.

[33] Rao, V. M., Behal, A., Marzocca, P., and Rubillo, C.M., "Adaptive aeroelastic vibration suppression of a supersonic airfoil with flap," *J. Aerospace Science and Technology*, vol. 10, Issue 4, pp. 309–315, May 2006.

[34] Theodorsen, T. and Garrick, I. E., *Nonstationary flow about a wing-aileron-tab combination including aerodynamic balance*, National Advisory Committee for Aeronautics NACA Report, no. 736, pp. 137-138, 1942.

[35] Stepanyan, V. and Kurdila, A. "Asymptotic tracking of uncertain systems with continuous control using adaptive bounding," *IEEE transactions on neural networks*, vol. 20, pp. 1320–1329, Aug. 2009.